School of Applied Science

Prediction of Slamming Occurrence of Catamarans

Kristoffer Grande

This thesis is presented as part of the requirements for
the award of the Degree of Master of Science(Physics)
of the Curtin University of Technology

August 2002

This thesis contains no material which has been accepted for the award of any other degree or diploma in any university. To the best of my knowledge and belief this thesis contains no material previously published by any other person except where due acknowledgement has been made.

ABSTRACT

In this work the problem of slamming on the cross structure of catamarans is studied. An introduction and overview of the problem is given. Methods for predicting the slamming occurrence of high-speed power catamarans and sailing catamarans are presented. Emphasis is placed on developing methods that are practical to use in order to facilitate prediction of slamming occurrence at the design stage. The methods used consist of three steps: Ship motion prediction, slamming identification and slamming pressure calculations. Existing linear and non-linear ship motion prediction theories are used for high-speed power catamarans while a new strip theory has been developed specifically for motion prediction of sailing multihulls. Predicted ship motion results are compared to full-scale experiments, both for high-speed power catamarans and sailing catamarans. A new direct method for identification of slamming occurrence in the time domain is presented, as well as results using probabilistic methods. A comparison between the two methods is presented. Slamming pressure calculations are done using an existing two dimensional slamming theory and are compared with analytical results. A parametric study is done on two case study ships to investigate the effect of various hullform parameters on the slamming occurrence. The methods and results presented are of use to designers of high-speed power catamarans and sailing catamarans.

ACKNOWLEDGEMENTS

Writing this thesis would not have been possible without the many persons that have helped me along the way. I would especially like to thank my principal supervisor, Dr Jinzhu Xia, for his encouraging guidance and all the time he has spent working together with me on this project. I would also like to thank Dr Jørgen Krokstad who was my initial supervisor who organized the use of the software packages VERES and SLAM 2D from Marintek, Norway. Thanks also go to Emeritus Professor John Penrose, one of my co-supervisors who has been very helpful and a source of inspiration with his humour. Dr Tony Armstrong of Austal Ships has also been very helpful, and besides being a co-supervisor he has provided me with a case study design from Austal ships. Dr Armstrong has also been very helpful by sharing some of his practical experience from high-speed catamarans and giving useful comments. I would also like to thank Dr Andrew Tuite from Crowther Multihulls for providing a sailing catamaran case study design and for useful input along the way. Thanks also go to Marintek, Norway for providing the software packages VERES and SLAM 2D.

All the staff at Centre for Marine Science and Technology have been very friendly. A special thanks go to Mr Kim Klaka who initially suggested I should travel from Norway to Western Australia to do this degree. Even though he has not had any formal involvement in my work he has been extremely helpful all the way. Mr Alec Duncan, Mr Amos Maggi and Mr Frank Thomas have all been a great help with their knowledge about full-scale trials, data processing and Matlab. Thanks also go to Mr Malcom Perry for his hard work with the equipment for my full-scale trials. Thanks also go to Mr Ian Walker for kindly letting me use his sailing catamaran Sally Malay for my full-scale trials. Finally a big thanks go to Mr Philippe Peche for sharing of his vast practical experience acquired through years of racing high performance catamarans around the world.

NOMENCLATURE

a	sectional added mass
A	added mass
b	sectional damping
B	damping
β	wave heading angle
β_T	true wind angle
bwl	sectional waterline beam
c	sectional restoring coefficient
C	restoring coefficient
CG	boats centre of gravity
C_M	midship coefficient
C_P	prismatic coefficient
ε	slenderness parameter
η	displacement at CG
η_A	displacement amplitude
f	sectional Froude-Krylov force
F	exciting force
F^d	diffraction force
F^f	froude-Krylov force
g	gravitational acceleration
h	sectional diffraction force
Hs	significant wave height
i	complex operator
k	wave number
LCB	longitudinal centre of buoyancy
LCF	longitudinal centre of flotation
LPP	length between perpendiculars
M	mass
ω	wave circular frequency
ω_e	wave circular encounter-frequency
RAO	response amplitude operator

S	spectral ordinate
τ	waveform parameter
t	time
T_{mean}	wave spectra mean period
U	boat speed
V	wind speed
V_1	wind speed parallel to x axis
V_2	wind speed parallel to y axis
xc	sail strip chord length
ξ	relative displacement between the ship and wave surface
ζ	wave elevation
ζ_A	wave amplitude

TABLE OF CONTENTS

LIST OF TABLES

LIST OF FIGURES

CHAPTER 1: INTRODUCTION

1.1 Background

Although not a new problem the slamming of a ship hull against waves has become a more important problem with the increasing popularity of high-speed catamarans in recent years. A special concern for catamarans is the structure between the hulls, i.e. the wetdeck (bridgedeck) or the crossbeams (Fig 1.1). This structure is often flat or nearly flat, and is located a distance above the waterline.

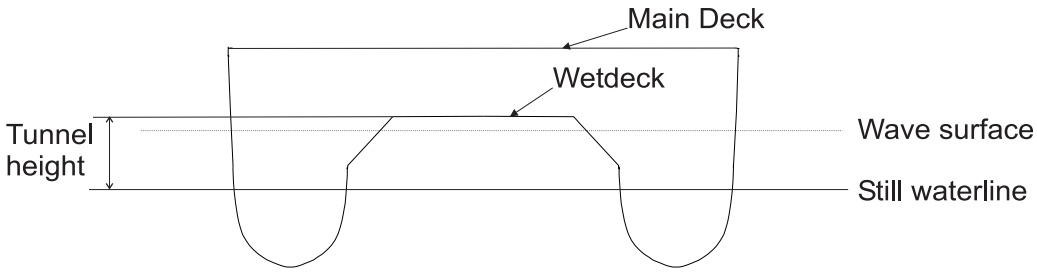

Fig. 1.1 Typical fast ferry catamaran cross section

Slamming on this flat, large area cross-structure can potentially give very high slamming pressures. High-speed catamarans add to the problems with their high speed and usually also light weight. Light weight and high speed often leads to higher vertical displacements, velocities and accelerations. Light weight is the result of a carefully optimised structure and modern materials, often with a smaller tolerance against failure than conventional ships. Slamming is clearly recognized as a problem by shipmasters, and they routinely reduce speed or abort operation when the vessel slams frequently. Designers of fast ferries have recognized slamming as an important problem for quite a long time, and slamming is now usually taken into account in the design, construction and operation of fast ferries. Nevertheless damage still occurs, both to local plating and reinforcements and global structure.

Slamming has also been a problem for sailing catamarans, and with the recent trend for large high-speed ocean-crossing sailing catamarans slamming has quickly become one of the major concerns for this type of boat. Compared to high-speed ferries sailing catamarans are considerably lighter and in some conditions sail with a

speed comparable to that of a fast ferry. For cruising catamarans the cross structure is often called the bridgedeck and is used for accommodation (Fig. 1.2).

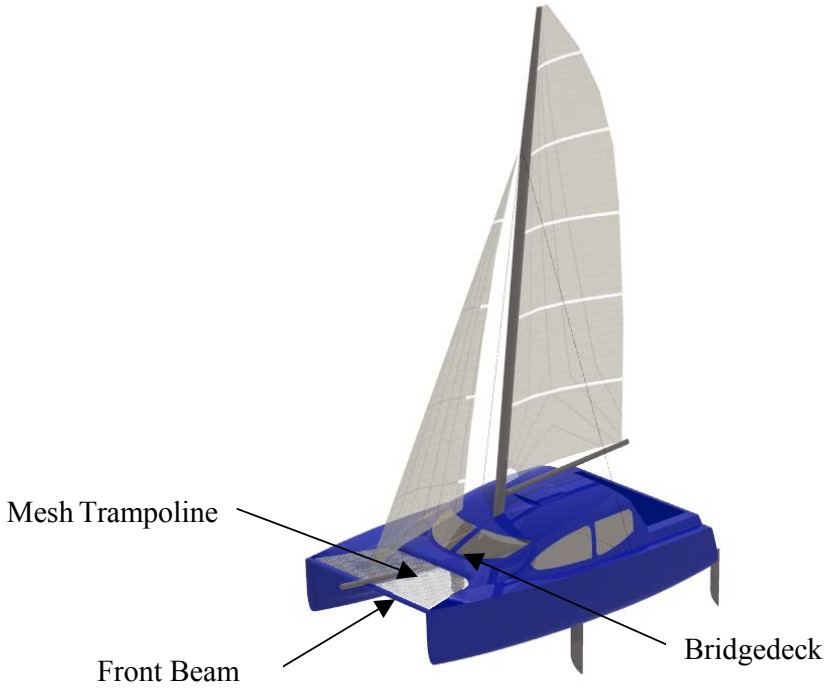

Fig. 1.2 Typical cruising catamaran (30ft)

The bridgedeck is usually kept as low as possible to keep weight and windage down as well as improving the overall appearance. Although a cruising catamaran sails at relatively low speeds the area and shape of the bridgedeck makes it very vulnerable to slamming loads. Ocean going racing catamarans have a simpler cross structure compared to the full decks of both fast ferries and cruising catamarans. Usually a main beam under the mast and an aft beam take the majority of the rigging loads while a smaller front beam gives support to the forestay (Fig. 1.3).

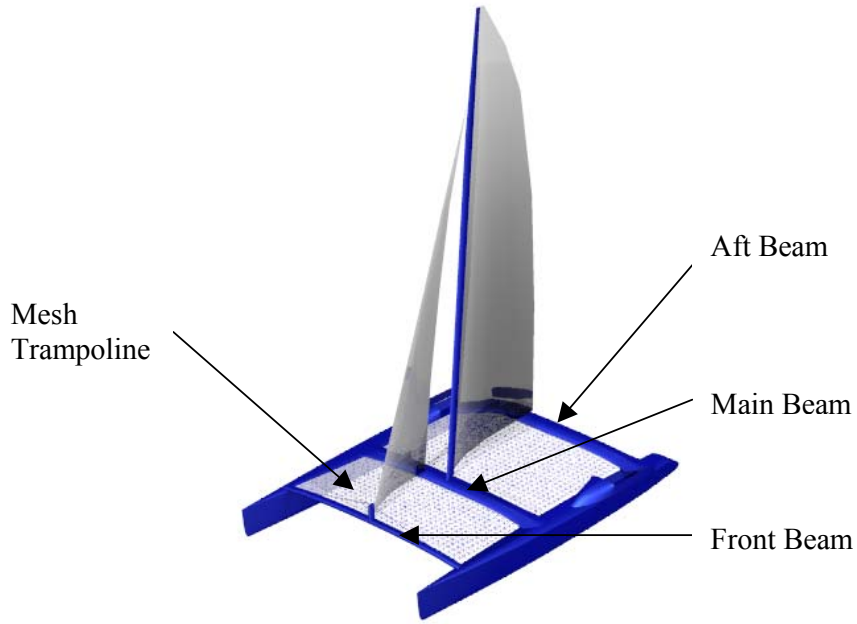

Fig. 1.3 Typical ocean going racing catamaran (120ft)

Fig. 1.4 110ft ocean racing catamaran ORANGE

The possibility of extreme speeds does however make slamming one major drawback for ocean racing catamarans (Fig. 1.4).

The main beam in such craft is especially vulnerable. On a racing catamaran the main beam takes the compression loads from the mast, typically 70 tonnes on a

110 ft racing catamaran, and a large part of the global sea loads. Slamming exacerbates the load regime; delamination on the underside of the main beam is not uncommon. Most often the failure is due to fatigue.

Race yachts differ from conventional yachts in that they are often designed for a specific race. Sailing multihulls are very weight-sensitive, added weight will reduce the speed. Except for basic safety requirements and sometimes class regulations there are no guidelines or regulations for the structural design of racing sailing multihulls. As a consequence the boats are designed for minimum weight, with small safety margins. More often than not they require a significant structural inspection and rebuild between major races. There are no real statistics available on the reliability of racing multihulls, but it is interesting to follow the history of the boats that entered THE RACE in 2001. A polish entry was WARTA POLPHARMA. Their boat was old, but had previously sailed around the world once. Problems were experienced with the main beam and a broken mast prior to the start but the craft completed the race. Team Legato also sailed an old boat, from 1983. This boat had been around the world once, while a second attempt ended with a broken mast in the southern ocean. They completed the race. Team Philips was a new, novel design with twin rigs and a central pod. The boat had severe problems from the start. One bow broke off completely during the initial trials. After a long rebuild they experienced problems with the mast-foot. After another rebuild the boat was taken for a long offshore sea trial. In rough conditions the pod started to crack from the hull and the boat also suffered control problems. The ship was abandoned and never recovered. Playstation was the first of a new generation catamarans to be launched for THE RACE. The boat was modified with more volume in the bows prior to THE RACE, but retired early due to problems with the keels and mainsail. However the boat has proven its value later and now holds the transatlantic record. Three sisterships were built by the French yard Multiplast for THE RACE. Club Med won the race, but had extensive delamination on the intersections between the hulls and beams when crossing the finishing line. The boat has been rebuilt and has recently set a new 24hr record of 697nm. Innovation Explorer, the second of the three sister-ships came second in THE RACE without any major damage. The boat was subsequently rebuilt and reinforced and has sailed around the world again to claim the Jules Verne Trophy. During this attempt the boat suffered damage from slamming, but the crew repaired it at sea. Team Adventure, the last of the Multiplast yachts, suffered

extensive delamination on the main beam during the RACE, and had to make two stops for emergency repairs. The boat attempted to break the transatlantic record after the race but the port bow broke off after colliding with a submerged object at high speed.

Investigations into slamming of fast ferries are not novel, but the problems have traditionally received far less attention than, for example, resistance and seakeeping problems. More research has been done specifically for fast ferries lately, mostly focusing on the calculation of loads from a given slamming impact. Little work has been published on the prediction of slamming occurrence.

Seeing the problem from a designer's perspective one recognizes that there are at least two sides of the problem. Firstly, the designer seeks to design the boat to avoid slamming as much as possible. Avoiding slamming totally would involve an impractical height of the cross structure, so some slamming must be tolerated. Secondly, the impact loads for the expected impacts must be calculated and the structure dimensioned accordingly. A method to predict the slamming occurrence of a catamaran would be an important tool for choosing important parameters such as cross structure height and different hull form parameters early in the design stage.

To the author's knowledge no research has been done into the slamming occurrence of sailing catamarans. Sailing multihulls are certainly not a new invention, but it is only in the last two decades that they have fixed their position as safe high-performance offshore sailing yachts. As with Formula 1 motor racing offshore racing has moved away from a trial and error mentality to become a highly professional industry. Empirical rules and guesswork are slowly being replaced by research. To this day most research for sailing catamarans is in the fields of resistance, rig design and structural design. As catamarans spend most of their time sailing in waves a more correct performance optimisation should be done by taking seakeeping and slamming into account.

1.2 Statement of problem

Presented herein is a study into the prediction of slamming occurrence of catamarans. Methods have been developed to investigate under what conditions slamming occurs. The frequency and severity of slamming is also investigated. This

work focuses on a theoretical approach to the problem, but the work is validated with experimental work as much as practically possible. Both fast ferry type catamarans and sailing catamarans are treated in this report. The problems for fast ferry catamarans and sailing catamarans are nearly identical, but there are differences in ship motion prediction methods available.

The work is partly based on existing methods. Ship motion predictions for fast ferry catamarans are based on an existing high-speed strip theory program (Faltinsen & Zhao 1991; VERES User manual, Marintek).Ship motion predictions for sailing catamarans are based on the same theory as used for fast ferry catamarans but a new strip theory program has also been developed by the author extending the well known theory of Salvesen, Tuck and Faltinsen (1970) to incorporate features that are important for sailing catamarans. A new method has been developed to identify and classify slamming events from predicted ship motions. Slamming pressure calculations are done using an existing computer program, employing a 2 dimensional non-linear slamming theory (Zhao & Faltinsen 1993).

1.3 Historical review

The calculation of slamming pressure was first studied theoretically by Von Karman in 1929 to estimate the impact load on a seaplane during landing. He idealized the problem and employed linear potential theory, neglecting gravity effects. The added mass and impact load is calculated neglecting the water surface pile up during the slam. In 1932 Wagner derived a more realistic theory, taking the water pile up into account. Wagner's theory is sometimes criticized for a theoretical inconsistency giving infinite velocities at the edge of the wetted area. Wagner's theory is simple, but is still in use today as it gives accurate peak impact pressures for practical use. A detailed description of both Von Karman's and Wagner's theory can be found in textbooks by Bertram (Bertram 2000) and Faltinsen (Faltinsen 1990).

One of the most important contributions to the prediction of slamming occurrence was made by Michel K. Ochi in 1964. In the papers Extreme Behaviour of a Ship in Rough Seas - Slamming and Shipping of Green Water(Ochi 1964a) and Prediction of occurrence and severity of ship slamming at sea (Ochi 1964b) he studied the probability of occurrence and severity of slamming for a 13ft scale model of a Mariner cargo ship. His work was experimental and was performed at the David Taylor Model Basin. In these two papers Ochi derives formula that are still in wide

use today. By assuming that the probability of water entry and the probability of exceeding a threshold value of relative vertical velocity are statistically independent he calculated the probability of slamming as the joint probability of water entry and exceeding a threshold value of relative vertical velocity. The method also assumes that the maxima of the relative vertical velocity follow a Rayleigh distribution. Ochi calculated the probability of slams per cycle of wave encounter as

$$P(slam) = e^{-\left(\frac{\dot{\xi}_{cr}^2}{2\sigma_v^2}+\frac{d^2}{2\sigma_r^2}\right)} \qquad (1.1)$$

where $\dot{\xi}_{cr}$ is the critical or threshold relative vertical velocity, d is the local draft, σ_v^2 is the variance of the relative vertical velocity and σ_r^2 is the variance of the relative vertical displacement.

Ochi also found that a minimum relative vertical velocity must be exceeded in order to classify a water entry as a slam. He found an empirical relationship linking this threshold value to the ship length L.

$$\dot{\xi}_{cr} = 0.093\sqrt{gL} \qquad (1.2)$$

The relative vertical motions can be found for example from linear strip theory. The formulas are still in wide use, and they provide a simple way of predicting slamming occurrence.

In recent years the increasing popularity of fast ferries and high speed craft have seen renewed interest for the slamming problem. Several interesting papers have been published.

Hayman, Haug and Valsgård (1991) investigated the Response of Fast Craft Hull Structures to Slamming Loads by full-scale tests, drop tests and theoretical calculations. They also presented an interesting comparison of their results to the classification rules requirements at the time. Their work was related to semi planing monohulls.

Zhao and Faltinsen presented a 2 dimensional theory for calculating slamming impact pressures in the paper Water entry of two-dimensional bodies (1993). They

developed a non-linear boundary element method for calculating slamming pressure on arbitrary shaped two-dimensional sections. They included a jet flow approximation at the edge of the wetted area during the impact, removing the singularity present in Wagner's theory.

Several researchers have presented papers on hydroelastic effects on slamming in recent years. For flat catamaran wetdecks the structure will deform under the impact load, and this may influence the peak slamming pressure. Kvålsvold and Faltinsen (1994) found that hydroelastic effects reduce the peak impact pressure compared to rigid body theory.

Some investigations have been done into the effects of slamming on composite panels, for example (Parga-Landa et al. 1999).

Rosén and Garme (1999) and Milchert and Stråby (1999) made investigation into slamming of planing and semi-planing monohulls. Both papers present full scale slamming data of the same 11m combat craft. Both papers also perform seakeeping simulations to provide input data for slamming pressure calculations, but different theories are used. Rosén and Garme propose a simplified non-linear seakeeping model for planing craft, while Milchert and Stråby apply linear and non-linear strip theory to semi-planing to predict motions of a semi-planing craft. Fair to good agreement is reported between simulations and full-scale trials.

Varyani, Gatiganti and Gerigk (2000) investigated motions and slamming impact on a catamaran. A 3D pulsating source method was used for motion prediction and a 3-dimensional finite volume computational fluid dynamics method was presented to calculate slamming pressure. Only 2-dimensional results were presented and the 3-dimensional calculations were reported to require extensive computing facilities. The motion prediction was used to find typical relative vertical velocities for use in the slamming computations.

Faltinsen presented an overview to recent advances in slamming computations (2001). The paper acknowledges that slamming is a 3-dimensional problem, but due to the complexity of the problem it is presently preferred to use 2-dimensional calculations. On a typical bow flare section 3-dimensional effects would typically reduce the pressure by 10 – 20% from the values expected from 2-dimensional theory. Hydroelastic effects were reported to be important for sections with small deadrise angles.

Some investigations have been made into slamming problems for sailing yachts, but only for monohulls. Ward (1985) studied the impact-loading problem as a dynamic problem. A simply loaded beam was studied, but with the load travelling at a constant rate along the beam. Brown and Joubert (1990) and later Brown, Joubert and Yan (1996) investigated sailing yacht hulls that had failed due to slamming, and reverse engineered the estimated pressure necessary to cause the damage. Recently Manganelli and Wilson (2001) presented initial results from a research program established to investigate the slamming loads on the "Open 60" class of sailing yachts. The research is based on acquisition of full-scale results from accelerometers during races.

Ship motion predictions are an important part of the prediction of slamming occurrence. Ship motion prediction is a problem that has received a lot of attention from scientists and researchers in the last 50 years. In 1957 Korvin-Kroukovsky and Jacobs (1957) presented a strip theory for predicting heave and pitch motions in head sea, arguably the first numerical motion prediction theory with engineering accuracy. The theory was criticised for some mathematical inconsistency, but has later been recognized as one of the most important contributions to ship motion prediction. Modified strip theories for head sea followed, for example Gerritsma and Beukelman (1967) and Söding (1969). The strip theory that has been most widely acknowledged was proposed by Salvesen, Tuck and Faltinsen (1970), widely known as the STF theory. They extended the strip theory to five degrees of freedom in arbitrary wave headings. Moreover their theory had an improved theoretical foundation. Although the basic principles are the same as in Korvin-Kroukovsky and Jacobs (1957) there are important differences in the calculations of forward speed terms and end terms.

Apart from the different theoretical foundation there are also differences in how the sectional properties are calculated. The simplest method is conformal mapping, where the ship sections is mapped to a circular cylinder using Lewis forms(1929) or multiparameter mappings. The solution for a circle can be found analytically, following the work of Ursell(1949). Panel methods are able to reproduce the sections exactly and are of particular benefit for complex section shapes like bulbous bows, but are more computationally intensive. Several implementations of panel methods can be found, for example the technique known as Frank Close Fit(1967).

Two important limitations of linear strip theory are that it is not suitable for prediction of ship response in severe seastates and for high speed ships. Several non-

linear strip theories have been proposed to adress these issues, for example (Xia, Wang & Jensen 1998).

Zhao and Faltinsen (1991) introduced the high-speed strip theory following initial work by Chapman (1975) and Faltinsen (1983). The theory has later been extended to account for non-linear motions, for example (Wu & Moan 1996). An extension to the high-speed strip theory has also been presented (Hermundstad 1996), taking into account the interaction of the two demi-hulls on a catamaran. A closely related theory that shows promise is the 2D + t theory, reviewed in (Beck & Reed 2001). In the 2D + t theory the calculations are performed in a stationary reference frame. The ship is sent through the reference frame, and hence the cross sections are changing with respect to time.

3D panel methods have a better theoretical foundation than strip theories and its derivatives. Both linear and non-linear 3D panel methods have been presented, for example the SWAN code(Kring, Huang & Sclavounos 1997). 3D panel methods are far more involving to use than strip theory, both in terms of computational power and the input specifications. This factor, together with the fact that they so far have failed to produce significantly better results than strip theories can explain why 3D panel methods are rarely used except in research applications. Most likely this will change in the future as the theories are refined and more powerful computers are available for design work.

1.4 Present work

The problem of predicting slamming occurrence on catamarans has been divided into three steps. In the first step the global rigid body motions are calculated in a simulated irregular sea. In the second step all downwards crossings of the sea surface and the accompanying relative vertical velocity is calculated at positions of interest on the cross structure, using the results from step 1. Finally in the third step the local slamming pressures are calculated using the calculated local relative vertical velocity from step 2 and the local geometry.

1.4.1 Ship motion prediction

There are several ways to predict seakeeping of ships. Experimental methods, typically tests with scale models, can provide accurate data but are time consuming and expensive. Theoretical models or computer predictions are more interesting early in the design phase as it is often a quicker and more cost effective way of getting estimates of seakeeping qualities of a ship. There are different methods available for predicting the motions of ships in waves, but today there are three general methods in use. The simplest method is strip theory. It is essentially a 2-dimensional theory, with some effects of forward speed included. The theory is simple and regarded by some as quite crude, but it has shown to give good estimates of seakeeping for a range of ship types over the years. There are a number of different versions of strip theory, the most commonly used is the strip theory proposed by (Salvesen, Tuck & Faltinsen 1970 hereafter referred to as STF). Most strip theory programs employ linear theory and are known to over predict pitch motion, especially in severe seastates. In linear theory the ship motions are computed in regular waves, most often in the frequency domain. Results can be obtained for irregular seas by linear superposition of the regular wave results. Some strip theory programs have been extended to include non-linear effects such as bow flare and bow emergence. Most non-linear programs are formulated in the time domain, and the results can be simulated directly for irregular seas.

The high-speed strip theory tries to account for part of the steady wave system created by the ship while still keeping the simplicity of strip theory. It is done by using the information calculated at upstream strips as boundary conditions at the next strip. The solution is started at the bow and stepped downstream. The method accounts for upstream flow, but does not include waves propagating in the opposite direction of the ships movement. It is often called $2^1/_2$D theory. The theory is appropriate for slender ships with a Froude number of 0.4 or higher when neglecting the transverse wave system can be justified, and when the waveform parameter $\tau = \omega U/g > ¼$. The latter requirement indicates that there are no waves propagating upstream. The high-speed strip theory has been formulated both as a linear theory and as a non-linear theory. Both strip theory and High-speed strip theory will be explained in more detail in appendix 1.

Three-dimensional methods have the best theoretical foundation for predicting ship motions. At the present stage the methods are not yet mature and suitable for routine calculations. In many cases the advanced 3-dimensional methods have failed to produce better results than the simpler strip theory, and the extra complications are hard to justify.

1.4.1.1 High-speed catamarans

Strip theory, high-speed strip theory and 3-D methods are used for high-speed catamarans. Strip theory should in theory not be well suited to this problem due to the high Froude number, but has been widely used with mixed success. high-speed catamarans are ideally suited for the high-speed strip theory, especially when the interaction between the two hulls is included in the theory. High-speed catamarans sometimes have motion control fins, either active or passive. The effect of motion control devices can be incorporated in seakeeping prediction programs. For this project the software package VERES was kindly made available by Marintek, Norway. The software package includes a linear and non-linear strip theory module, as well as a linear and non-linear high-speed strip theory module. The high-speed module was used for all work involving high-speed power catamarans.

1.4.1.2 Sailing catamarans

A sailing catamaran can be operated in two modes; when the sail generated heeling moment is under a threshold value the boat will sail with both hulls in the water, with a slight heel angle generating a righting moment. When the heeling moment increases above this threshold value the windward hull will lift clear of the water and the righting moment curve will reach its maximum value. Further heeling will only reduce the righting moment. This is not a stable condition, but a well-balanced racing boat with a good crew can sail the boat with a hull flying at a nearly steady heel angle. A simplified approach can be taken when the boat is sailing on one hull. By neglecting unsteady sail-forces and assuming no roll motion the boat can be analysed as a slender monohull. This allows a standard ship motion prediction program to be used. The assumption of no roll motion might seem a gross simplification, but when sailing on one hull the roll motion is largely governed by sail-forces. The hydrodynamic and hydrostatic roll moments are small for the slender hulls, and are easily dominated by the sailforces. The crew controls the sail-force to

keep the boat steady, and roll motion is largely governed by their response time. This is a separate problem, and for now it suffices to assume an ideal crew.

The windward hull will be clear of the water and will only contribute through its mass forces. In a similar fashion a catamaran sailing at a small heel angle with both hulls in the water can be treated as a symmetric catamaran with no heel angle, and analysed as a normal catamaran neglecting the sail forces. The non-linear strip theory version of VERES was used for these simplified methods. To study a more realistic situation where the boat heels moderately without flying the windward hull the boat can no longer be considered symmetric, and the asymmetry will influence the motions. Similar to the coupling between heave and pitch when the hull is asymmetric fore and aft there will be a coupling between heave and roll and heave and pitch when the boat is asymmetric in the longitudinal centre plane.

Unsteady sail-forces are important for high performance sailing catamarans with a high sail area / displacement ratio. Pitch and roll motion will result in a height depending variation of angle of attack and relative wind strength for the sails, especially for tall masts and sail combinations seen on racing catamarans. The variation in inflow over the sails will provide a damping force that has a significant effect on the motions. A linear strip theory program following the theory of STF was written specifically for analysing sailing catamarans, with extensions to account for the effect of heeling and sail-forces. The theory will be presented in full in Chapter 2.

1.4.2 Slamming identification

From the seakeeping prediction the relative vertical displacement and velocity between the wave surface and a point on the hull can be calculated. A slam in a specified location is identified by finding when the point crosses the wave surface from above, with a downwards relative velocity. Traditionally the relative vertical velocity also had to exceed a threshold value (Ochi 1964a; Ochi 1964b) dependent on the ship length. Since this threshold value has been empirically derived for a ship type with very different motion characteristics, hull shape and construction than the catamarans treated here it is doubtful whether it is applicable.

Slamming events can be identified in either a probabilistic manner or a deterministic manner. Ochi (1964a; 1964b) developed simple formulae for calculating the

probability of slamming. A more accurate method is proposed here where slamming events are identified directly in the time domain. The method is especially suitable when the motion prediction is performed in the time domain. Further, the method fully utilises the increased accuracy possible when using non-linear motion prediction while the probabilistic methods are only suitable for linear theories. The procedure is presented in full in chapter 4. As no threshold value is used in identifying slamming events many of the slams found will in fact be very light. The impacts are classified in groups according to the relative vertical velocity, now the impact velocity. This allows the designer to judge the distribution of impact velocities and impact pressures. Knowing the vessel construction details the designer can remove from consideration the lightest impacts that give negligible impact loads.

1.4.3 Slamming pressure calculations

Using the impact velocities found in the slamming identification the slamming pressure can be calculated. In real life each slamming event will be different as the ship hits the wave in a slightly different way each time. The problem is simplified here by calculating the pressure when the hull section is forced through an initially calm water surface with a constant velocity. Forward speed is not included. Calculation of slamming pressure is a problem that is still on the research stage, with a few very different methods under investigation at this time. The methods available for practical use today are 2-dimensional methods, either analytical methods or panel methods. In the present project the computer program SLAM 2D (*SLAM 2D users manual, Marintek*) is used. It is a non-linear 2 dimensional boundary element method. The structure is assumed rigid (no hydroelastic effects) and the creation of air pockets is not included. For conventional ships slamming analysis is normally done on transverse sections, as the transverse curvature is greater than the longitudinal curvature. For catamaran wetdecks and cross-structure the most significant curvature is in the longitudinal direction, and the analysis is done here on longitudinal strips.

More advanced methods for calculating slamming pressure may be feasible in the future. It is widely recognized that 3-dimensional effects, forward speed effects, hydroelastic effects and the effect of air pockets can be important.

CHAPTER 2: SHIP MOTION PREDICTION

2.1 Available methods

As stated in the previous chapter strip theory, high-speed strip theory and 3-dimensional theories can be used for seakeeping prediction. Only strip theory and high-speed strip theory are used in this work. The STF strip theory and the high-speed strip theory are described in full in Appendix 1 for completeness.

2.2 Present development

2.2.1 Asymmetric strip theory

The simplified treatment of a sailing catamaran using normal strip theory is a useful and effective method to investigate slamming and seakeeping of catamarans when flying a hull. However, some catamarans spend a lot of time in a steady heeling but non-flying condition, sailing as an asymmetric multihull. To investigate the seakeeping properties of a heeled catamaran a linear frequency domain strip theory program capable of handling asymmetric multihulls is developed based on the strip theory proposed by Salvesen, Tuck & Faltinsen (1970), as explained in detail in appendix 1. In strip theory the calculation of added mass, damping, stiffness and excitation forces is usually simplified by assuming the ship to be symmetric. For a symmetric ship heave and pitch can be calculated independently from sway, roll and yaw motions. In the general asymmetric case they cannot be considered independent. Limiting the motions of interest to heave, roll and pitch a coupling between heave and roll as well as coupling between roll and pitch must be considered.

Equations of motion

The general equations of motions in heave, roll and pitch can be written as

$$\sum_{k=3}^{5}\left[(M_{jk}+A_{jk})\ddot{\eta}_k+B_{jk}\dot{\eta}_k+C_{jk}\eta_k\right]=F_j e^{i\omega t} \quad ,\mathrm{j}=3\ldots5 \qquad (2.1)$$

where η_3 is heave, η_4 is roll and η_5 is pitch displacement. A right handed coordinate system with the x-axis pointing forward and the z-axis pointing up is used. The origin is located in the still-water-plane.

The only coefficients to be considered in the mass matrix M when Cg is located at (0, ycg, zcg) is

$$M = \begin{bmatrix} - & - & - & - & - & - \\ - & - & - & - & - & - \\ - & - & m & my_{cg} & mz_{cg} & - \\ - & - & my_{cg} & mr_{44} & mr_{45} & - \\ - & - & mz_{cg} & mr_{54} & mr_{55} & - \\ - & - & - & - & - & - \end{bmatrix} \qquad (2.\ 2)$$

and similarily for added mass

$$A = \begin{bmatrix} - & - & - & - & - & - \\ - & - & - & - & - & - \\ - & - & A_{33} & A_{34} & A_{35} & - \\ - & - & A_{43} & A_{44} & A_{45} & - \\ - & - & A_{53} & A_{54} & A_{55} & - \\ - & - & - & - & - & - \end{bmatrix} \qquad (2.\ 3)$$

damping

$$B = \begin{bmatrix} - & - & - & - & - & - \\ - & - & - & - & - & - \\ - & - & B_{33} & B_{34} & B_{35} & - \\ - & - & B_{43} & B_{44} & B_{45} & - \\ - & - & B_{53} & B_{54} & B_{55} & - \\ - & - & - & - & - & - \end{bmatrix} \qquad (2.\ 4)$$

and restoring coefficients

$$C = \begin{bmatrix} - & - & - & - & - & - \\ - & - & - & - & - & - \\ - & - & C_{33} & C_{34} & C_{35} & - \\ - & - & C_{43} & C_{44} & C_{45} & - \\ - & - & C_{53} & C_{54} & C_{55} & - \\ - & - & - & - & - & - \end{bmatrix} \quad (2.5)$$

Calculation of hydrodynamic coefficients

The total added mass, damping and excitation forces can be calculated as

$$A = A^0 + A^F + A^T \quad (2.6)$$

$$B = B^0 + B^F + B^T \quad (2.7)$$

$$F = F^0 + F^F + F^T \quad (2.8)$$

where subscript 0 represents Zero speed coefficients, subscript F represents forward speed corrections and subscript T represents corrections for a transom stern.

The restoring coefficients and zero speed added mass and damping coefficients are obtained by integrating the sectional restoring coefficients along the hull

$$C_{jk} = \int c_{jk} dx \; ; j,k = 3..5 \quad (2.9)$$

where c is sectional restoring coefficient

$$A^0_{jk} = \int a_{jk} dx \; ; j,k = 3..5 \quad (2.10)$$

where a is sectional added mass coefficient

$$B^0_{jk} = \int b_{jk} dx \; ; j,k = 3..5 \quad (2.11)$$

where b is sectional damping coefficient

$$F_j^0 = \rho \int (f_j + h_j) dx \, , j = 3,4 \qquad (2.\ 12)$$

where f is sectional Froude-Krylov force and h is sectional diffraction force

$$F_5 = -\rho \int \left[(f_5 + h_5) + \frac{U}{i\omega} h_3 \right] dx \qquad (2.\ 13)$$

excitation force in pitch is calculated directly including forward speed term

Forward speed terms and transom terms are added to give the total added mass and damping coefficients.

STF gives most forward speed terms and transom terms necessary:

$$A_{33}^F = 0 \qquad B_{33}^F = 0$$

$$A_{35}^F = -\frac{U}{\omega_e{}^2} B_{33}^0 \qquad B_{35}^F = U A_{33}^0$$

$$A_{53}^F = \frac{U}{\omega_e{}^2} B_{33}^0 \qquad B_{53}^F = -U A_{33}^0$$

$$A_{55}^F = \frac{U^2}{\omega_e{}^2} A_{33}^0 \qquad B_{55}^F = \frac{U^2}{\omega_e{}^2} B_{33}^0$$

$$A_{44}^F = 0 \qquad B_{44}^F = 0 \qquad (2.\ 14)$$

and

$$A_{33}^T = -\frac{U}{\omega_e{}^2} b_{33}^A \qquad B_{33}^T = U a_{33}^A$$

$$A_{35}^T = \frac{U}{\omega_e{}^2} x_A b_{33}^A - \frac{U^2}{\omega_e{}^2} a_{33}^A \qquad B_{35}^T = -U x_A a_{33}^A - \frac{U^2}{\omega_e{}^2} b_{33}^A$$

$$A_{53}^T = \frac{U}{\omega_e^{\,2}} x_A b_{33}^A \qquad B_{35}^T = -U x_A a_{33}^A$$

$$A_{55}^T = -\frac{U}{\omega_e^{\,2}} x_A^{\,2} b_{33}^A + \frac{U^2}{\omega_e^{\,2}} x_A a_{33}^A \qquad B_{55}^T = U x_A^{\,2} a_{33}^A + \frac{U^2}{\omega_e^{\,2}} x_A b_{33}^A$$

$$A_{44}^T = -\frac{U}{\omega_e^{\,2}} b_{44}^A \qquad B_{33}^T = U a_{44}^A$$

$$F_3^T = \rho \frac{U}{i\omega} h_3^A$$

$$F_4^T = \rho \frac{U}{i\omega} h_4^A$$

$$F_5^T = -\rho \frac{U}{i\omega} x_A h_3^A \qquad (2.\ 15)$$

The remaining forward speed and transom terms can be calculated from the following relationships given by STF

$$T_{jk} = T_{jk}^0 + \frac{U}{i\omega_e} t_{jk}^A \,, j,k = 1,2,3,4 \qquad (2.\ 16)$$

$$T_{5k} = T_{5k}^0 - \frac{U}{i\omega_e} T_{3k}^0 + \frac{U}{i\omega_e} t_{5k}^A \;\; ; k = 1,2,3,4 \qquad (2.\ 17)$$

$$T_{j5} = T_{j5}^0 + \frac{U}{i\omega_e} T_{j3}^0 + \frac{U}{i\omega_e} t_{j5}^A - \frac{U^2}{\omega_e^{\,2}} t_{j3}^A \;\; ; j = 1,2,3,4 \qquad (2.\ 18)$$

where $T_{jk} = \omega_e^{\,2} A_{jk} - i\omega_e B_{jk}$ and $t_{jk} = \omega_e^{\,2} a_{jk} - i\omega_e a_{jk}$

The remaining forward speed terms are then

$$A_{34}^{F} = 0 \qquad B_{34}^{F} = 0$$

$$A_{43}^{F} = 0 \qquad B_{43}^{F} = 0$$

$$A_{45}^{F} = -\frac{U}{\omega_e^{\,2}} B_{43}^{0} \qquad B_{45}^{F} = UA_{43}^{0}$$

$$A_{54}^{F} = \frac{U}{\omega_e^{\,2}} B_{34}^{0} \qquad B_{54}^{F} = -UA_{34}^{0} \qquad \text{(2. 19)}$$

and the remaining transom terms are

$$A_{34}^{T} = -\frac{U}{\omega_e^{\,2}} b_{34}^{A} \qquad B_{34}^{T} = Ua_{34}^{A}$$

$$A_{43}^{T} = -\frac{U}{\omega_e^{\,2}} b_{43}^{A} \qquad B_{43}^{T} = Ua_{43}^{A}$$

$$A_{45}^{T} = -\frac{U}{\omega_e^{\,2}} b_{45}^{A} - \frac{U^2}{\omega_e^{\,2}} a_{43}^{A} \qquad B_{45}^{T} = Ua_{45}^{A} - \frac{U^2}{\omega_e^{\,2}} b_{43}^{A}$$

$$A_{54}^{T} = -\frac{U}{\omega_e^{\,2}} b_{54}^{A} \qquad B_{54}^{T} = Ua_{54}^{A} \qquad \text{(2. 20)}$$

Calculation of sectional properties

The calculation of sectional properties may be simplified by assuming each hull to be symmetric about its own center-plane. The roll moment about each hull's own axis is also assumed negligible compared to the total roll moment of the ship, an assumption valid when the demihull separation is high compared to the beam of the individual hulls. The sectional properties in heave, roll and pitch can then be

calculated from the sectional properties in heave for each hull. This simplification is valid for small roll angles, consistent with linear theory.

The sectional properties in heave can be easily calculated from the individual sectional properties of each hull in heave. Superscript j denotes sectional property of a single hull.

$c_{33}^j = \rho g bwl^j$ is the sectional restoring coefficient of hull j, where bwl is the waterline beam of the section

a_{33}^j is the sectional added mass in heave of hull j

b_{33}^j is the sectional damping in heave of hull j

f_3^j is the sectional Froude-Krylov force in heave of hull j

h_3^j is the sectional diffraction force in heave of hull j

y^j is the transverse distance from global zero point to local hull centreline

x is the distance from CG in the longitudinal direction

In heave we have

$$a_{33} = \sum_{j=1}^{2} a_{33}^j \qquad b_{33} = \sum_{j=1}^{2} b_{33}^j \qquad c_{33} = \sum_{j=1}^{2} c_{33}^j \tag{2. 21}$$

$$f_3 = \sum_{j=1}^{2} f_3^j * e^{-ik(x\cos\beta - y^j \sin\beta)} \tag{2. 22}$$

$$h_3 = \sum_{j=1}^{2} h_3^j * e^{-ik(x\cos\beta - y^j \sin\beta)} \tag{2. 23}$$

Similarly for pitch,

$$a_{55} = \sum_{j=1}^{2} x^2 a_{33}^j \qquad b_{55} = \sum_{j=1}^{2} x^2 b_{33}^j \qquad c_{55} = \sum_{j=1}^{2} x^2 c_{33}^j \tag{2. 24}$$

$$f_5 = \sum_{j=1}^{2} x f_3^j * e^{-ik(x\cos\beta - y^j \sin\beta)} \tag{2. 25}$$

$$h_5 = \sum_{j=1}^{2} xh_3^j * e^{-ik(x\cos\beta - y^j \sin\beta)} \tag{2. 26}$$

roll,

$$a_{44} = \sum_{j=1}^{2} y^2 a_{33}^j \qquad b_{44} = \sum_{j=1}^{2} y^2 b_{33}^j \qquad c_{44} = \sum_{j=1}^{2} y^2 c_{33}^j \tag{2. 27}$$

$$f_4 = \sum_{j=1}^{2} yf_3^j * e^{-ik(x\cos\beta - y^j \sin\beta)} \tag{2. 28}$$

$$h_4 = \sum_{j=1}^{2} yh_3^j * e^{-ik(x\cos\beta - y^j \sin\beta)} \tag{2. 29}$$

pitch-heave coupling,

$$a_{35} = -\sum_{j=1}^{2} xa_{33}^j \qquad b_{35} = -\sum_{j=1}^{2} xb_{33}^j \qquad c_{35} = -\sum_{j=1}^{2} xc_{33}^j$$

$$a_{53} = a_{35} \qquad b_{53} = b_{35} \qquad c_{53} = c_{35} \tag{2. 30}$$

roll-heave coupling,

$$a_{34} = \sum_{j=1}^{2} ya_{33}^j \qquad b_{34} = \sum_{j=1}^{2} yb_{33}^j \qquad c_{34} = \sum_{j=1}^{2} yc_{33}^j$$

$$a_{43} = a_{34} \qquad b_{43} = b_{34} \qquad c_{43} = c_{34} \tag{2. 31}$$

and roll-pitch coupling,

$$a_{45} = -\sum_{j=1}^{2} yxa_{33}^j \qquad b_{45} = -\sum_{j=1}^{2} yxb_{33}^j \qquad c_{45} = -\sum_{j=1}^{2} yxc_{33}^j$$

$$a_{54} = c_{45} \qquad b_{54} = c_{45} \qquad c_{54} = c_{45} \tag{2. 32}$$

The coupling terms for roll-heave and roll-pitch will all be zero for a symmetric hull, but must be included for an asymmetric hull-shape. An effect of the asymmetric coupling with only academic interest for sailing catamarans is the possibility of roll motion in pure head sea!

Calculation of sectional coefficients in heave

A panel method by Heinrich Söding described in detail in (Bertram 2000) is used for the calculation of 2-dimensional added mass coefficient, damping coefficient, Froude Krylov force and diffraction force in heave.

2.2.2 Modelling of sail-forces

A simple model to investigate the effect of sail forces on the motion may be implemented in the linear frequency domain strip theory. To this end, linearized sail damping coefficients are obtained based on a simple time domain model of the sail forces. The relative wind is composed of the true wind, the boat speed and an unsteady contribution from roll and pitch motion. Contributions from surge and sway are neglected, and the heel angle is assumed small. Summing the velocity components in longitudinal and transverse directions we obtain for a strip located at height z over the waterline

$$V_1(z,t) = V_0 \cos\beta_T + U + U_{pitch}(z) \tag{2. 33}$$

$$V_2(z,t) = V_0 \sin\beta_T + U_{roll}(z) \tag{2. 34}$$

$$U_{roll}(z,t) = \dot{\eta}_4 * z = \omega_e \eta_4^A z e^{i\omega t} \tag{2. 35}$$

$$U_{pitch}(z,t) = \dot{\eta}_5 * z = \omega_e \eta_5^A z e^{i\omega t} \tag{2. 36}$$

The relative wind is now given by

$$V_{rel}(z,t) = \sqrt{V_1^{\,2} + V_2^{\,2}} \tag{2. 37}$$

And

$$\beta_R(z,t) = a\tan\frac{V_2}{V_1} \tag{2. 38}$$

For upwind sailing the unsteady drag force is an order of magnitude smaller than the unsteady lift force, and is neglected. Assuming small variations in the relative wind angle the side force and driving force can be calculated using a constant lift coefficient, supported by wind tunnel data given by (Larsson & Eliasson 2000). Any hysteresis effect from the oscillatory motions is neglected.

$$C_S(z,t) = C_L\cos(\beta_R) \tag{2. 39}$$

$$C_D(z,t) = C_L\sin(\beta_R) \tag{2. 40}$$

The side force and drive force for a strip is now calculated as

$$S(z,t) = \frac{1}{2}\rho_{air}xc(z)C_S V_{rel}^{\,2} \tag{2. 41}$$

$$D(z,t) = \frac{1}{2}\rho_{air}xc(z)C_D V_{rel}^{\,2} \tag{2. 42}$$

where xc is the chord length of a strip and total heel and pitch moment can be calculated as

$$M_{roll}(t) = \int_{z_{\min 1}}^{z_{\max}} S(z) * z * dz \tag{2. 43}$$

$$M_{pitch}(t) = \int_{z_{\min}}^{z_{\max}} D(z) * z * dz \tag{2. 44}$$

with the integration performed over the total height of the sail.

The forces are unfortunately non-linear, and must be linearized in order to be used in a linear frequency domain theory. The damping moments are calculated as

$$B_{roll} = \sqrt{\frac{\int_0^{\frac{2\pi}{\omega}} M_{roll}^2(t)dt}{\int_0^{\frac{2\pi}{\omega}} \sin^2 \omega t dt}} \tag{2. 45}$$

$$B_{pitch} = \sqrt{\frac{\int_0^{\frac{2\pi}{\omega}} M_{pitch}^2(t)dt}{\int_0^{\frac{2\pi}{\omega}} \sin^2 \omega t dt}} \tag{2. 46}$$

The damping coefficients can finally be calculated,

$$B_{sail44} = \left.\frac{B_{roll}}{\hat{\eta}_4}\right|_{\hat{\eta}_5=0} \tag{2. 47}$$

$$B_{sail45} = \left.\frac{B_{roll}}{\hat{\eta}_5}\right|_{\hat{\eta}_4=0} \tag{2. 48}$$

$$B_{sail54} = \left.\frac{B_{pitch}}{\hat{\eta}_4}\right|_{\hat{\eta}_5=0} \tag{2. 49}$$

$$B_{sail55} = \left.\frac{B_{pitch}}{\hat{\eta}_5}\right|_{\hat{\eta}_4=0} \tag{2. 50}$$

The method is quite crude, and ignores effects from flow separation, hysteresis and flexibility of the sail. A more complete implementation would have been possible if the motion prediction program was formulated in the time domain, but within the limitations of linear theory it is believed that the present theory gives some insight into the effect sail-forces have on the motion of a sailing multihull.

2.2.3 Implementation

The strip theory for sailing multihulls was coded in Fortran 90/95 by the author. The program runs efficiently under Windows 2000. Subroutines for the calculation of sectional properties in heave was available as Fortran 77 source code, and could easily be adapted to the program. An efficient input format for hull geometry description and run control parameters makes the program easy to run. Besides being able to write detailed results including intermediate calculations to files the program also writes the RAOs in VERES output format, making it easy to compare results with VERES using the VERES postprocessor.

2.4 Work automation and visualisation

The VERES program is an efficient program, but for the present purposes it was desirable to run the program in batch mode when performing time domain simulations. The standard version of VERES can only run one simulation at a time, and with a typical computational time of 30-60 min per run it can be very time consuming to do multiple runs. A macro was written to facilitate overnight computations of predetermined lists of wave conditions, heading and velocities. Being able to perform 72 simulations easily over the weekend meant that computational time was not an issue when planned for.

A method for making a 3D animation of time domain simulations was developed, to investigate some discrepancies between linear and non-linear time domain results from VERES, but also as a visual check for slamming identification procedures. The method implemented was crude, but effective and produced high quality visualisation.

A small Fortran program was written to translate results from time domain simulations into a script readable by the 3D program Rhino 3D. The fortran program calculated the wave elevation over an area at each time step and fitted a surface to the

points using the wave components from the simulation. The ship hull was predefined and imported in to the 3D scene at each time step. The hull was moved and rotated in 6 degrees of freedom with the rigid body displacements from the time domain results. Finally a snapshot was taken, and the process proceeded to the next time step. The result was a set of numbered still images that could be stitched together to a computer animation with very little effort.

CHAPTER 3: SHIP MOTION PREDICTION RESULTS AND VALIDATION

3.1 High-speed strip theory results

3.1.1 Crowther 318

Crowther design 318 (fig. 3.1) is a 50ft high-performance racing sailing catamaran designed by Crowther Multihulls of Sydney, Australia.

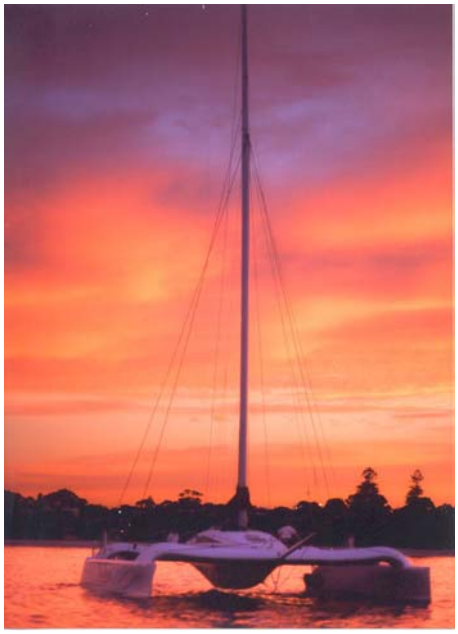

Fig. 3. 1 Crowther Design 318

The main parameters are given in the table below(table 3.1).

Loa	15.2m
Boa	10.8m
Displacement (sailing condition)	3700kg

Table 3.1 Crowther 318 data

Compared to a typical fast ferry catamaran this is a very lightweight catamaran. The hulls are very slender, with an extreme length to beam ratio around 22. The forward sections of the hull have a semi-swath form, a typical feature of many Crowther Multihulls designs. The semi swath hull form reduces the waterline line width in the bow, and produces a very fine entry. It is also believed that this hullform reduces pitching motions. Excessive pitching is a problem for lightweight sailing catamarans and is a limiting factor when sailed hard in rough conditions. Pitching also causes a variation of apparent wind angle and apparent wind speed for the sails, especially evident on high masts.

To investigate the importance of non-linear motions for this catamaran it has been analysed in the hull flying condition, with only the leeward hull in the water. The hulls of Crowther design 318 are canted outward, and the leeward hull is vertical and symmetric when the windward hull lifts out of the water. The boat is treated as a symmetric slender monohull, with no sail-forces.

The RAOs were calculated in heave and pitch from both linear frequency domain high-speed strip theory (VERES linear) and from a 60min simulation in irregular sea with non-linear high-speed strip theory (VERES non-linear). Calculation of RAOs is strictly speaking not valid for a nonlinear system, but for a weakly non-linear system it is considered to be a useful way of comparing and presenting motions characteristics. It must be noted however that the RAOs are only valid for the sea state they were calculated in, as opposed to RAOs for a truly linear system. All calculations were performed for upwind sailing, 10 knots heading 45 degrees into the waves. The non-linear simulation was performed in an irregular sea simulated by a Bretschneider spectrum (Lloyd 1989) with Hs = 1m and Tp = 5s.

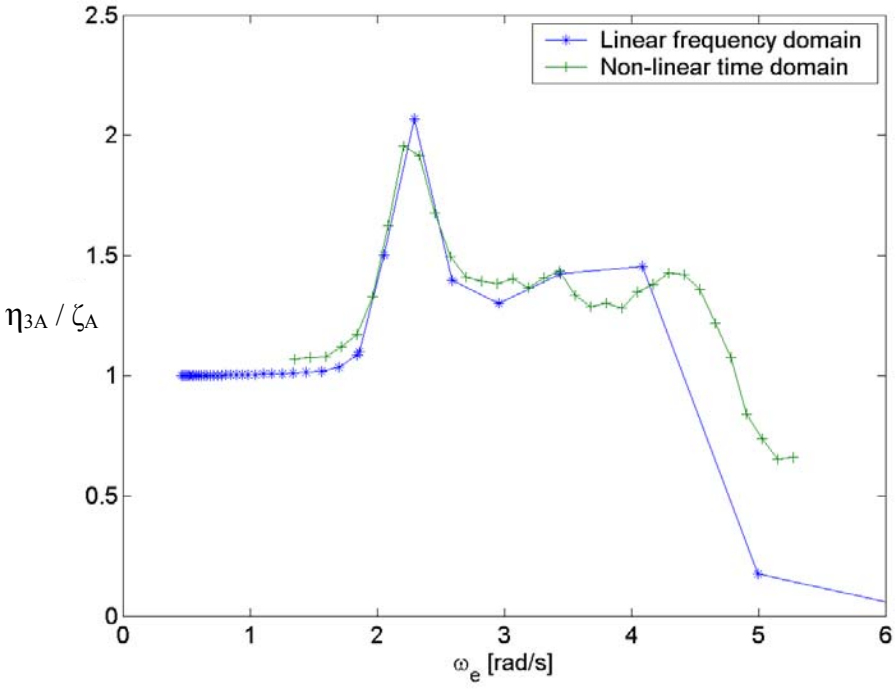

Fig. 3. 2 Calculated Heave RAOs, Crowther 318 orig

The linear theory and the non-linear simulation predict similar results in heave (fig. 3.2). The non-linear simulation results show some irregularities at high frequencies, the reason is unclear.

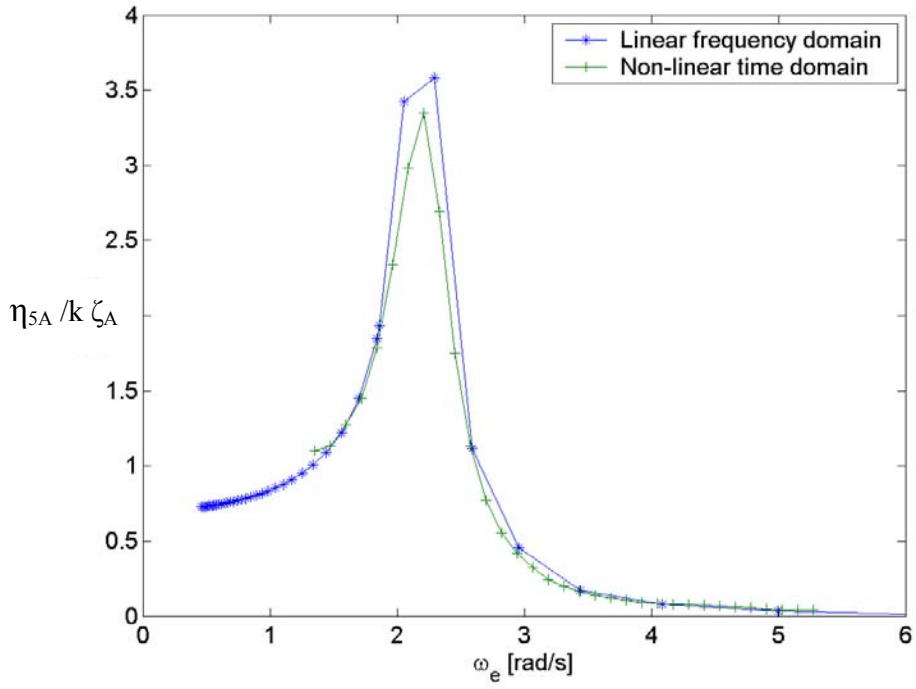

Fig. 3. 3 Calculated Pitch RAOs, Crowther 318 orig

The agreement in pitch (fig. 3.3) is very satisfying. As expected the non-linear theory predicts a smaller peak response than found from linear theory. It is worth noting that the peak response in pitch is large for this hull. This agrees well with practical experience for sailing catamarans, known to pitch excessively at certain encounter frequencies in rough conditions.

In a moderate sea-state, Hs = 1m, non-linear effects as included in the non-linear VERES code are not found to be very important.

3.1.2 Crowther 318 modified

To improve the performance further, especially in waves the Crowther design 318 was subsequently lengthened to 17.1m(56ft). As an interesting exercise the modified hull was analysed, and the RAOs were calculated.

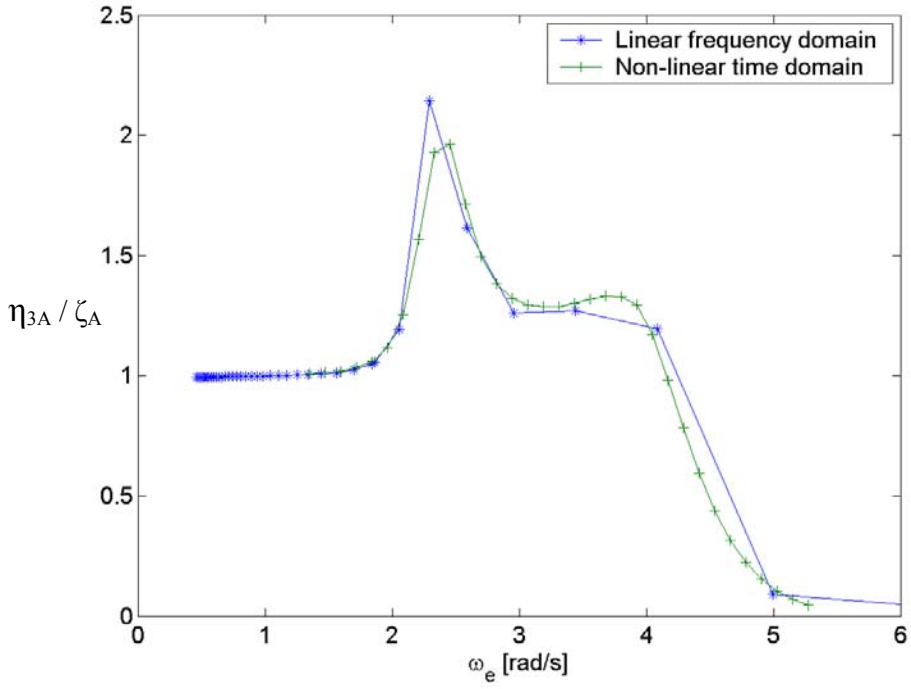

Fig. 3. 4 Calculated Heave RAOs, Crowther 318 mod

The heave RAO (fig. 3.4) is very similar to the original hull-shape (fig. 3.2). The non-linear simulation is very well behaved for this hull.

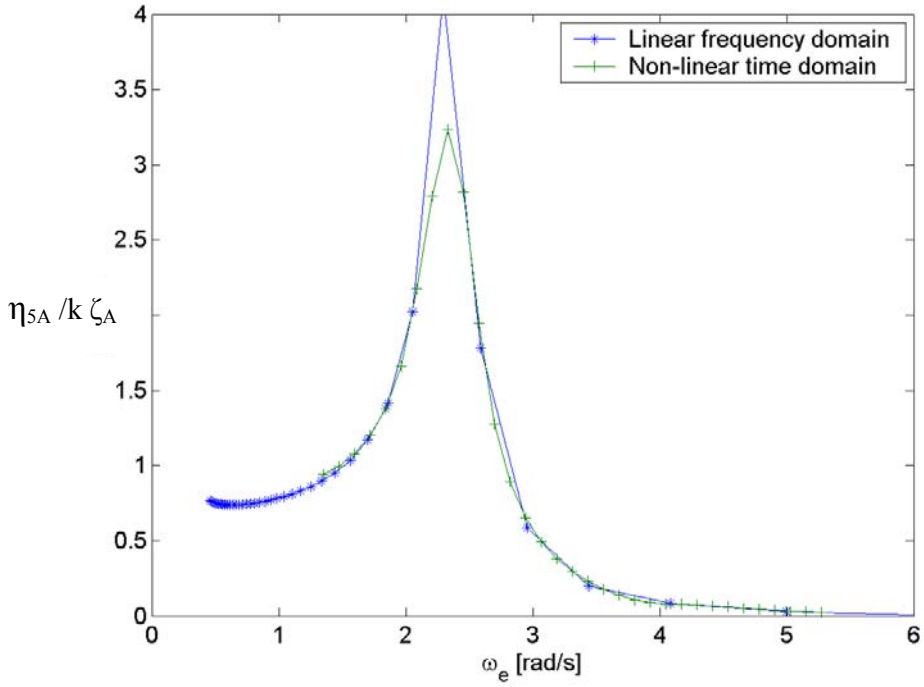

Fig. 3. 5 Calculated Pitch RAOs, Crowther 318 mod

The linear pitch RAO (fig. 3.5) has a larger peak response than found for the original hull, but the non-linear simulation prediction (fig. 3.5) is similar to the original hull (fig. 3.3).

Again, possibly except the peak response in pitch, non-linear effects are not extremely important for this hull in an Hs = 1m seastate. For this boat this can be considered as a moderate sea-state.

3.1.3 Austal Hull 63

Fig. 3. 6 Austal Hull 63

Austal Hull 63 (fig. 3.6) is a high-speed catamaran ferry built by Austal Ships and delivered to Istanbul, Turkey in 1998. The vessels main parameters are given below (table 3.2).

Loa	86.6m
Boa	24.0m
Service Speed	40 knots

Table 3.2 Austal Hull 63 data

This hull has a hull-form often described as semi-swath. The forward part of the hulls have SWATH (Small Waterplane Area Twin Hull) sections with a very narrow waterline which blends in to more conventional U shaped sections in the aft body. The semi-swath hull form is believed to give reduced wave making resistance due to the fine entry and narrow waterline beam in the bow, and give favourable motion characteristics due to a smaller waterplane area in the bow.

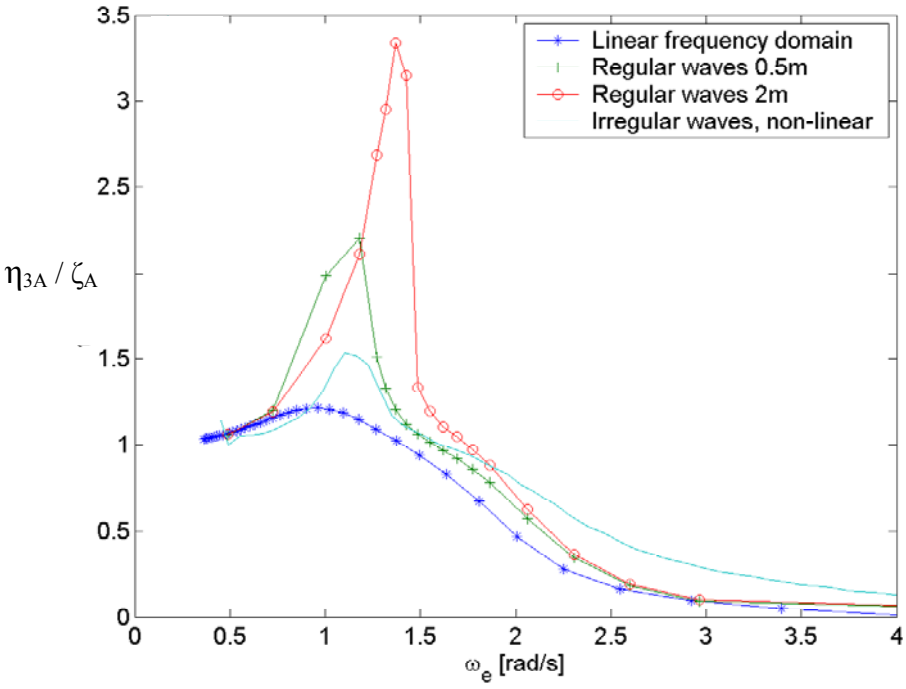

Fig. 3. 7 Calculated Heave RAOs, Austal Hull 63

The RAOs were calculated in heave (fig. 3.7) using the linear frequency domain version of VERES, non-linear simulation in 0.5m regular waves, non-linear simulation in 2m regular waves and a 60min non-linear simulation in a 2m Bretschneider seastate with 9s peak period. All computations were performed at 34.51 knots, with the incoming waves 6 degrees off the bow. The high speed strip theory with hull interaction was used in all computations shown, but a similar trend was found using low-speed strip theory. The differences between the methods are significant, both in the location and value of the peak response. It was expected that the non-linear simulation in 0.5m regular waves would give similar results to linear theory, but there is a large discrepancy except for high frequency waves. One would also expect that the non-dimensional motion amplitude decreases with increasing wave amplitude, which is at least a better studied trend for conventional ships(Xia, Wang & Jensen 1998; O'Dea, Powers & Zselecsky 1992). No physical or computational explanation for the discrepancies has been found.

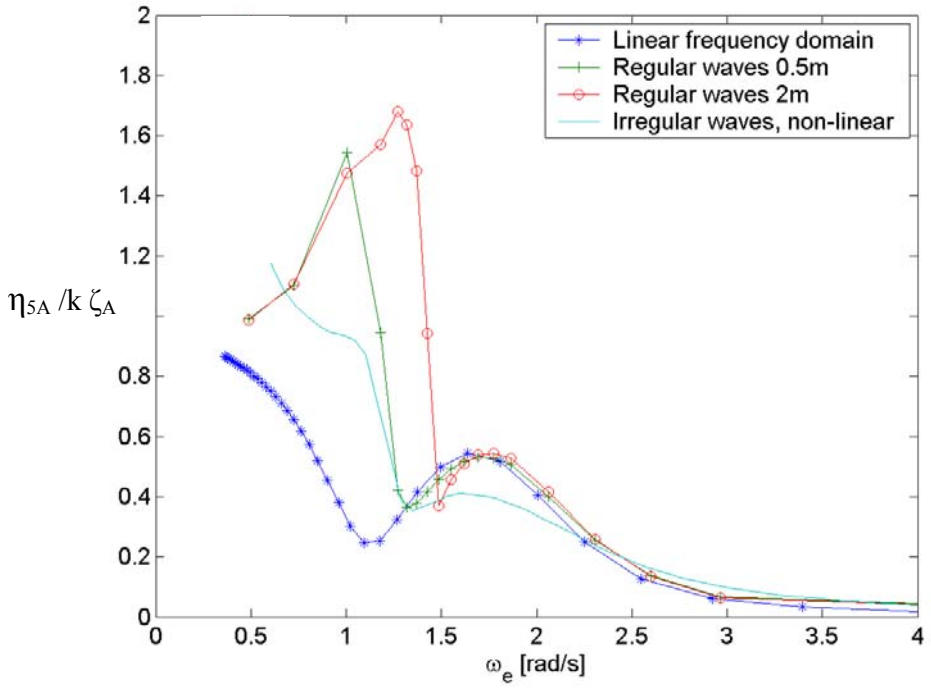

Fig. 3. 8 Calculated Pitch RAOs, Austal Hull 63

A similar trend is seen for the calculated pitch RAOs (fig. 3.8). The pitch RAO is double peaked. All computations except the non-linear simulation in irregular sea give a similar result for the highest frequency peak, but large variations are found in the shape, location and value of the low frequency peak. There are also large variations in the position of the trough between the two peaks, especially the linear frequency domain result has a markedly different location than predicted by non-linear theory. It was expected to see a lower response in pitch for the non-linear codes than found from linear theory, but this did not happen. The importance of the observed differences can be studied further by looking at simulated time series from the different methods. A time series was generated from the linear frequency domain RAOs using the same wave components used in the non-linear time domain simulation. The time domain computation gives both linear and non-linear results. The comparison is done for both heave (fig. 3.9) and pitch (fig. 3.10), and ideally the linear time domain results should match those obtained from linear frequency domain theory. Instead, it seems that the differences between the time domain

implementation and the frequency domain implementation are much larger than acceptable, most likely larger than the non-linearities the method tries to capture. This hull is the only hull-shape that has shown this problem to such a degree, and it is very possible that the time domain VERES software has problems with the semi-swath hull-shape. Unfortunately the program does not show any intermediate results so the exact cause remains unknown. In any case it is unfortunate since this hull is an example of a typical hull that is used in the fast ferry industry. Note: It is now known that this problem was due to errors in the program, and the latest version of VERES gives satisfactory results. Unfortunately this version was only available after the thesis was submitted for examination.

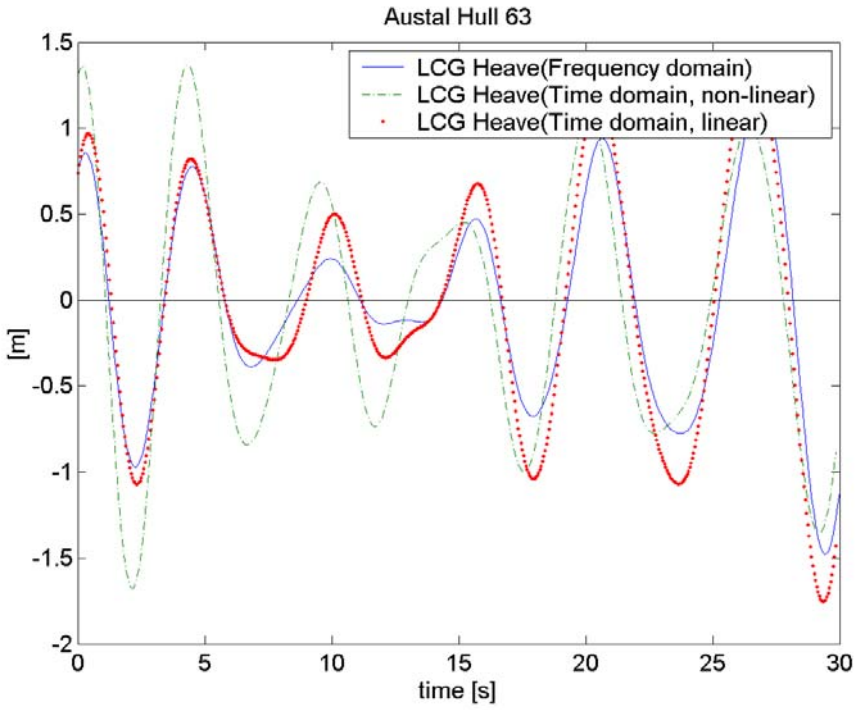

Fig. 3. 9 Heave Time series

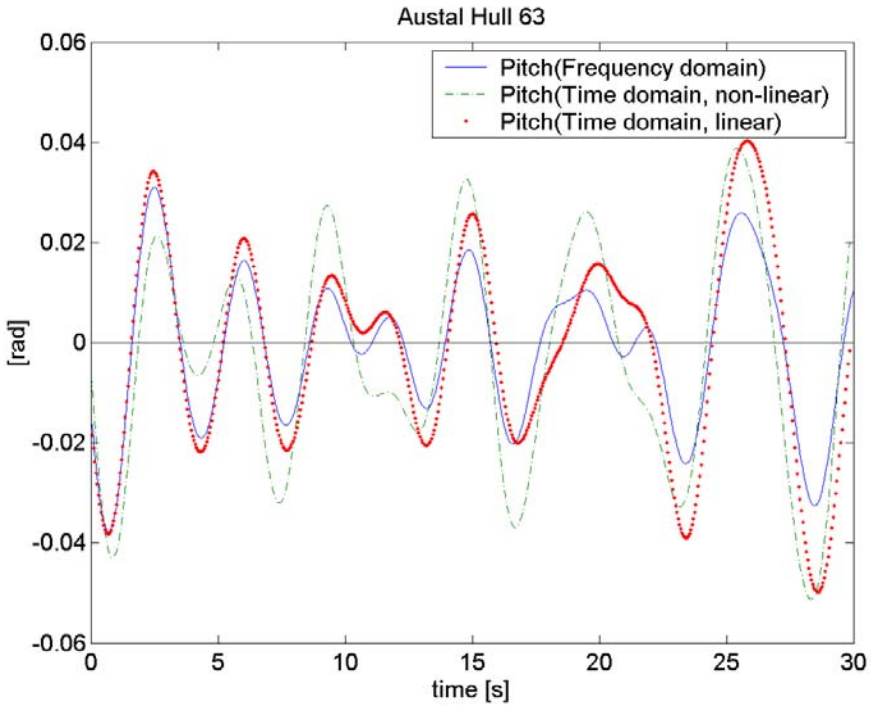

Fig. 3. 10 Pitch Time series

3.2 Seakeeping validation

3.2.1 Educat Full-scale Trials

The Centre for Marine Science and Technology operates an 8m research vessel called 'Educat' which was designed by Hercus Marine Design, Australia and commissioned by the Australian Maritime Engineering CRC. Educat was designed to be a scale model of a typical fast ferry, and has previously been used for global loads measurements, motion measurements and marine education. The vessels main parameters are given below

Loa	8m
Lwl	6.80m
Boa	2.79m
Disp	~2.0t

Table 3.3 Educat data

Fig. 3. 11 Educat

Fig. 3. 12 Educat

Onboard equipment

To measure the motions a TSS motion sensor measuring heave, roll and pitch was fitted. The TSS motion sensor has an internal signal processing system and gives heave, roll and pitch displacements from an array of 3 linear accelerometers and 3 angular rate sensors. The data from the TSS unit was logged digitally to a laptop. Further, two linear accelerometer measuring heave acceleration in each hull and a triaxial accelerometer measuring surge, sway and heave in the bow of the port hull were fitted. The signals from the accelerometers were low-pass filtered at 20Hz to avoid aliasing and sampled at 100 Hz using a 12 bit Data Acquisition Card. The data were logged using a second laptop. Heading, speed and position were determined with a GPS, and logged using the second laptop. A brief technical description of the instrumentation is given in appendix 3.

Wave logging

Four CMST wave recorders(Maggi & Klaka 1999) were used to measure the waves in the trial area. They were suspended from a surface float and

mounted in pairs at 13m and 15m below the surface respectively, in 18m deep water (fig. 3.13). Wave heading was estimated visually.

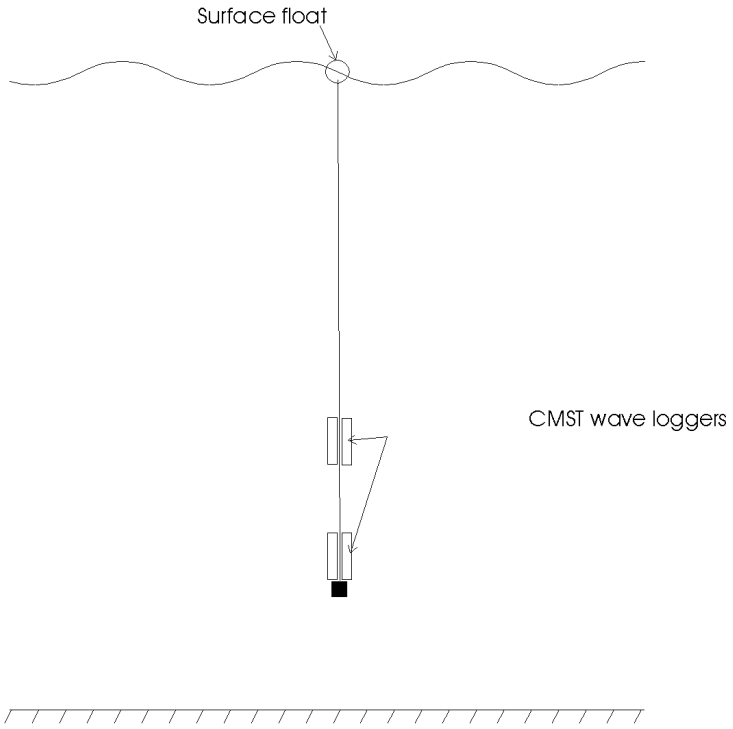

Fig. 3. 13 Wave logger setup

Trial Area

The trials were performed in Cockburn Sound, inside Garden Island, S/SW of Fremantle (fig. 3.14).

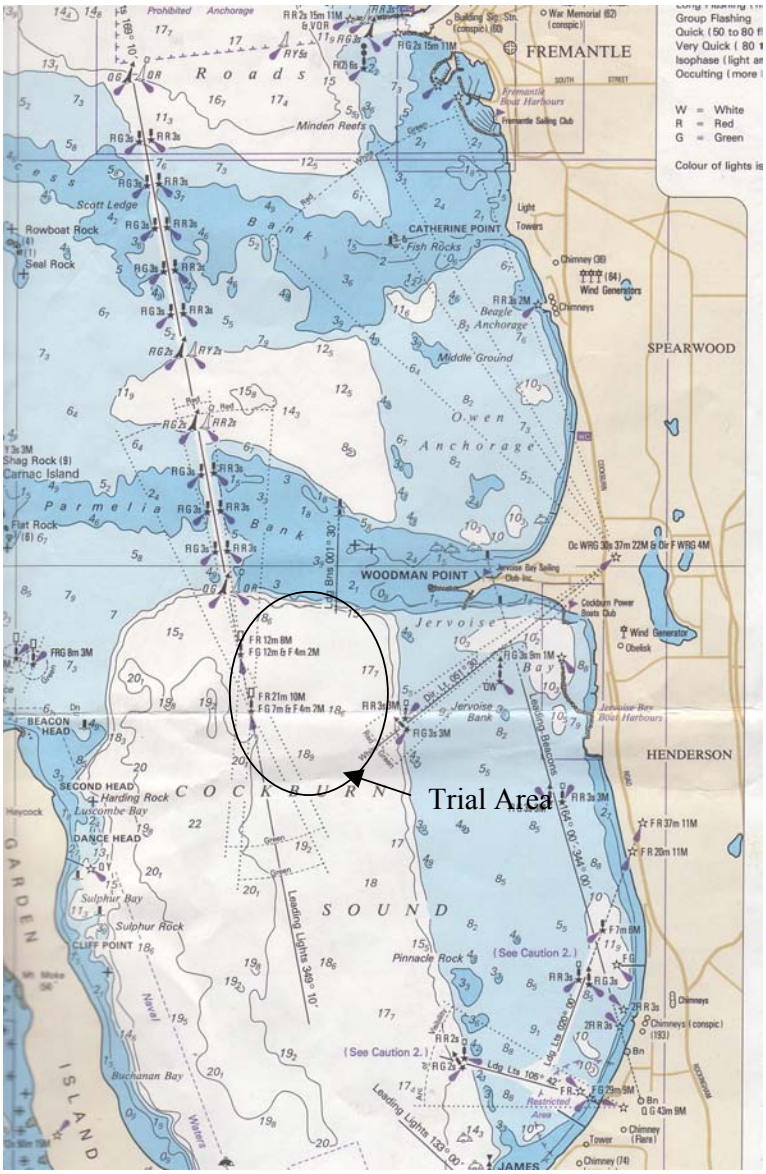

Fig. 3. 14 Trial Area

Weather conditions

The trial was performed in late May 2002. The wind was S/SW at 10-15 knots. The water in Cockburn Sound was chosen, as the water directly out from Fremantle was too rough. The S/SW wind direction was perfect, as it gave a reasonably long fetch of about 4-5 nautical miles. This means that the wind waves had time to build up in front of the trial area, reducing the variation of wave-heights over the trial area. The significant wave height was about 0.5m, with a reasonably unidirectional wave direction. Very little swell comes into

Cockburn Sound, and consequently most of the wave energy was concentrated at high wave frequencies.

Trial procedure

To keep close to the wave buoy a series of 10 min trials were performed. A speed of 10.5 knots was chosen, and all trials were performed in head sea. A total of 4 head sea runs were completed.

Data processing

To obtain a better statistical estimate of the wave and motion spectra the four headsea runs were combined into one 40min run. The motion data from the TSS were high-pass filtered and decimated to 7Hz prior to the calculation of motion power spectra. The spectra were calculated using Welch's averaged, modified periodogram method (Press et al. 1986). 50% overlapped segments were used, with 512 samples in each segment. Each segment was windowed with a 10% cosine taper window.

The wave spectra were calculated with identical parameters, but the calculation procedure involves corrections for sensor height and waterdepth. The calculation procedure is described in (Maggi & Klaka 1999). The stationary wave spectrum (fig. 3.15) was used to calculate the wave spectrum in the moving reference frame, using the boat's speed and course information from the GPS and visual estimates of the wave heading. The non-dimensional heave RAO was calculated by dividing the square root of the heave spectrum with the square root of the wave power spectrum. The non-dimensional pitch RAOs were calculated by dividing the square root of the pitch spectrum with the square root of the wave-slope power spectrum.

$$RAO_n = \sqrt{\frac{S_{\eta_n}}{S_\zeta}} \quad \text{for } n = 1,2,3 \tag{3.1}$$

$$RAO_n = \sqrt{\frac{S_{\eta_n}}{S_\zeta * k^2}} \text{ for } n = 4,5,6 \tag{3.2}$$

Results

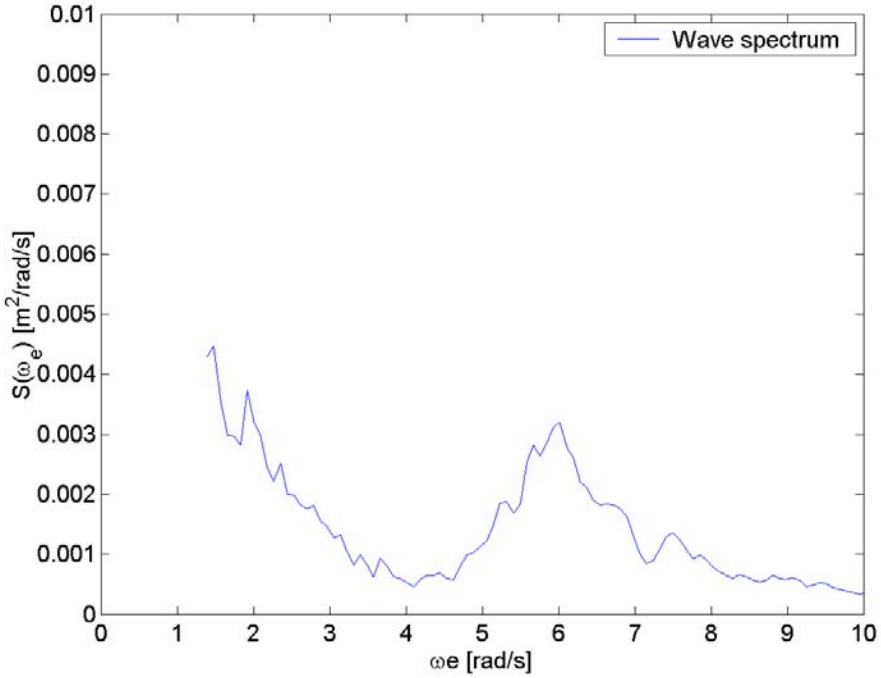

Fig. 3. 15 Wave spectrum

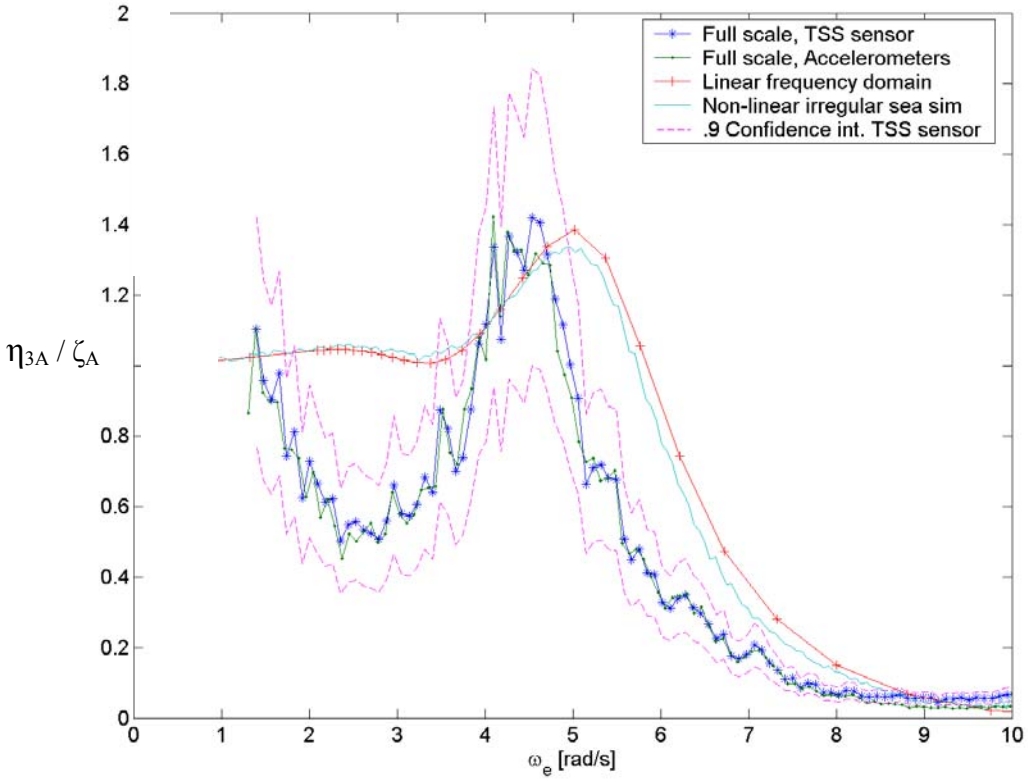

Fig. 3. 16 Educat heave RAOs

The measured heave RAOs (fig. 3.16) obtained by both the TSS and the accelerometers are virtually identical, giving some confidence in the accuracy of the motions measurements. The RAOs are quite jagged, but the trend is very clear. The results at the low frequency end are inaccurate due to insufficient low frequency energy in the wave spectrum and noise amplification in the processing of the wavedata. Some seakeeping experiments have been performed with Educat previously, and the shape of the heave RAO is similar to what has been found previously. Predicted results from linear and non-linear versions of the VERES high-speed strip theory (2½D) have been plotted for comparison. The same procedure was used for calculating RAOs from simulated time series. In order to get the same degree of non-linearity in the full-scale results and the simulations the simulations were run with the same wave spectrum as calculated from the full-scale data. At 10.5 knots Educat runs with a significant trim angle. The mean trim angle was measured by the TSS motion sensor, and all

simulations were performed with this trim angle. At low frequency the full-scale results indicate a dip below unity in the RAOs, this is poorly predicted by both versions of VERES. The location of the peak response is shifted to the right for the predicted RAOs, but the value of the peak response is very well predicted by both codes. The difference between the linear and the non-linear version of VERES in heave is negligible for this sea state.

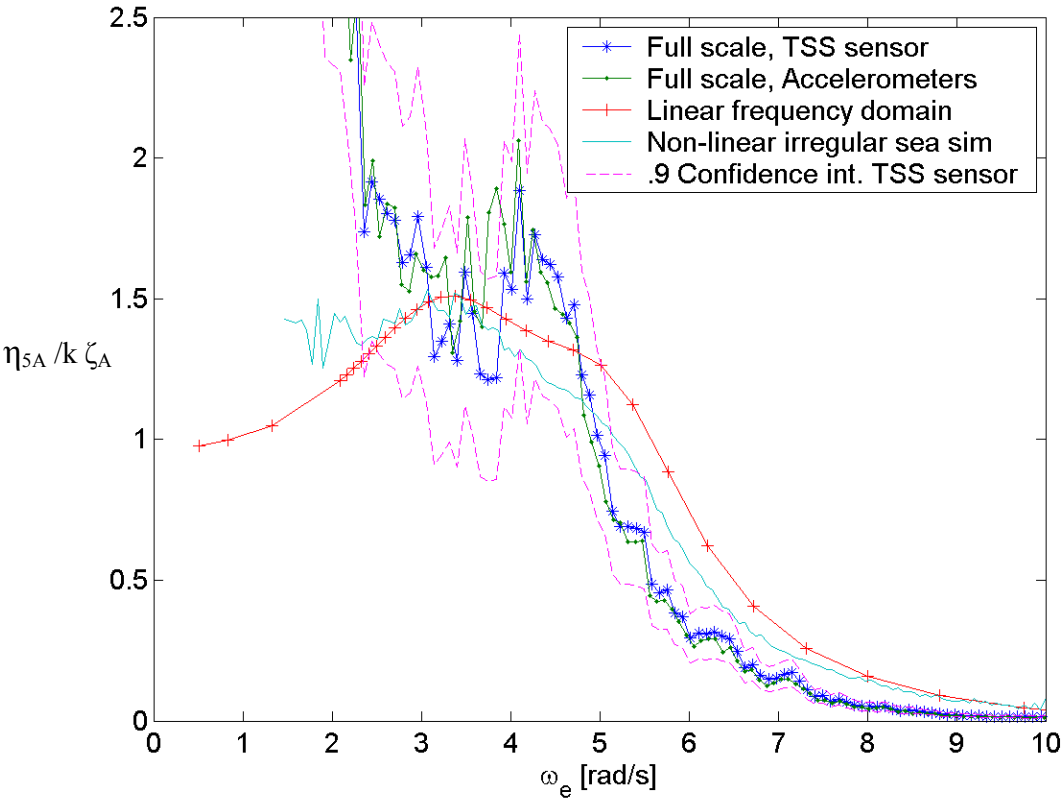

Fig. 3. 17 Educat pitch RAOs

The full scale RAOs in pitch (fig. 3.17) suffers more from insufficient low frequency energy, and blows up quickly at low frequencies. Again it is encouraging to se that the results found from accelerometers match the results found from the TSS sensor. It is difficult to make a good comparison with predicted RAOs as the peaks of the full scale RAOs are not well defined, but it looks like the peaks of the full-scale RAOs are both slightly higher and found at a higher frequency than the peaks of the predicted RAOs. Also, the full scale RAOs drop down much more quickly at high frequency than the predicted

RAOs. The linear and non-linear VERES pitch RAOs are slightly different, the non-linear version fitting the experimental high-frequency trend best.

Conclusions

A full-scale trial has been performed and the motion characteristics of Educat have been estimated. The measured RAOs are believed to be a good estimate of the Vessel's RAOs.

Both the linear and the non-linear version of VERES do a reasonable job of predicting the motions of Educat, but fail to reproduce some of the measured RAOs' features. There is not much difference between the linear and the non-linear theories in the moderate seastates analysed.

3.2.1 Austal Hull 63 full scale – simulation comparison

A large full-scale data set is available from Austal Hull 63. During a delivery voyage from Fremantle to Istanbul the ship was fitted with an extensive instrumentation system. A large amount of recorded data is available, including accelerometer data, measured wave data, strain gauge data and ship speed, course and loading data.

Wave conditions were monitored using a TSK wave meter (*TSK Remote Wave height meter, operating manual*), which measures the relative motion between the ship and wave. The true wave height can be calculated by subtracting the displacement of the sensor. An accelerometer signal is integrated in the TSK wave meter, enabling calculation of the displacement by double integrating the accelerometer signal. Wave heading was estimated visually.

Translatory accelerations at several locations were recorded using accelerometers, and can be double integrated to give ship displacements. Only heave motion is considered important of the translatory motions in this work. Rotational displacements in roll and pitch were recorded directly with angular sensors.

After suitable filtering of the data both wave and motion encounter-spectra can be calculated. Having calculated both wave and motions energy spectra the ship's response amplitude operators (RAOs) can be calculated.

Equipment

The full-scale test procedure and equipment is described in the paper "Global and Slamming Sea Loads Acting on an 86m High Speed Catamaran Ferry" (Steinmann, Fach & Menon 1999). The ship was instrumented with a total of six vertical axis accelerometers and pitch and roll gyros for measuring motions. Two onboard wave meters were used to monitor the sea conditions. Strain gages were fitted at 16 locations around the ship.

Procedure

Test data from 61 30 minutes trials were available. About half the trials were carried out with the vessel's ride control system on, and were therefore not suitable for a comparison. Some trials with a dominating wind sea had very little energy in the low frequency region, making the RAOs useable only for high encounter frequencies. A group of trials with suitable sea conditions and near head sea were selected for comparison.

Calculation of RAOs

For the calculation of RAOs the data were low pass filtered to 4 Hz and decimated. Prior to the calculation of wave spectra the true wave height and the heave displacement had to be calculated. The acceleration signals from LCF and the TSK were double integrated in the frequency domain. Prior to the integration a high pass filtering had to be performed, to avoid a blow up of the low frequency content during the integration. Different cut off frequencies were evaluated both by looking at the full-scale data, and using simulated data. A cut-off frequency of 0.1 Hz was found to be suitable. The Discrete Fourier transform of the signal was calculated using a Fast Fourier Method. The double integration was performed by dividing the Fourier transforms of each frequency by the

frequency (in radians per second) squared. The signal was finally transferred to the time domain again with an inverse Fourier transform. The displacement is also calculated internally in the TSK wave meter, as a running time domain double integration. The two methods gave a similar answer, but the TSK internal calculations had slightly more low frequency noise. The frequency domain double integration used has been tested against time domain integration using simulated data, and found to give very accurate results. No data about how the double integration was performed in the TSK are available, and it was decided to use the frequency domain method. The true wave height was calculated by subtracting the displacement of the sensor (double integrated acceleration signal from the TSK accelerometer) from the TSK relative wave height.

The Power Spectral Densities (PSD) were calculated using Welch's averaged modified periodogram method (Press et al. 1986) of spectral estimation. Each trial was broken down into 50% overlapped sections, each with 512 data points. Each section was linearly detrended and windowed with a 512 point Hanning window.

Simulations

Simulations were run with the computer program VERES, a 2 ½ D linear and non-linear high-speed strip theory program. The simulations were run with the calculated full-scale wave spectrum. The sea-keeping program simulates an irregular seaway using a user-defined spectrum, with random phase angles. From the full scale trials the angle of the encountered waves and swell estimated visually were available, recorded in the logbook. The simulations were only performed in long crested seas, and a mean heading was used. The effect of foils is included in the program, and the forward T-foils were modelled. The performance of the motion control system is difficult to reproduce exactly, so only full-scale runs where active foils were not used were chosen for comparison. The effects of the interceptors (motion control devices with similar effect as a trim tab) is not incorporated in the program, but they are believed to have a negligible effect on the motions in passive state. A 60 minute simulation time was chosen for the comparison. The calculation of RAOs from the simulation was done in a similar manner as the full-scale calculations.

Simulations were also done in regular wave heights of 0.5m and 2.0m. A linear frequency domain version of VERES was also used for comparison.

Errors

As is often the case with full-scale seakeeping trials there is a certain level of uncertainty in the wave measurements. The accuracy of the TSK wave sensor is not absolute, and a small error in the relative velocity measurement can be expected. The relative velocity is integrated to give the displacement. This integration requires a high pass filtering to avoid blow up of the low frequency content. This will introduce a small error, mostly in the low frequency region. The TSK does not measure wave direction, this was done visually during the trials. Similarly the double integration of the acceleration to displacement introduces a low frequency error, and the accelerometer itself can be expected to give a slight error. The accelerometer at the TSK is gyro mounted, and should be free of influence from pitch and roll. These errors all sum up to around 10% of the measured wave height according to (*TSK Remote Wave height meter, operating manual*).

The measurement of motions has error sources as well. The acceleration data is contaminated by mechanical vibration, mostly at high frequencies. The sources of mechanical vibrations can be the engine, auxiliary equipment and cavitation on foils. Usually mechanical vibrations have both a much higher frequency than the rigid body motions and a significantly lower energy, enabling the noise to be filtered out. The double integration of the acceleration signal to obtain displacement introduces an error in the low frequency region as discussed for wave measurement. A cut-off frequency of 0.1 Hz = .628 rad/s was found necessary to get a good result from the integration, leaving spectra and RAO values below 0.1 Hz useless. Above this frequency the double integration routine has been tested and found accurate.

Rotational motions were measured using gyros, and no integration had to be performed. A value for the typical error of the angle sensors has not been found.

The error in the calculation of wave and motions spectra is dependent of the length of the trial. It is especially the accuracy in the low frequency region that

suffers. As discussed above results below 0.1Hz are useless because of filtering in any case. (Lloyd 1989) states that a full-scale trial should cover at least 100 mean periods Tmean. A 30 min trial corresponds to 180 0.1Hz waves, and satisfies the minimum requirement.

The simulations are run with long crested seas, but as long as roll is not considered to be very important it is believed that this can be justified. The effect of short crested seas on the encountered wave frequencies is automatically included as the spectrum from the full-scale trial is used. The draft and trim of the ship during the trials were calculated from departure and arrival conditions. The effect of speed on trim is not known however, but the simulations were run with different trim angles and the effect on seakeeping was found negligible.

Results and discussion

Heave RAOs

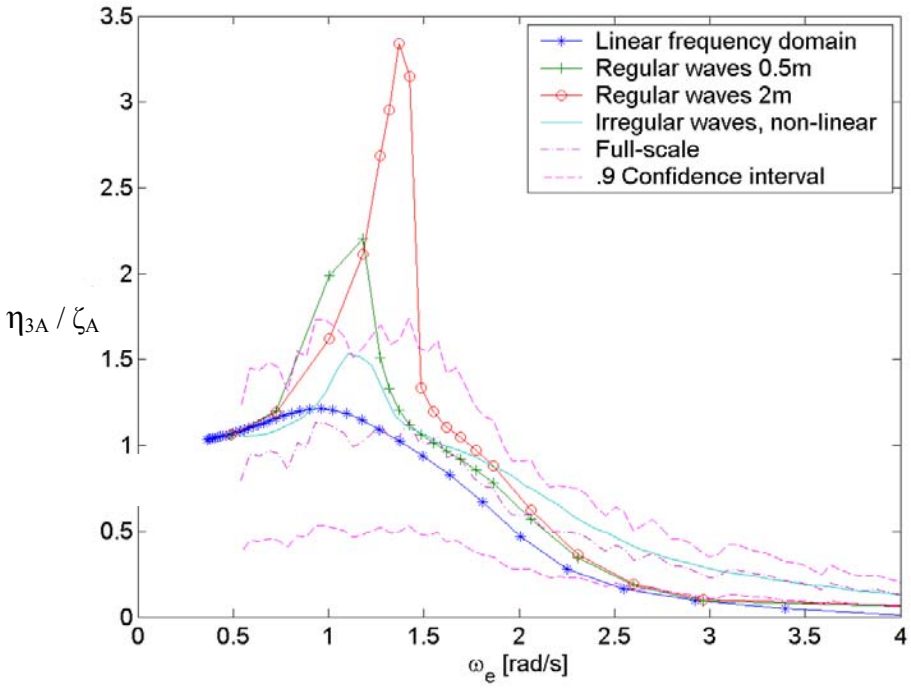

Fig. 3. 18 Full-scale heave RAOs, Austal Hull 63

The full scale RAO in heave (fig. 3.18) is quite jagged, and does not quite converge to 1 at low frequency. It also seems there might be some noise in the high frequency region as the RAO doesn't drop as quickly as expected. As found in section 3.1.3 the time domain versions of VERES are not well behaved for this ship. The linear frequency domain version of the high-speed strip theory does however predict the heave RAO reasonably well. At encounter frequencies below ~1.3 rad/s the linear theory over-predicts the motions slightly compared to the full-scale results, and at encounter frequencies above ~1.3 rad/s the linear theory is predicting lower response than seen in full-scale. Considering the error sources in the full-scale trials as discussed above and the limitations of linear theory the comparison is good.

Pitch RAOs

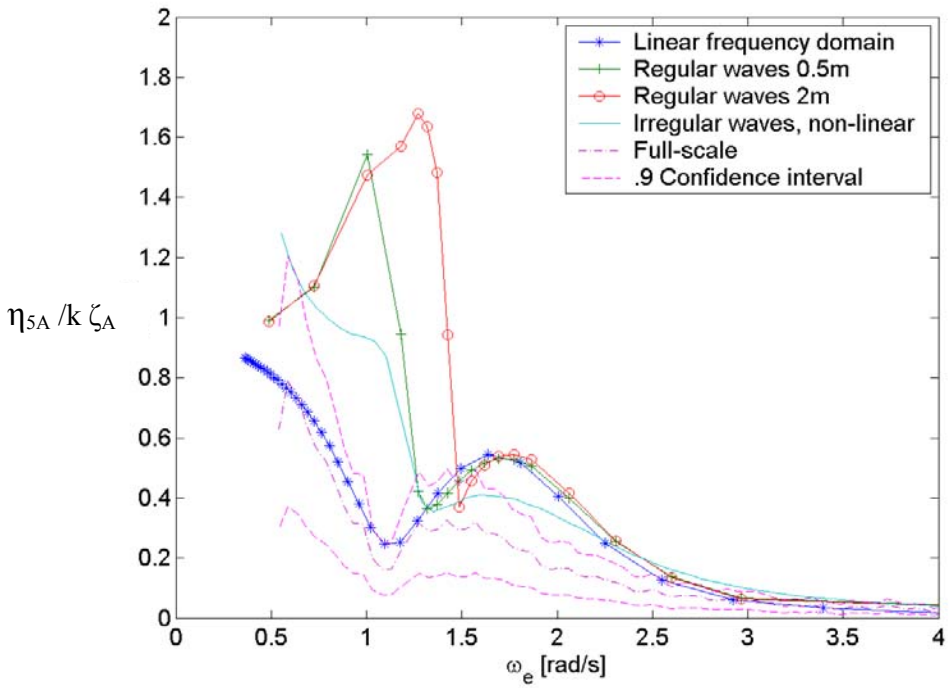

Fig. 3. 19 Full-scale pitch RAOs, Austal Hull 63

The full-scale RAO for pitch (fig. 3.19) is believable, and is well behaved except a blow up at low frequency due to the high-pass filtering of the wave data.

Again the linear high-speed theory gives a closer fit than the non-linear method. The pitch RAO is double peaked with a dip in the non-dimensional motion amplitude around 1.1 rad/s. The linear high-speed theory predicts the lower frequency peak and the dip well, but over-predicts the higher frequency peak. At least for conventional ships linear theory is generally considered to over-predict pitch motions so this result is not unexpected. The non-linear irregular wave simulation predicts the second peak better than linear theory, but generally the linear method has the best fit.

Conclusions

As discussed earlier in this chapter the non-linear version of VERES does not give a good seakeeping prediction for this hull, but the linear theory gives a good prediction.

3.2.2 Marin model test

Background

In the paper "Hydrodynamic Development for a Frigate for the 21 Century" (Kapsenberg & Brouwer 1998) a parametric investigation of the effect of different hull form parameters on seakeeping performance was carried out. It was discovered that linear strip theory did not predict the seakeeping characteristics accurately for all hulls considered, especially a hull the author labelled COFEA. The COFEA hull is characterized by an extreme aft location of LCF, which leads to a very narrow waterline in the forward half of the hull. This is in fact quite similar to many catamaran semi-swath hull forms. Catamarans hulls are usually a bit narrower than the COFEA hull form, and lacks the added waterline beam in the stern that the COFEA hull has.

The problem of strip theory for this hull form, and the similarity to the hull form of Austal Hull 63 made it interesting to see how the VERES strip theory package

compared with the published simulated and experimental results from Marin (Kapsenberg & Brouwer 1998).

Input data

The body plan (fig. 3.20) together with main dimensions (table 3.4) of the COFEA hull form was published in the paper, as well as the experimental results. A problem with the published body plan was the small scale, so some inaccuracies can be expected in the digitising process. An evidence of this was that some longitudinal smoothing was required to produce a smooth hull from the digitised lines. Main dimensions for the digitised hull are listed together with published figures below

	Published COFEA	**Digitised COFEA**
L_{PP}[m]	120	120
B_{WL}[m]	20	20
T[m]	4.6	4.6
Δ[ton]	4242	4229
C_P[-]	0.633	0.592
C_M[-]	0.925	0.948
LCB[m]	-0.336	2.107
LCF[m]	-16.452	-13.458

Table 3.4 COFEA data

As can be seen from the table the displacements are quite similar, while there are quite large differences in LCB, LCF and CP. The difference in LCB and LCF can be due to different longitudinal datum, difference in calculations or errors in the digitised hull. The difference in C_P can be due to calculation differences, or errors in the digitised hull. LPP/2 is used as longitudinal datum for both hulls, and should be the same. The published COFEA data are probably calculated accurately using the whole hull, while the data calculated for the digitised hull are calculated using only the published cross sections(accurate bow and stern description was impossible). Since the agreement with the displacement is so good, it is reasonable to believe that the digitised hull (fig.

3.21) is a good approximation to the COFEA hull used in the paper(Kapsenberg & Brouwer 1998).

A further unknown quantity is the pitch radius of gyration, which was not published. It has been assumed to be 0.25*LPP, an engineering approximation.

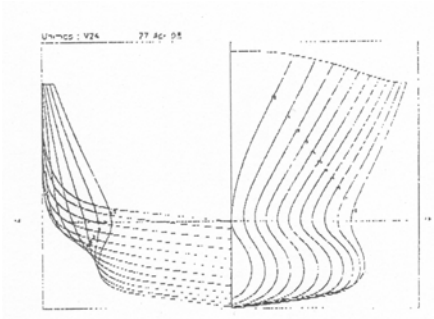

Fig. 3. 20 Published COFEA body plan

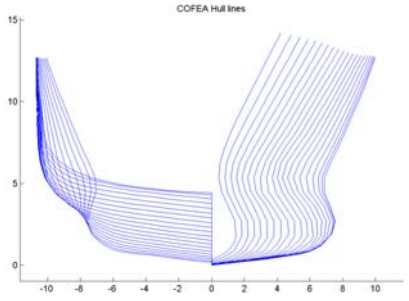

Fig. 3. 21 Digitised COFEA body plan

Simulations

The VERES sea-keeping package has 4 analysis options: Linear 2D strip theory, non-linear 2D strip theory, linear $2^1/_2$D strip theory and non-linear $2^1/_2$D strip theory.

The digitised COFEA hull was run in head sea in regular waves at 15 knots and 25 knots, with 9 wave periods. The analysis was done using all 4 VERES' analysis options. For the linear cases the response amplitude operators are calculated directly, while for the non-linear cases the calculations are performed in the time domain. Wave amplitude is 1m, as used in the Marin experiment.

Results

15 knots

As can bee seen from the heave plot (fig. 3.22) there are quite substantial differences between the Marin experiments and the simulations. The three linear cases are clearly the worst, and all drastically over predict the heave motions around the peak frequency. The two non-linear cases are slightly better, but surprisingly the $2^1/_2$D code is giving the better result. At 15 knots the Froude number of the full-scale ship is about 0.225, and one would expect the 2D strip theory to give better results than $2^1/_2$D. This ship does however have a very

special hull-form (fig. 3.24) that may not be well suited for the 2D problem, but it can also be a coincidence that the 2½D theory works better for this hull at this low speed. In any case there is still a large difference between the best simulated result and the experiments.

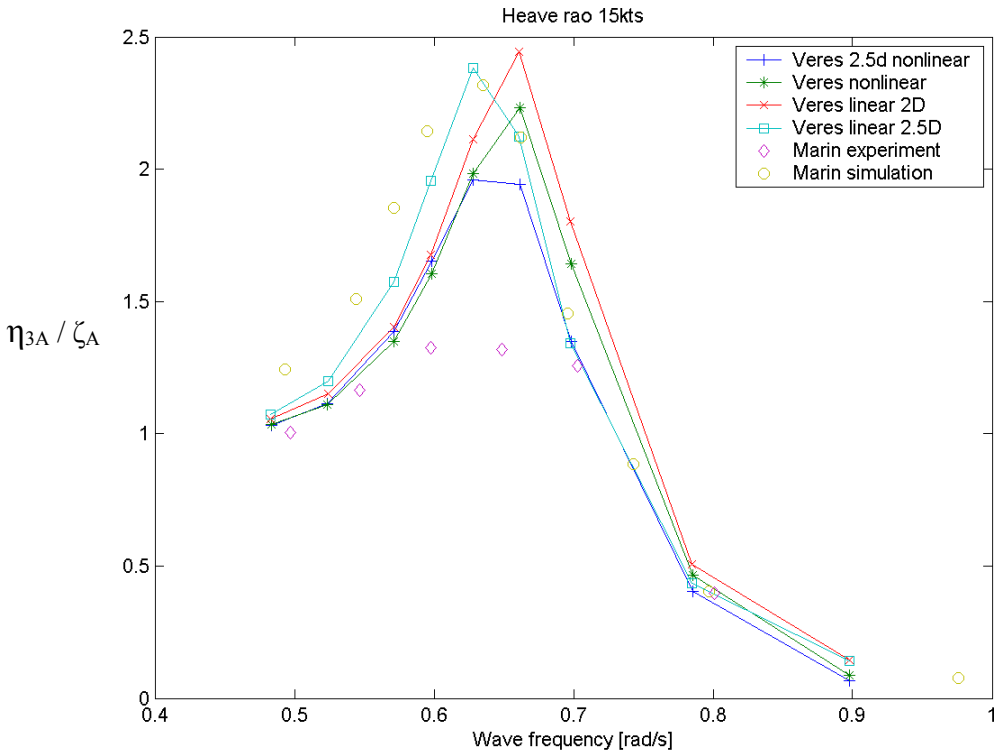

Fig. 3. 22 Cofea heave RAOs

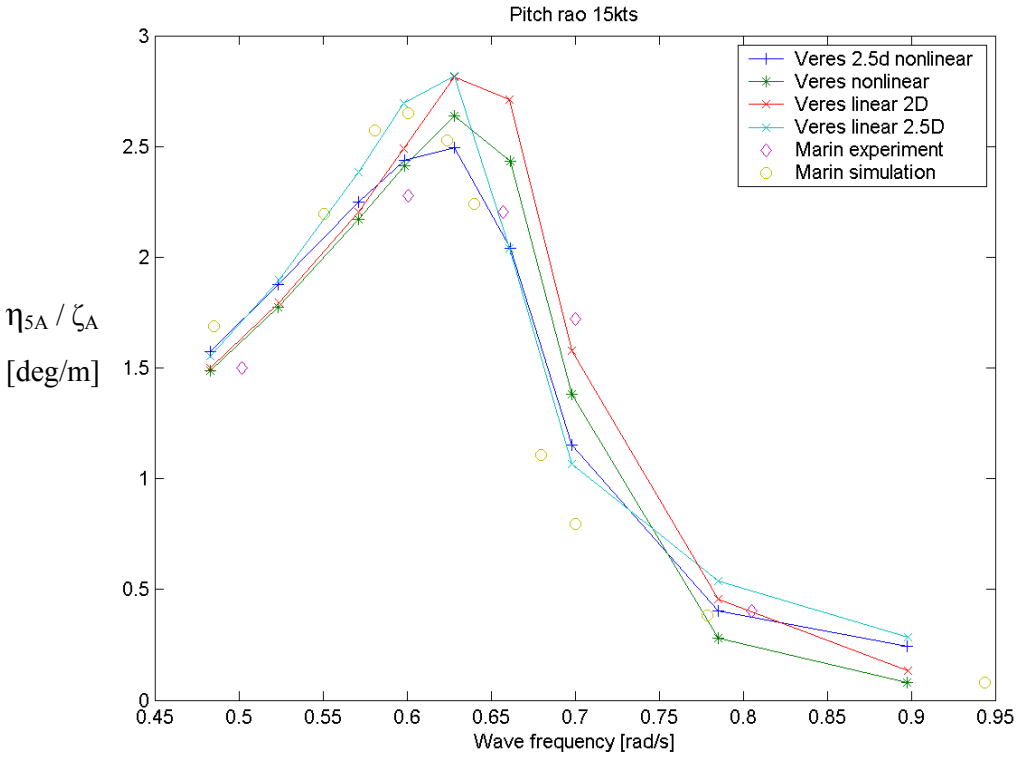

Fig. 3. 23 Cofea pitch RAOs

Looking at pitch (fig. 3.23), the differences are smaller, but the trend is still that the non-linear simulations compare better against the experiments than the linear. At least for the peak frequency it can also be seen that the $2^1/_2$D theory gives better results than the 2D results. However the peak of the $2^1/_2$D RAO seems to drop down a lot quicker than both the 2D theory and the experiments.

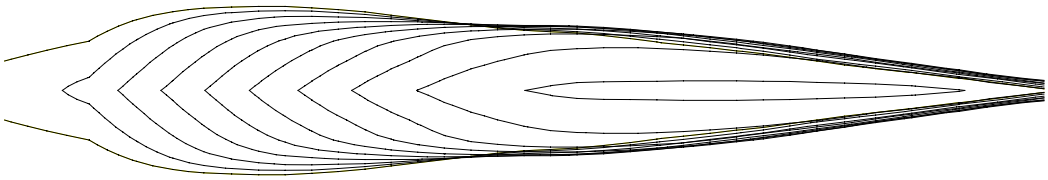

Fig. 3. 24 Cofea Waterlines

25 knots

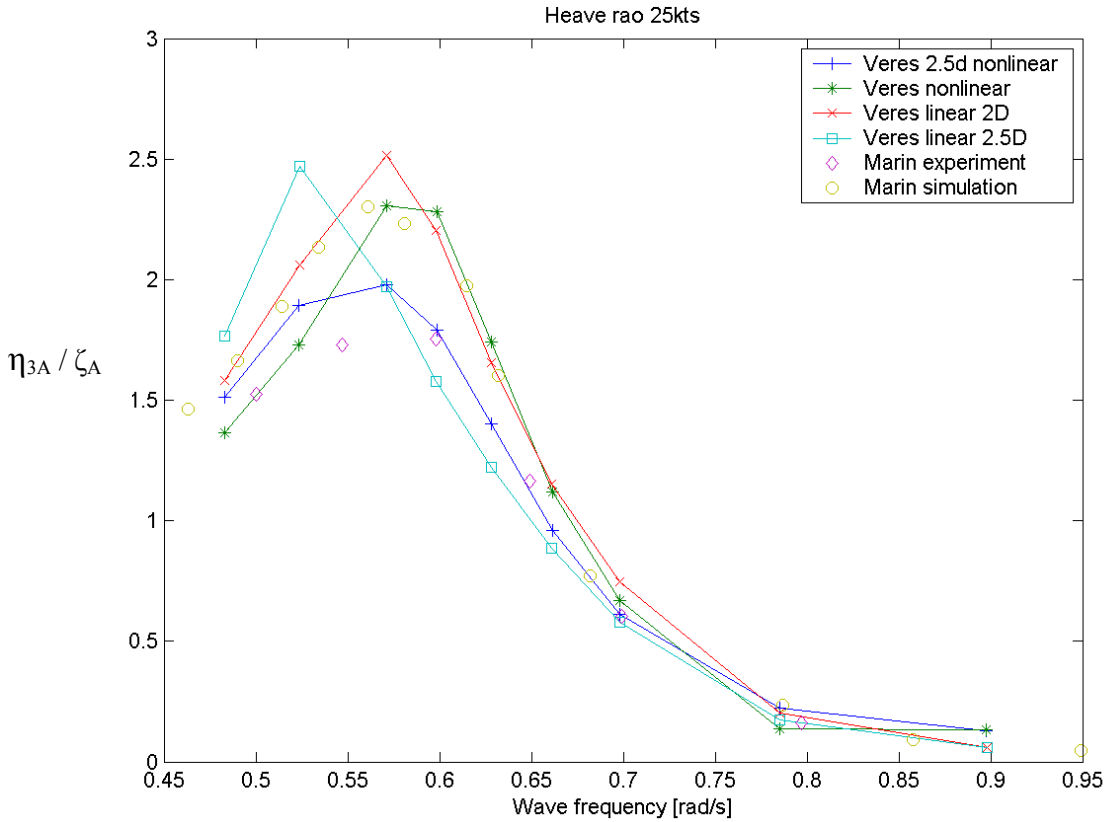

Fig. 3. 25 Cofea heave RAOs

In heave at 25 knots (fig. 3.25) there is a constant over prediction of the response by the linear theories. The linear $2^1/_2$D theory is a little inconsistent with the others and is partly over predicting, partly under predicting the response. It cannot be said that the linear $2^1/_2$D theory is any better than the linear 2D theories, as one would expect. The non-linear $2^1/_2$D theory gives the closest match, and except for a slightly over predicted peak value gives a good agreement with the experiment.

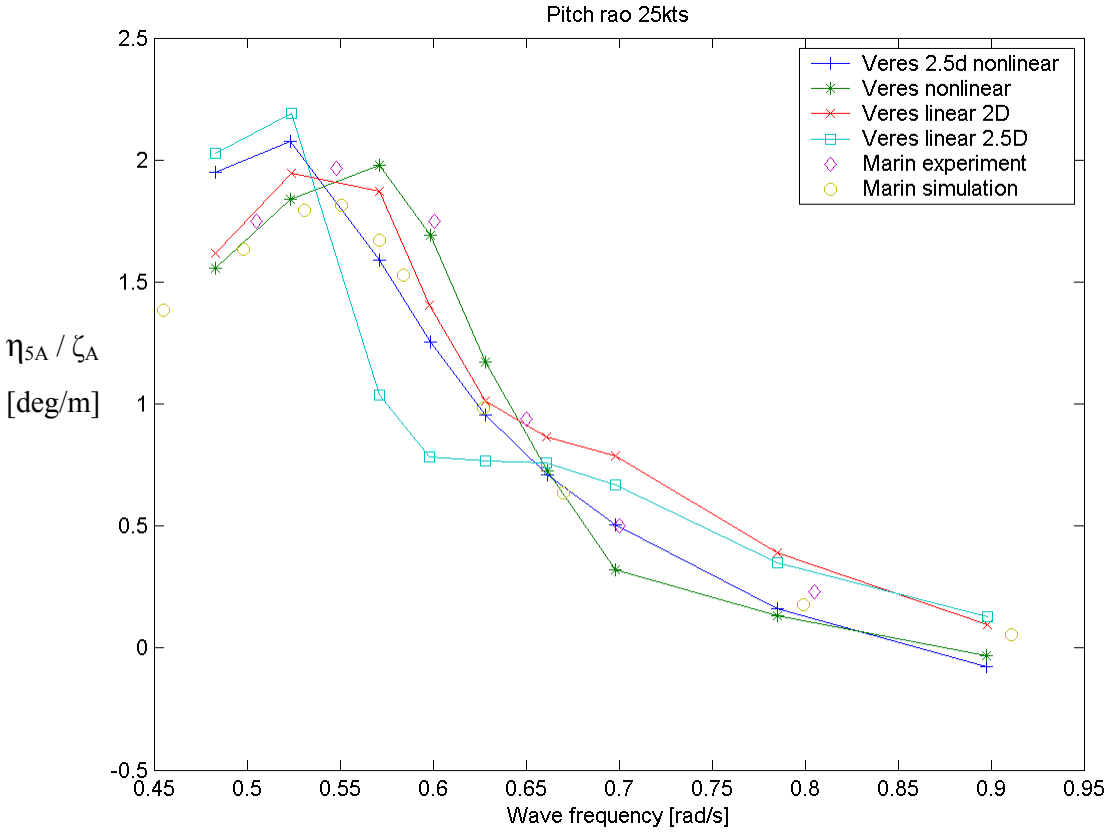

Fig. 3. 26 Cofea pitch RAOs

Again looking at pitch response (fig. 3.26), the results for pitch motion at 25 knots are interesting. Most theories here show a mixed behaviour with partly over- and partly under prediction compared to the experiments. Surprisingly the 2D linear theory gives excellent agreement with the experiments, while the $2^1/_2$D non-linear theory shows a marked shift in the peak frequency. No reason has been found for this. At 25 knots the Froude number of the full-scale ship is about 0.375, which ideally should make the $2^1/_2$D theory more suitable for the computation than the 2D theory.

Conclusion

A comparison of different codes for predicting seakeeping characteristics has been done. Unfortunately the input data for the comparison is not consistent, and is a source of uncertainty. However with the variation of the results it was not possible to detect any trends that might originate from errors in the digitised

hull lines, and it is believed that the hull lines used are accurate enough for the comparison.

Generally the results are as expected in the sense that the nonlinear theories seem to predict the response values better than the linear theories. It is interesting to see that the $2^1/_2$D theory is more effective than the 2D theory even at a fairly low speed for this particular hull. Except for the pitch response at 25 knots it can be said that the $2^1/_2$D theory gives reasonably good agreement with the experiments, and performs better than any of the other codes. Looking at the overall picture of prediction of slamming occurrences, it is worth noticing that the most interesting motion is relative vertical motion. Relative vertical motion in the bow is influenced by heave, pitch and the phase relationship between heave and pitch. Errors in pitch can have a large influence on the relative vertical motions in the bow. The phase relationship also has a strong influence, but unfortunately no information about this was published in the paper.

3.3 Sailing multihull strip theory results

3.3.1 Crowther Design 318

The results obtained from the new strip theory for sailing multihulls have been compared to the results from the linear version of VERES. The RAOs have been calculated at 0 degrees heel angle(sailing as a symmetric catamaran), at 5 degrees heel angle(sailing on one hull) for both VERES and the new strip theory, and sailing on two hulls with 2 degrees heel angle with the new theory. VERES cannot analyse a heeled catamaran because of the asymmetry. Sailing upwind with zero heel angle is not a realistic condition, as the hull will always heel over to generate the necessary righting moment. The speed when sailing at one hull only will also be higher due to reduced resistance, but for the comparison the speed has been kept constant. Ideally the two theories should give identical results at 0 degrees and at 5 degrees when sailforces are not included. Both results from the linear 2D version of VERES and the linear 2½D(high-speed) version of VERES have been presented for comparison.

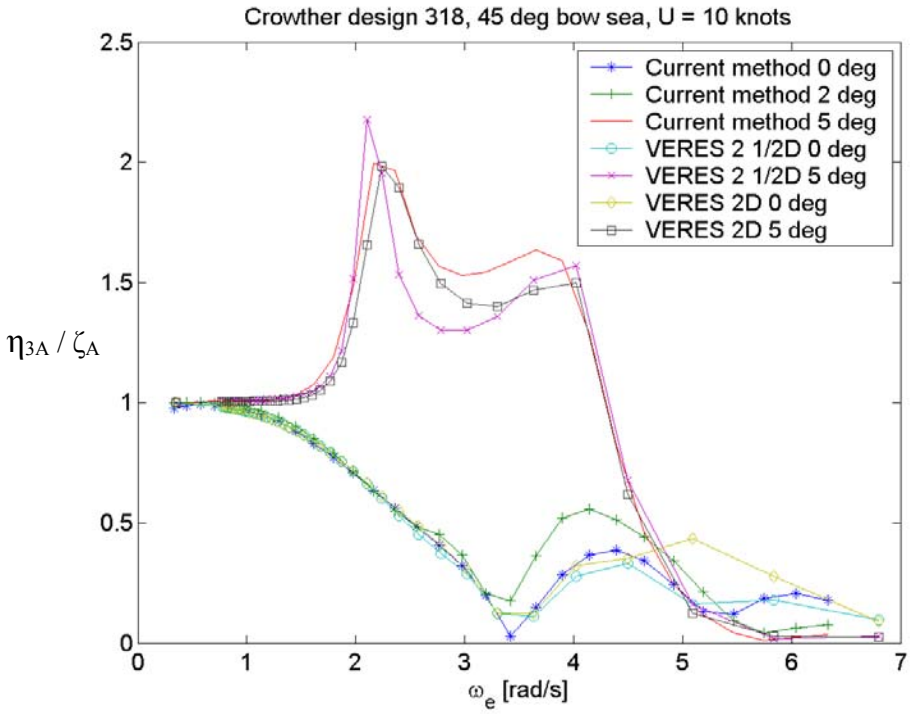

Fig. 3. 27 Heave RAO without sail forces

The comparison in heave (fig. 3.27) is very good. There is a marked difference between having two hulls in the water and sailing on one hull only. When sailing on one hull the mass matrix is effectively kept constant. The hydrodynamic properties are changed when two hulls are substituted with a single hull with deeper draft. This is also supported by practical experience. The RAO for 2 degrees heel is very close to the 0 degree heel case for heave.

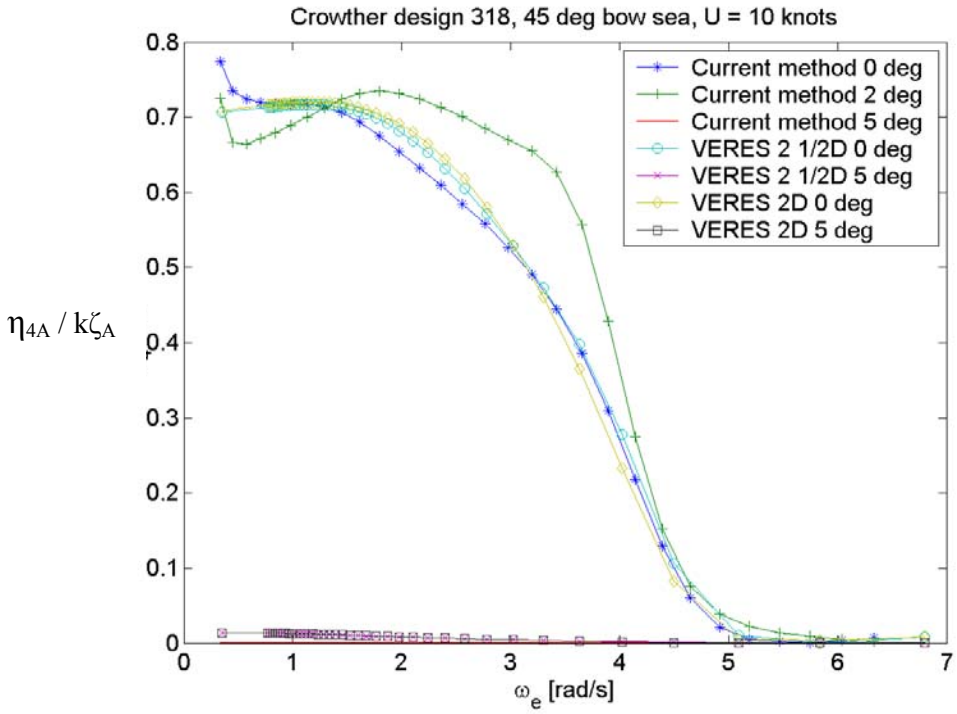

Fig. 3. 28 Roll RAO without sail forces

The comparison for roll (fig. 3.28) is also very good. For the 5 degrees heel angle case the boat has been locked in roll as this is an unstable condition and any results in roll would be meaningless. Sailing with 2 degrees of heel increases the roll motions at high frequencies. This is both due to coupling between heave, roll and pitch but also because the hydrodynamic properties have changed as a result of the individual change in draft in the two hulls.

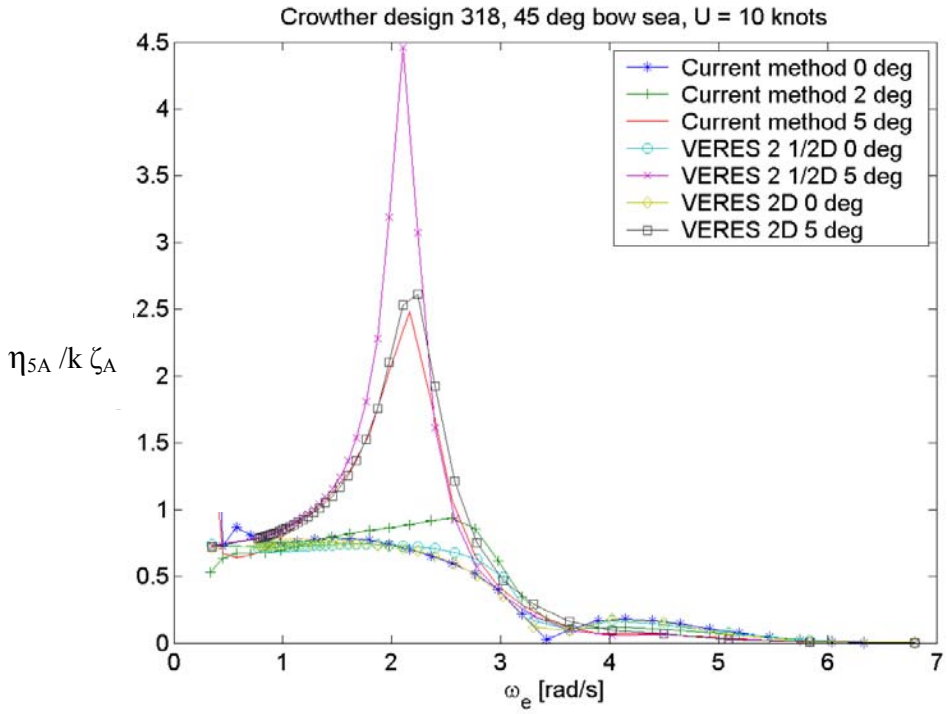

Fig. 3. 29 Pitch RAO without sail forces

The comparison in pitch (fig. 3.29) is also very good, but VERES 2½D predicts a higher peak response than the VERES 2D theory and the sailing multihull strip theory. Again the motions are worst when sailing on one hull (5 degrees heel) and best at 0 degrees of heel.

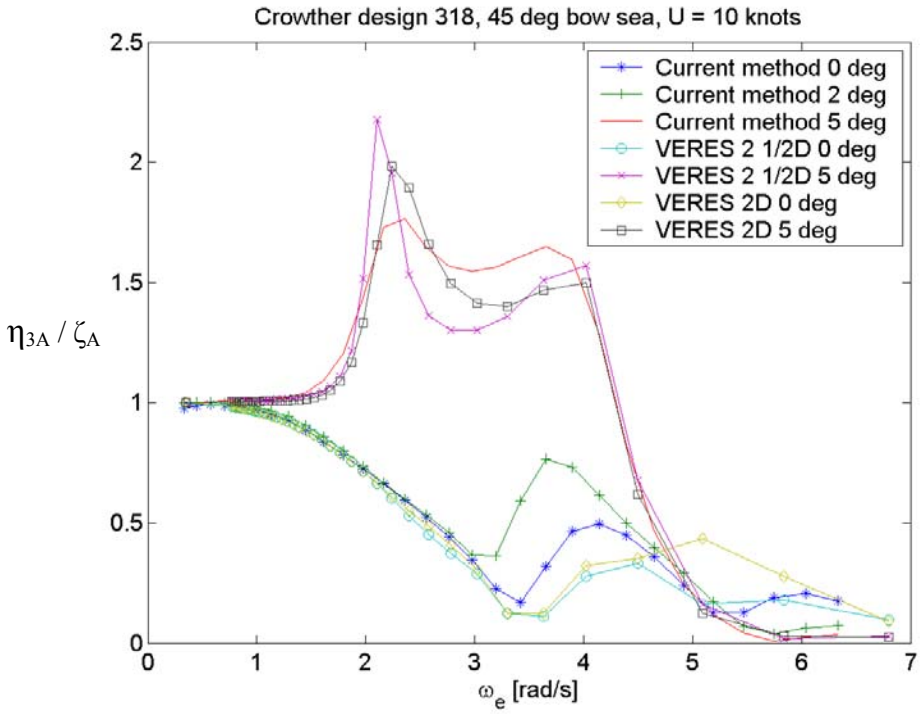

Fig. 3. 30 Heave RAO with sail forces

In calculating the sail-forces a wind speed of 8m/s has been used, a wind speed where most sailboats develop full power from their sails. The wind direction is identical to the wave direction.

The sail forces have a direct effect on the motions in roll and pitch, and due to coupling effects have a slight influence in heave (fig. 3.30) also. For the 5 degrees heel angle case it is clearly visible that the peaks response have been reduced somewhat. For the 0 degrees and the 2 degrees cases the incorporation of sail-forces has led to an increase in the motions at high frequencies. The VERES results do not include sail-forces.

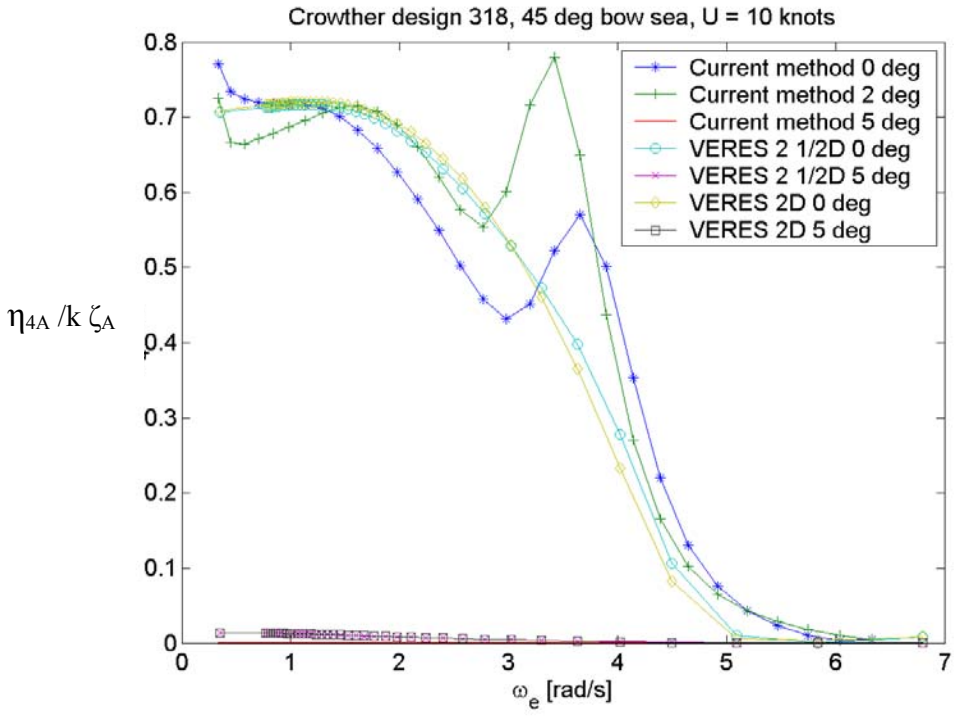

Fig. 3. 31 Roll RAO with sail forces

The effect in roll (fig. 3.31) is more pronounced. The sail-forces can be seen to reduce the motions at low frequencies, and increase the motions at high frequencies.

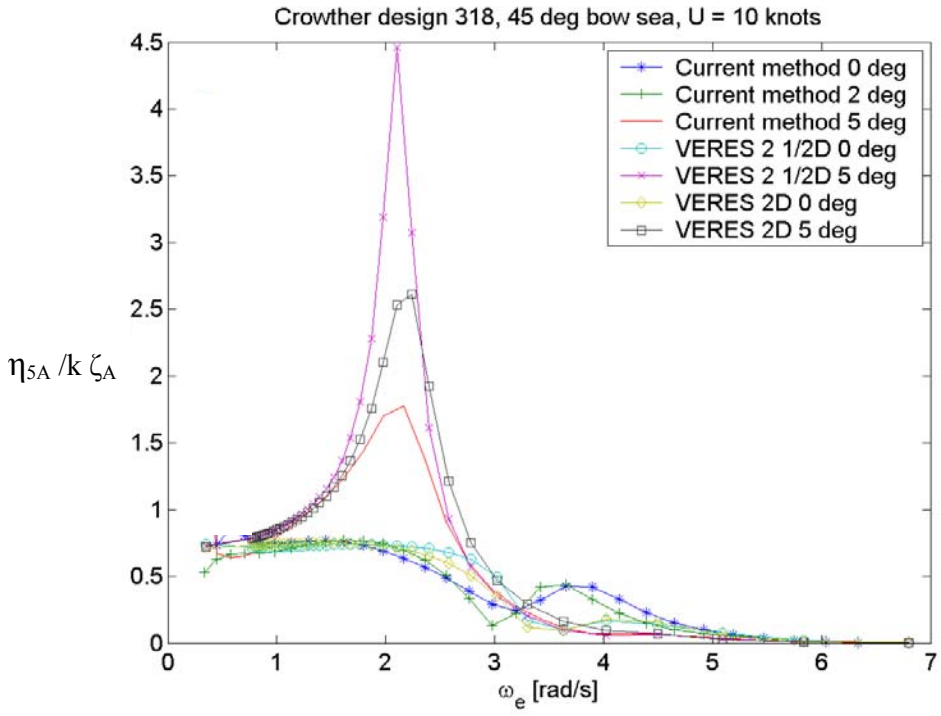

Fig. 3. 32 Pitch RAO with sail forces

A similar trend is seen for pitch (fig. 3.32) with a distinct reduction in the peak pitch response for the 5 degrees case, and increased motions at high frequencies for the 0 degree and 2 degrees case.

When sailing on one hull only the system is lightly damped, and the inclusion of sail-forces are important. The method used for calculating sail-forces is simple, but it is clear that sail-forces are an important consideration for high performance sailing catamarans with a high Sail Area / Displacement ratio.

3.3.2 Catamaran-Trimaran comparison

The single handed and grand prix racing in the 60 ft class is now completely dominated by trimarans, while the first edition of THE RACE (THE RACE is a no limits non-stop around the world race for sailing boats, first sailed in 2001) saw a fleet of giant catamarans. With the success of the race the interest is now building for round the world sailing in multihulls. A second edition of THE RACE is planned for 2004, and multiple teams are planning to attack the Jules Verne Trophy. The Jules Verne Trophy is the name of a non-stop around the world sailing record as opposed to a race, currently(2002) held by Bruno Peyron (French sailor, who in 1993 was the first man to get the Jules Verne trophy for circumnavigating the world in under 80 days. He sailed a catamaran) in his 110ft maxi catamaran at 64 days. After the first edition of THE RACE there were some comments that a giant trimaran could do better than a giant catamaran, especially with most of the catamarans suffering problems from slamming on the main beam. Olivier de Kersauson (another French sailor who held the record for several years with a trimaran until Peyron recently improved his time significantly) is trying to improve the record with his 115ft brand new trimaran Geronimo.

So what is really the difference between a catamaran and a trimaran? A trimaran is said to have both better seakeeping qualities as it sails with the main hull in the water in rough weather, while a catamaran needs to fly a hull to be fast. Also the beams on a trimaran are not stressed as hard as on a catamaran, and usually have smaller dimensions. As a case study two giant multihulls concepts were designed by the author, one 35m catamaran (fig. 3.33 and fig. 3.35) and one 35m trimaran (fig. 3.34 and fig. 3.36). For the sake of comparison as many parameters as possible were kept constant. Length, Beam, Displacement, sail area and main beam height (table 3.5) above the still waterline were kept constant. The hull shapes of the two yachts are obviously different, as is the size of the main beam. The designs were created for comparison only, and are not optimised. All the calculations were done for upwind sailing with a true wind angle and wave angle of 45 degrees. The speeds chosen are not necessarily realistic, but for the sake of comparison calculations have been performed for both two hulls in the water (both hulls on a catamaran, central hull and leeward

side-hull on a trimaran) and one hull in the water (The side-hull for a trimaran) for two speeds.

Loa	35 m
Boa	21 m
Main beam height	2.5 m
Sail area (upwind)	577 m^2
Displacement	24000 kg

Table 3.5 Catamaran/trimaran data

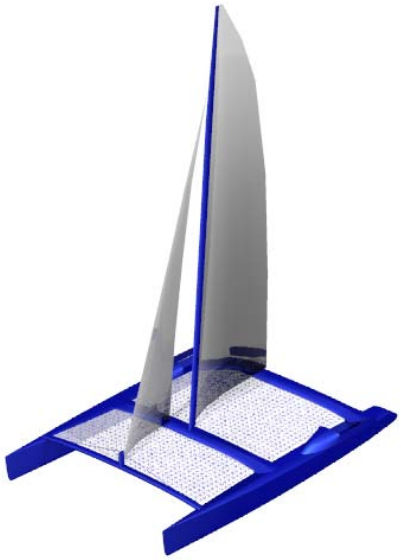

Fig. 3. 33 35m Catamaran (concept)

Fig. 3. 34 35m trimaran (concept)

Fig. 3.35 35m Catamaran lines plan

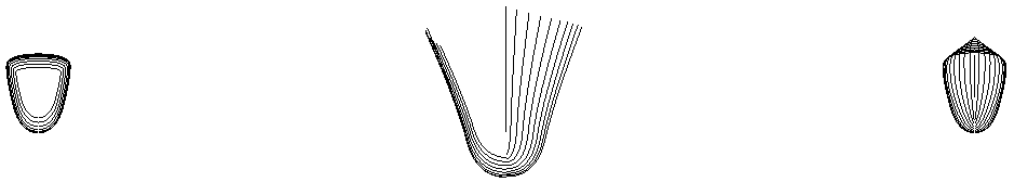

Fig. 3.36 35m Trimaran lines plan

RESULTS

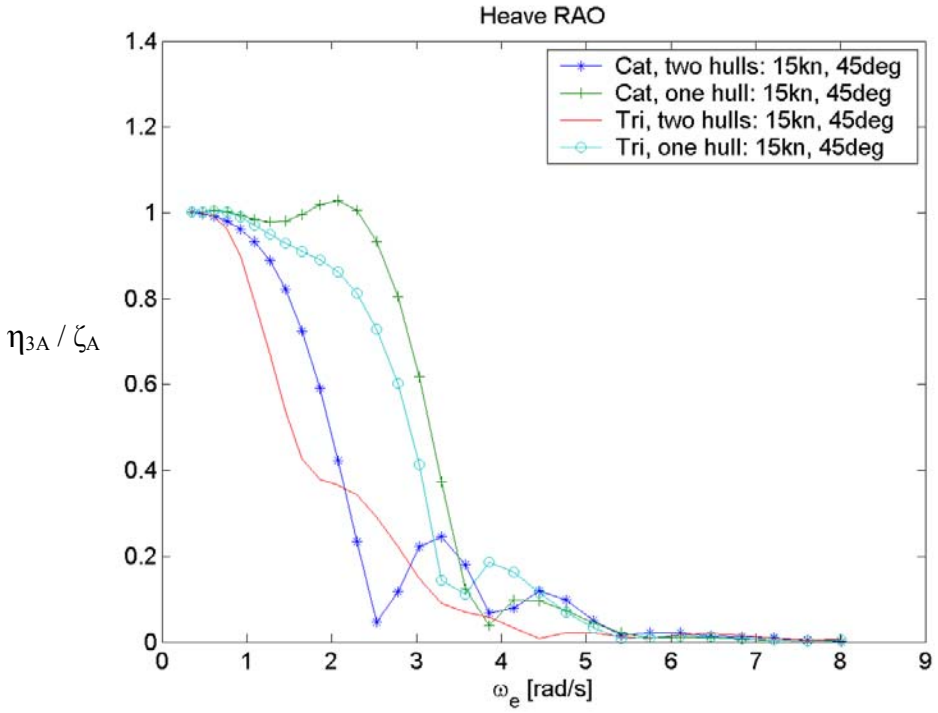

Fig. 3. 37 Heave RAO comparison 15 knots

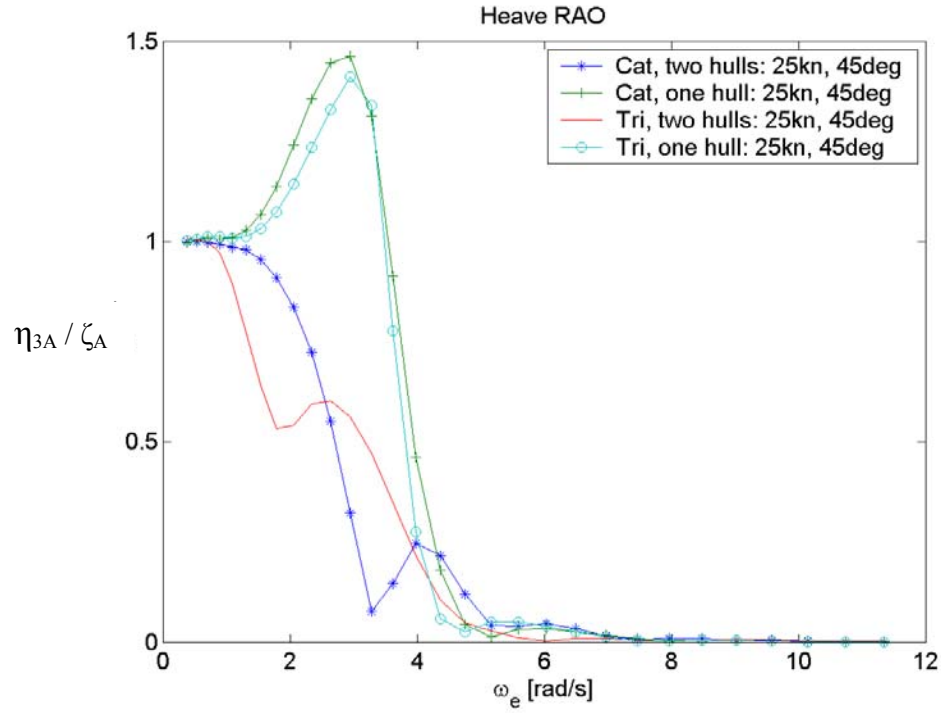

Fig. 3. 38 Heave RAO comparison 25 knots

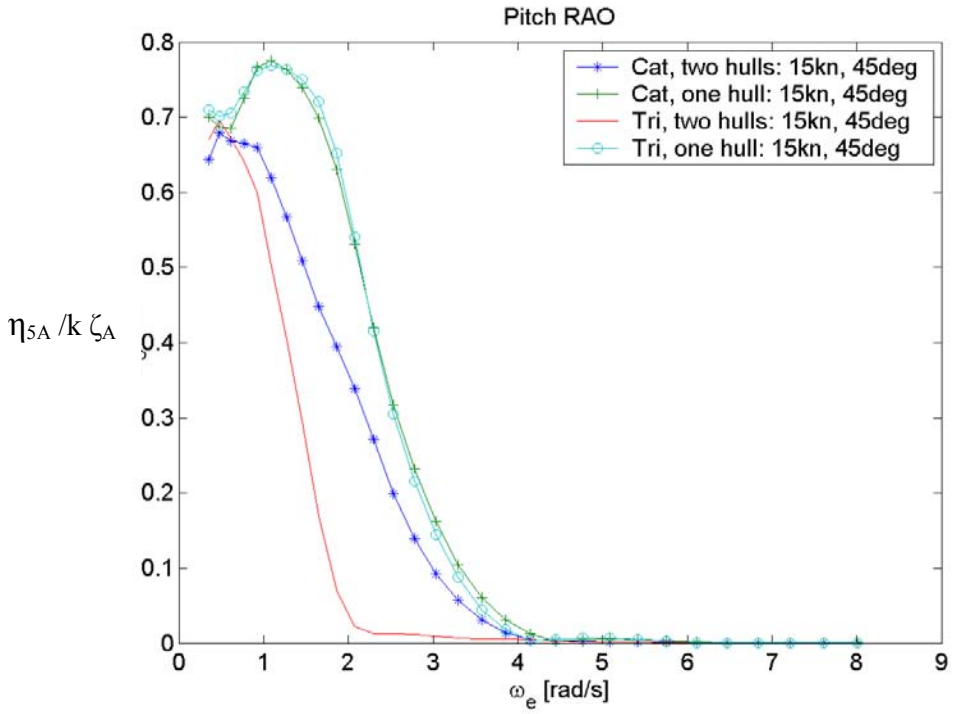

Fig. 3. 39 Pitch RAO comparison 15 knots

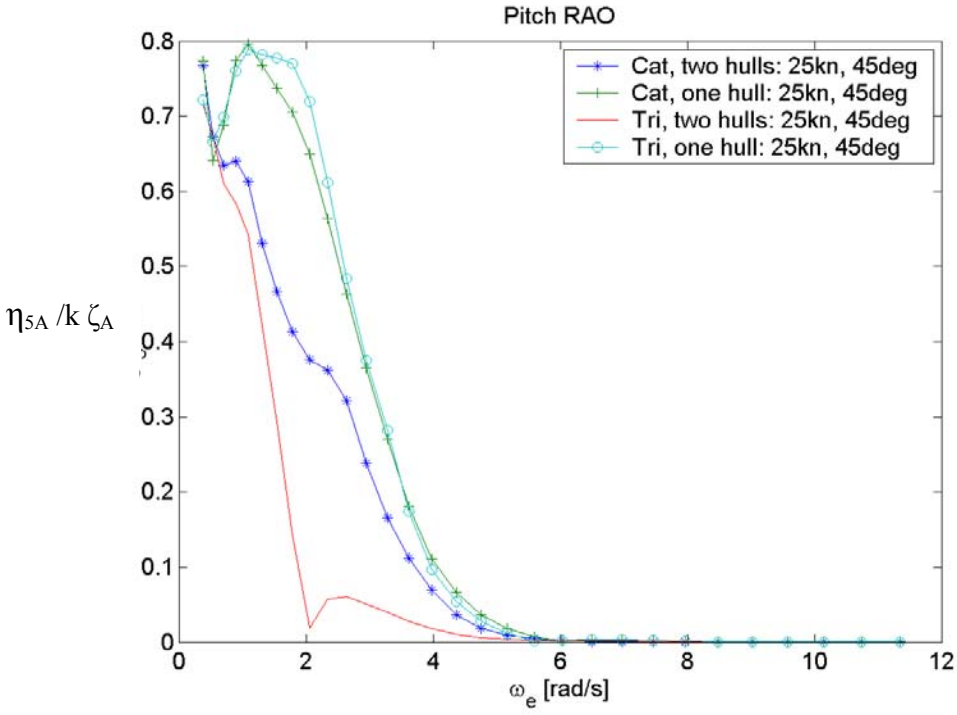

Fig. 3. 40 Pitch RAO comparison 25 knots

Comparing RAOs is a very useful way of comparing the seakeeping qualities of two yachts. Looking at the heave RAO in 15 knots (fig. 3.37) one can see that the trimaran gives a slightly smaller heave response at low frequency while the catamaran is better in high frequency waves. Both yachts experience less severe motions with two hulls in the water. The pitch RAO at 15 knots (fig. 3.39) shows that the catamaran and trimaran are very similar when sailed on one hull, while the trimaran is better when both yachts sails with two hulls in the water. Again sailing on two hulls reduces the motions. The trend continues at 25 knots (fig. 3.38 and fig. 3.40).

In conclusion it can be stated that the predicted seakeeping qualities for the trimaran are better than the predicted seakeeping qualities for the catamaran in most seastates, which corresponds well to experience.

3.4 Sailing multihull strip theory validation

3.4.1 Sally Malay seakeeping trials

In an attempt to validate the seakeeping predictions for sailing catamarans a full-scale trial was performed with a 36ft sailing catamaran (fig. 3.41). The catamaran was a cruiser/racer designed by Kurt Hughes Sailing Designs, Seattle, USA as a 30 footer, subsequently stretched to 36 foot before construction. Characteristic features of the boat are narrow, symmetric sidehulls, canted daggerboards in each hull, a low profile bridgedeck and a tall fractionally rigged sail-plan. It was built by the owner with plywood as the primary construction material, with local glass-fibre and carbon-fibre reinforcements. As a cruiser/racer the boat is normally sailed with both hulls in the water. Typical performance is 6-9 knots upwind and 6-20 knots downwind, depending on both wind and wave conditions.

Fig. 3. 41 Sally Malay

Onboard equipment

Onboard equipment and wave logging was identical to that used in the trials of Educat, as described in section 3.2.1

Trial Area

The trial area selected was outside of Hillary's Yacht club, north of Fremantle, Western Australia (fig. 3.43). To get approximately uniform waterdepth and waves in the trial area the trials were performed outside of the reefs.

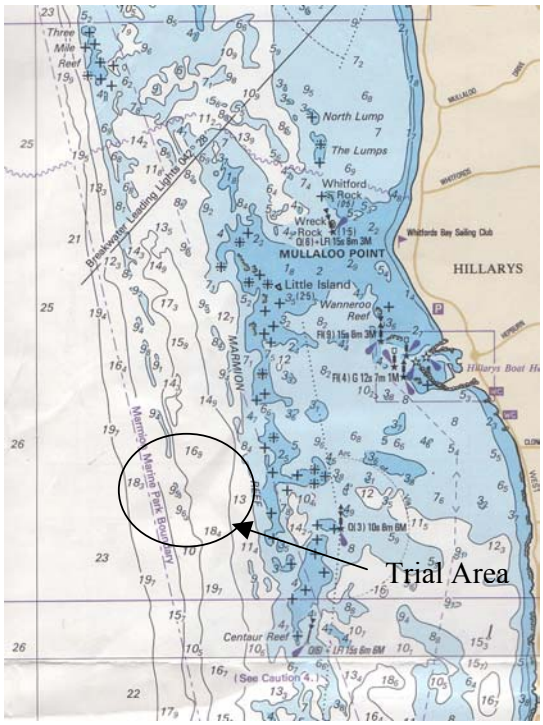

Fig. 3. 42 Trial Area

Weather conditions

The trial was performed in April 2002. A light morning south easterly wind veered to south-west around midday. The trials were performed in an unsettled sea-breeze from the south-west. The wind speed varied from about 5-7 knots during the trial. The sea was dominated by an almost long-crested westerly swell at approximately 0.7-0.8m wave height, 9-10 s period. The windsea was not fully developed and had considerable directional spread (fig. 3.44). The significant wave height was estimated visually to 1m.

Trial procedure

To keep close to the wave buoy a series of 10 min trials was performed. The first trial was performed by driving into the swell under motor. A series of upwind trials followed, and with the southwesterly wind direction there was a choice of either sailing directly into the swell or sailing at approximately right

angles to the swell. Sailing into the swell on port tack was thought to be most useful and 3 runs were carried out for this condition. One run was carried out sailing on starboard tack. The starting position of each run was adjusted to keep as close to the wave buoy as possible during the run.

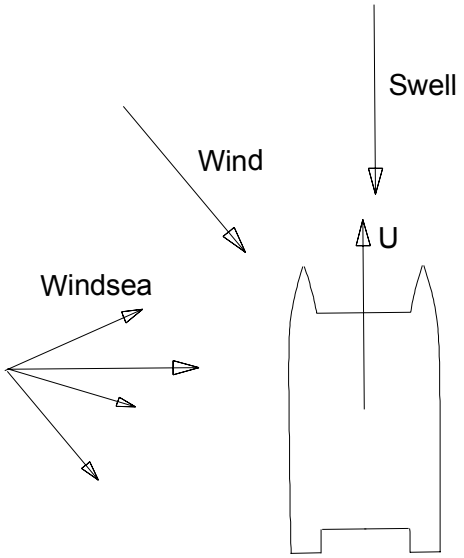

Fig. 3. 43 Typical port tack upwind trial run

Data processing

To obtain a better statistical estimate of the wave and motion spectra the three port tack upwind runs were combined into one 30min run. The motion data from the TSS was decimated to 4Hz prior to the calculation of motion power spectra. The spectra were calculated using Welch's averaged, modified periodogram method. 50% overlapped segments were used, with 256 samples in each segment. Each segment was windowed with a 10% cosine taper window. The wave spectra were calculated with the same procedure and identical parameters. The stationary wave spectrum was used to calculate the wave spectrum in the boat's reference frame, using the boat's speed and course information from the GPS and visual estimates of the wave heading. The non-dimensional heave RAO was calculated by dividing the square root of the heave spectrum with the square root of the wave power spectrum. The non-dimensional roll and pitch RAOs were calculated by dividing the square root of the pitch/roll spectra with the square root of the wave-slope power spectrum.

Results

Most of the wave energy was at the low frequency end of the spectrum, from the swell. This makes the calculation of RAOs difficult, as the signal to noise ratio of both the wave measurements and the motion measurements is not as good as it could have been. Nevertheless both the TSS sensor and the waveloggers proved capable of measuring small waves and motions quite accurately.

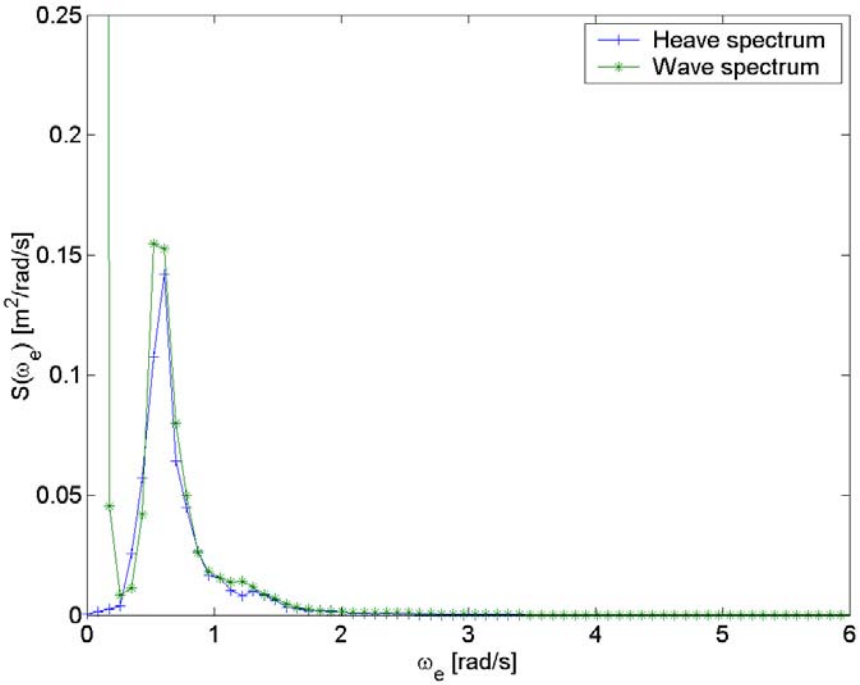

Fig. 3. 44 Heave and Wave spectra

The wave spectrum and the measured heave spectrum are plotted above (fig. 3.45).

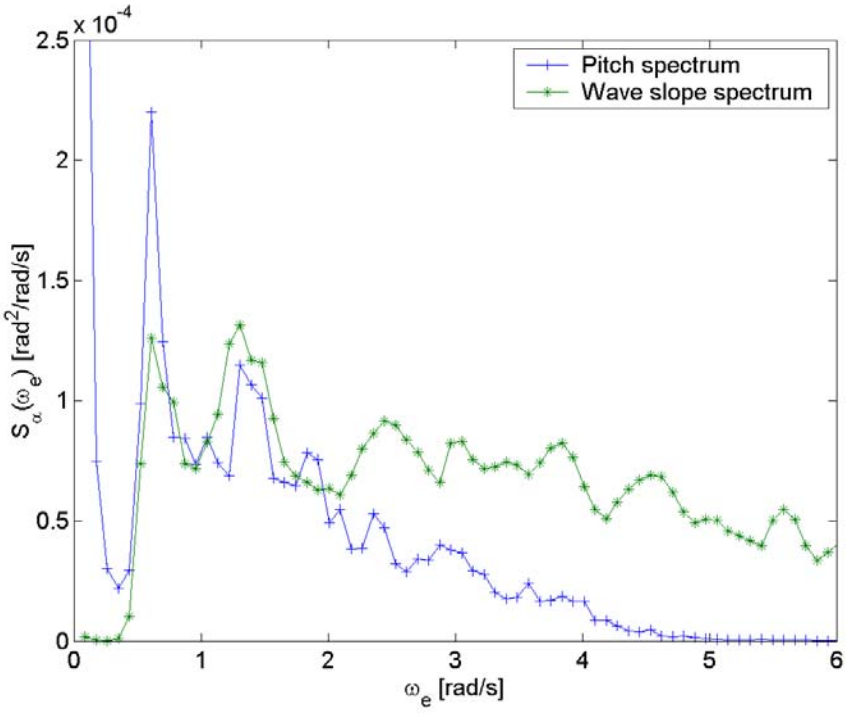

Fig. 3. 45 Pitch and wave slope spectra

The wave slope spectrum has been calculated from the wave spectrum, and is plotted against the pitch spectrum (fig. 3.46).

The RAOs have been calculated from the wave and motion spectra, and are plotted along with predicted RAOs obtained from linear strip theory. The full-scale trials were performed in a seastate with different directions of the swell and wind-sea. To reflect this the predicted RAOs were calculated for head sea and 50 degrees. The final predicted RAO was obtained by using the head sea RAO at low frequencies (<1.2 rad/s) and the 50 deg RAO at higher frequencies (>2.5 rad/s) and a weighted average for intermediate frequencies.

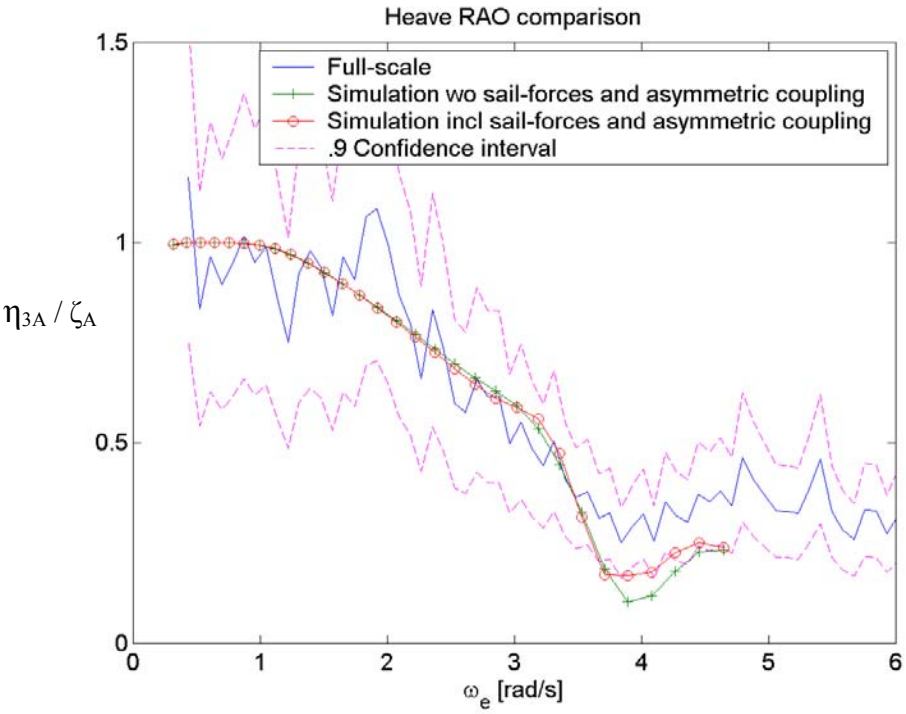

Fig. 3. 46 Full-scale heave RAOs

The heave RAO (fig. 3.47) is jagged, but its general shape is as expected. Due to a blow up of the wave spectrum at very low frequencies the full-scale heave RAO is inaccurate at very low frequencies. Some inaccuracies are also expected at medium-high frequencies as the wave energy was concentrated around the swell. With this in mind the comparison with the predicted RAOs is good, especially up to about 3 rad/s. Due to the low wind-speed and consequently heel-angle it is difficult to judge the importance of sail-forces and asymmetric coupling.

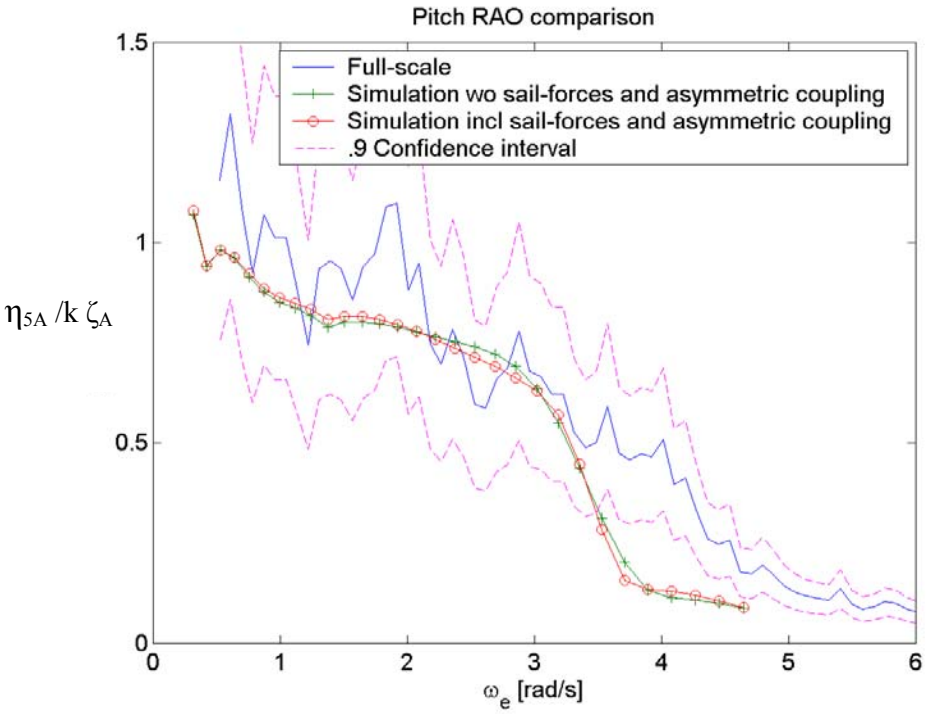

Fig. 3. 47 Full-scale pitch RAOs

The full-scale pitch RAO (fig. 3.48) is also jagged, but shows the usual behaviour. Again the very low frequency part of the RAO is contaminated by a blow-up in the pitch spectrum. The RAO is also inaccurate at high frequencies due to low energy content at high frequencies. The comparison is however good at frequencies up to about 3 rad/s, after which the predicted RAOs drop rapidly while the full-scale RAO drops more slowly.

Conclusions

A full-scale trial with the sailing catamaran Sally Malay has been performed and the boat's RAOs have been estimated. The wind and wave conditions on the trial day were not perfect, but the measured RAOs are a reasonably good estimate of the boat's RAOs.

Predicted RAOs have been compared to the measured RAOs, and found to give a reasonable prediction.

CHAPTER 4: SLAMMING IDENTIFICATION

4.1 Probabilistic method

As described in the historical review the probability of slamming can be calculated as the joint probability of water entry and exceedance of a threshold value of relative vertical velocity when the maxima of the relative vertical velocity follow the Rayleigh distribution. It is also assumed that the probability of water entry and the probability of exceeding a threshold relative vertical velocity are statistically independent. The formula is simple, and predicted motions from linear theory can be used as input. The probability of slamming per cycle of wave encounter is

$$P(slam) = e^{-\left(\frac{\dot{\xi}_{cr}^2}{2\sigma_v^2} + \frac{d^2}{2\sigma_r^2}\right)} \tag{4. 1}$$

Where $\dot{\xi}_{cr}$ is the critical or threshold relative vertical velocity, d is the local draft, σ_v is the variance of the relative vertical velocity and σ_r is the variance of the relative vertical displacement.

σ_v can be calculated as

$$\sigma_v^2 = \int_0^\infty S(\omega) \left| \frac{\dot{\xi}(\omega)}{\zeta} \right|^2 d\omega \tag{4. 2}$$

and σ_r can be calculated as

$$\sigma_r^2 = \int_0^\infty S(\omega) \left| \frac{\xi(\omega)}{\zeta} \right|^2 d\omega \tag{4. 3}$$

Where $\frac{\dot{\xi}(\omega)}{\zeta}$ and $\frac{\xi(\omega)}{\zeta}$ are the RAOs for the relative vertical velocity and the relative vertical displacement respectively.

Ochi (Ochi 1964b) also found that a minimum relative vertical velocity must be exceeded in order to classify a water entry as a slam. He found an empirical relationship linking this threshold value to the ship length L.

$$\dot{\xi}_{cr} = 0.093\sqrt{gL} \qquad (4.4)$$

4.2 Direct method

The strip theory time domain simulation gives the displacement and rotations at the centre of gravity as output. The output is given as a time series. In addition the wave components used are given. Together this information makes it possible to calculate heave displacements and velocities at arbitrary locations, and wave elevation and vertical velocity at arbitrary positions for the simulated regular or irregular sea. Further, the relative vertical position and velocity between arbitrary positions on the hull and the sea surface can be calculated. Finally slamming occurrences are identified by defining a slam to occur when a point on the hull breaks the wave surface, with a downwards velocity greater than a threshold value. In some instances the ships steady and unsteady wave systems will have an important effect on slamming, as they will effectively reduce the clearance under the wetdeck or bridgedeck. This is most likely to have a noticeable effect close to the stern where the divergent wave systems of the two hulls meet and a crest is formed. The effect of this can be included if the steady wave elevation is known for the desired location, for example from model tests or wave resistance programs. For some ships a jet is also formed from the bow wave, and this will sometimes influence slamming. Finally it is important to analyse the ship in its natural running trim. If the ship trims by the stern at speed this will greatly influence the probability of slamming.

Local origin

Local origin is positioned at Centre of gravity horizontally and in plane with the still water line vertically. The right handed coordinate system has the X-axis positive aft, and the Z-Axis positive upwards.

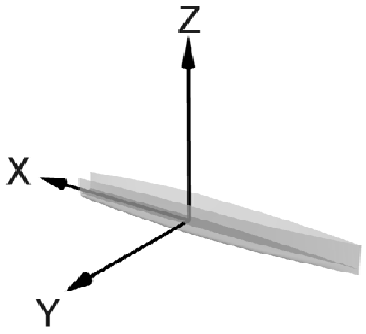

Fig. 4.1 Local origin

Displacements at centre of gravity

Vessel displacements at centre of gravity, CG, are given as

η_1 = surge displacement, positive in +X direction.

η_2 = sway displacement, positive in +Y direction.

η_3 = heave displacement, positive in +Z direction.

η_4 = roll displacement, about +X axis.

η_5 = pitch displacement, about +Y axis.

η_6 = yaw displacement, about +Z axis.

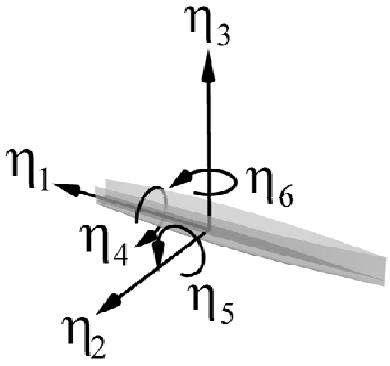

Fig. 4.2 Displacements

Calculation of heave motion at arbitrary positions

Given the displacements in 6 degrees of freedom at local origin, it is straightforward to calculate the heave motions at arbitrary positions on the vessel. The heave motion at remote location i is calculated as

$$\eta_{3i} = \eta_3 - X_i * \sin(\eta_5) + Y_i * \sin(\eta_4) \tag{4. 5}$$

The neglecting of the Z dependence in the calculation can be justified as it is both a higher order effect, and the Z coordinate of any position with a real possibility of slamming is small.

Calculation of velocities at centre of gravity

Given a time series of displacements at the centre of gravity the velocities at this point can be calculated by differentiation with respect to time. For the first time step a second order forward looking differentiation was used,

$$\dot{\eta}_i(t_1) = \frac{-3\eta_i(t_1) + 4\eta_i(t_2) - \eta_i(t_3)}{2 * \Delta t} \tag{4. 6}$$

The last time step is differentiated with a second order backward looking differentiation,

$$\dot{\eta}_i(t_n) = \frac{\eta_i(t_{n-2}) - 4\eta_i(t_{n-1}) + 3\eta_i(t_n)}{2 * \Delta t} \tag{4. 7}$$

The remaining majority of the time steps are calculated with a second order central differentiation,

$$\dot{\eta}_i(t_{2..n-1}) = \frac{\eta_i(t_{n+1}) - \eta_i(t_{n-1})}{2 * \Delta t} \tag{4. 8}$$

Finding velocities by numerical derivation is an approximate calculation, and it is important that the time steps are small to get the required accuracy.

Calculation of heave velocity at arbitrary positions

Following the same procedure as for heave displacement the heave velocity at arbitrary positions can be calculated from the velocities at the centre of gravity as follows:

$$\dot{\eta}_{3i} = \dot{\eta}_3 - X_i * \sin(\dot{\eta}_5) + Y_i * \sin(\dot{\eta}_4) \qquad (4.9)$$

Calculation of wave elevation at arbitrary positions

The wave elevation for a sinusoidal wave propagating along an axis x is given by

$$\zeta(x,t) = \zeta_a \sin(\omega t - kx + \varepsilon) \qquad (4.10)$$

where

ζ_a = Wave Amplitude, $\omega = \frac{2\pi}{\mathrm{T}}$, T = Wave Period, $k = \frac{2\pi}{\lambda}$, λ = Wavelength, ε = Phase angle

If forward speed is included

$$\zeta(x,t) = \zeta_a \sin(\omega_e t - kx + \varepsilon) \qquad (4.11)$$

, where ω_e is the encounter frequency. This formula is suitable for head sea, but it can be extended to include oblique seas. For long crested sea the wave elevation at an arbitrary point X,Y can be calculated by mapping the point X,Y onto an axis in the wave propagation direction.

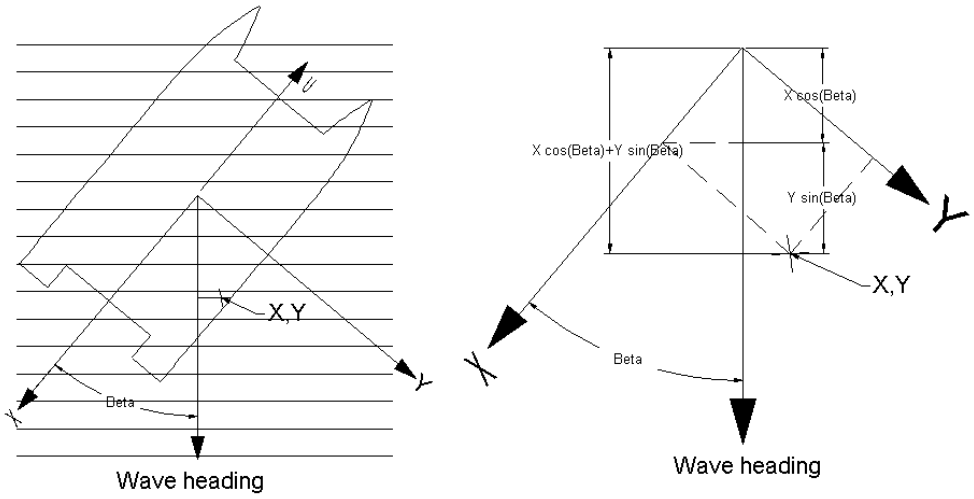

Fig. 4.3 Wave elevation at arbitrary location

Substituting x in the formula above with $X\cos(\beta)+Y\sin(\beta)$ we have

$$\zeta(X,Y,t)=\zeta_a\sin(\omega_e t-k(X\cos(\beta)+Y\sin(\beta))+\varepsilon) \qquad (4.\ 12)$$

where $\beta=$ Wave heading(0 rad is head sea) .

An irregular sea state can be simulated by superposition of sinusoidal waves, but to avoid repetition of the pattern random phase angles should be used for each wave component and the individual wave frequencies should be irregularly spaced. The wave elevation at an arbitrary point X_i,Y_i is

$$\zeta_i(t)=\sum_{j=1..n}\zeta_{aj}\sin(\omega_{ej}t-k_j(X_i\cos(\beta)+Y_i\sin(\beta))+\varepsilon_j) \qquad (4.\ 13)$$

Calculation of wave vertical velocity at arbitrary positions

The wave vertical velocity for a sinusoidal wave propagating along an axis x is found by taking the total derivative of the wave elevation.

$$\frac{D\zeta}{Dt}=\frac{d\zeta}{dt}+U\frac{d\zeta}{dx}= \qquad (4.\ 14)$$
$$(\omega_e-Uk)\zeta_a\cos(\omega_e t-kx+\varepsilon)=\omega\zeta_a\cos(\omega_e t-kx+\varepsilon)$$

Note that the encounter frequency is only used inside the cosinus term, as forward speed will have no effect on the amplitude on the vertical velocity. Following the same procedure as for wave elevation

$$\dot{\zeta}(X,Y,t) = \omega\zeta_a \cos(\omega_e t - k(X\cos(\beta) + Y\sin(\beta)) + \varepsilon) \tag{4. 15}$$

and for simulation of an irregular seastate we have

$$\dot{\zeta}_i(t) = \sum_{j=1..n} \omega_j \zeta_{aj} \cos(\omega_{ej} t - k_j(X_i\cos(\beta) + Y_i\sin(\beta)) + \varepsilon_j) \tag{4. 16}$$

Calculation of relative vertical motions

The relative vertical displacement at an arbitrary point X_i,Y_i,Z_i is calculated as

$$Z_{Ri} = Z_i + \eta_{3i} - \zeta_i \tag{4. 17}$$

In the calculation of the relative vertical velocity there will be a contribution due to forward speed and pitch, $U\sin(\eta_5)$.

$$\dot{Z}_{Ri} = \dot{\eta}_{3i} - \dot{\zeta}_i - U\sin(\eta_5) \tag{4. 18}$$

Finding water entry occurences

The first step to identify slamming occurrences is to identify water entry occurrences, or the time of all zero crossings of the relative vertical position. This means that the time the point considered breaks the sea surface, either on its way up or down will be identified. Given a time series of relative vertical position the time of all zero crossings can be found as follows:

Find all intervals where the relative vertical position changes sign.

Interpolate to find the zero cross time.

The use of interpolation will introduce a small error, but with a small time step it will be negligible.
Only half of the zero crossings found are water entry occurrences, and only crossings of the water surface from above will be used.

Calculating relative vertical velocity at zero crossings

Because all data are given as discrete points it is again necessary to interpolate to find the relative vertical velocity at the same instant as the hull breaks the sea surface. As above the error by interpolation will be negligible, providing the time step is small.

Identifying slammng occurrences

Identifying slamming occurrences is now a matter of how a slam is defined. A slam is here defined as a crossing of the wave surface from above, with a downwards relative velocity. Once a slam is identified the relative vertical velocity at the time of slam is taken as the impact velocity to be used in further calculations.

4.3 Grouping of slamming events

The Ochi threshold velocity (4. 4) could have been used, but instead it was chosen to classify the impact velocities into groups. Since slamming pressure is proportional to the impact velocity squared the total number of slams are placed into 5 groups according to the impact velocity squared. This simplifies the slamming pressure calculation as the slamming pressure needs only be calculated once for each group. Grouping the slamming events makes it possible to find the severity distribution of the slamming events, information that is valuable to a designer.

4.4 Practical implementation

The procedure was coded in Matlab. Matlab is ideally suited to this task since it has integrated plotting functions, and it has a useful library of efficient

matrix functions. The calculation of relative motions is computationally intensive and the program was written so a large set of time domain files could be post-processed overnight.

CHAPTER 5: SLAMMING IDENTIFICATION RESULTS AND VALIDATION

5.1 Austal Hull 63

As the non-linear theory gave unsatisfactory results for this hull it was decided to use the results obtained from linear high-speed strip theory. Slamming identification has been done using both the probabilistic method (Ochi's method) and the direct method presented in chapter 4. A comparison will also be given.
The total number of slams have been calculated for one location, shown below (fig. 5.1). After an initial study this location was found to be most exposed to slamming.

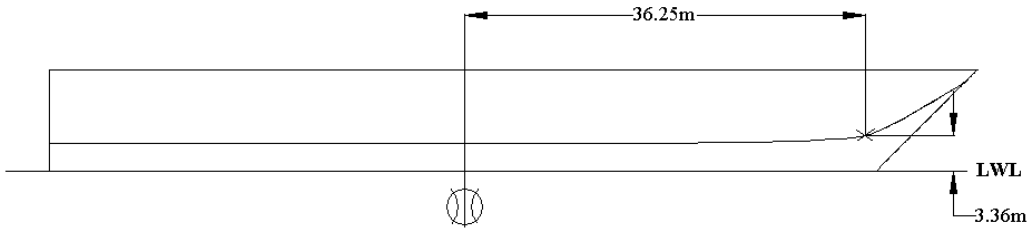

Fig. 5.1 Austal Hull 63 slamming location

5.1.1 Probabilistic method

The RAOs for Austal Hull 63 were calculated for a range of headings, speeds and wave periods. The conditions were chosen to reflect seastates where slamming may cause operability problems. The probability of slamming was then calculated according to the formulas given in chapter 4. The results have been presented as expected number of slams per hour vs heading angle to enable easy comparison with results calculated with the direct method. Results are only presented for head and bow sea operation as slamming is mostly a problem in bow sea. The total number of slams are shown, and it is expected that many of the slams will be very light (no threshold velocity is used) with a smaller number of more severe slams.

The number of slams per hour vs heading angle are plotted for U = 20 knots, U = 30 knots, U = 40 knots in seastates with Hs = 3m and Hs = 4m (Fig. 5.2 – 5.7). Head sea is 0 degrees. For all seastates the maximum number of slams are seen in head sea, and drops smoothly when the ship bears away from head sea. It is also evident that the most frequent slamming occurs in seastates with shorter mean period. This is a reasonable result given that the total number of waves will be greater in a shorter period. It is also seen that the number of slams decrease when the speed increased. This is in line with the practical experience expressed by the ships crew; when slamming occurs at full speed the problem is made worse by reducing speed. Finally the number of slams are seen to increase with increasing wave height. Even with linear motions as used here slamming is a highly non-linear phenomenon, increasing the significant wave height from 3 to 4 m results in a dramatic increase of the number of slams.

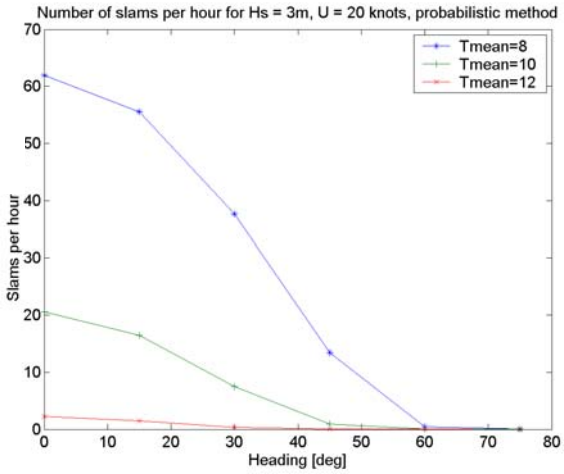

Fig. 5.2 Predicted slamming occurrence

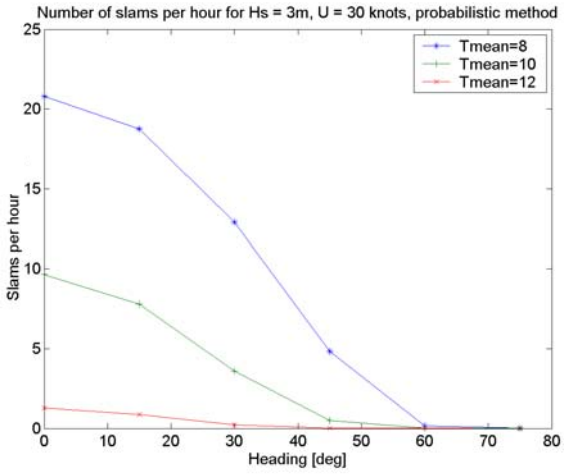

Fig. 5.3 Predicted slamming occurrence

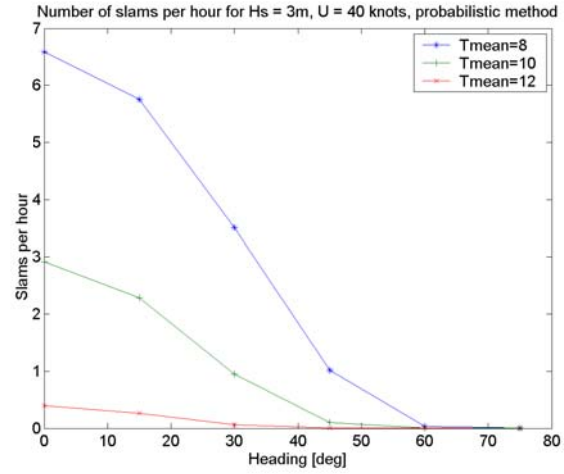

Fig. 5.4 Predicted slamming occurrence

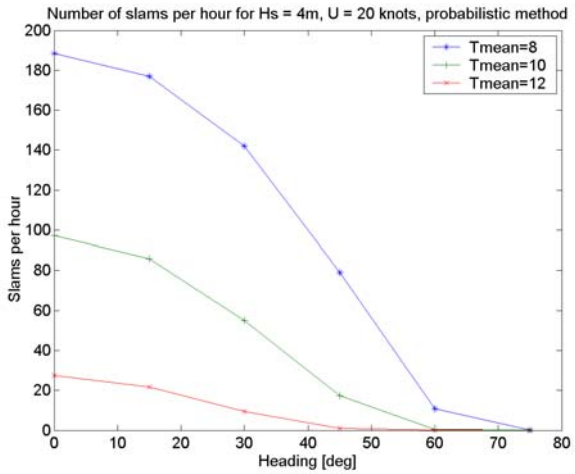

Fig. 5.5 Predicted slamming occurrence

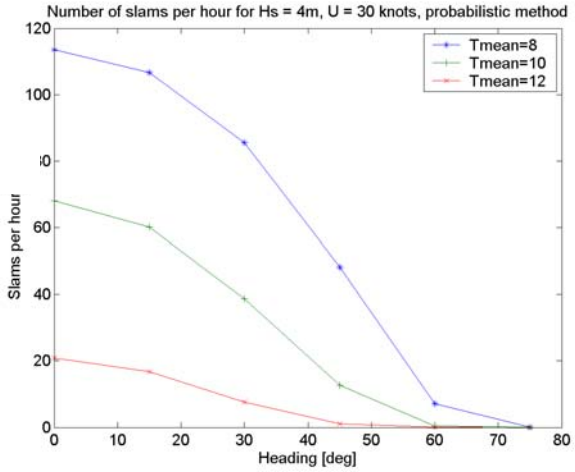

Fig. 5.6 Predicted slamming occurrence

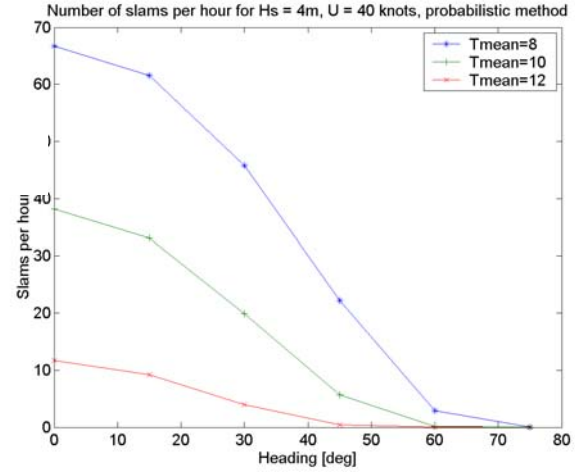

Fig. 5.7 Predicted slamming occurrence

5.1.2 Direct method

The same RAOs as used for the probabilistic method were used to generate 108 time series, covering the same conditions as used in the section above. Each run was 1hr. The results from each run was post processed and the results are shown below (fig. 5.8 – 5.13). The results are similar to the results obtained by the direct method, but for conditions with few slamming events the statistical uncertainty makes the predictions inaccurate.

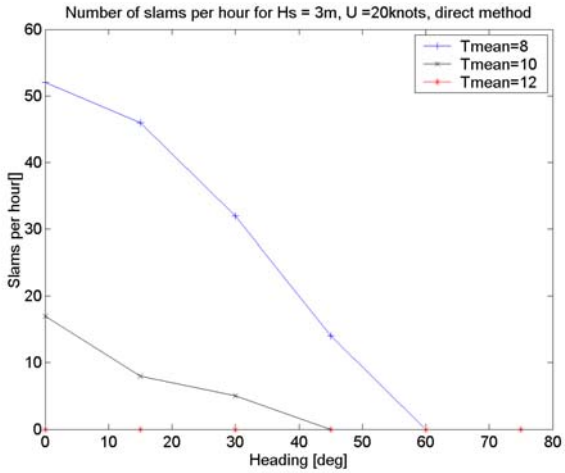

Fig. 5.8 Predicted slamming occurrence

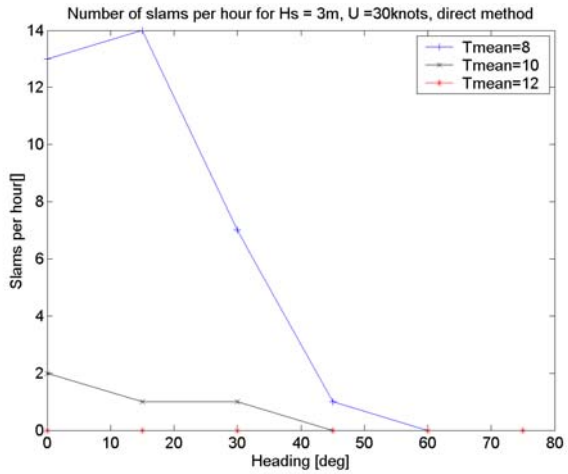

Fig. 5.9 Predicted slamming occurrence

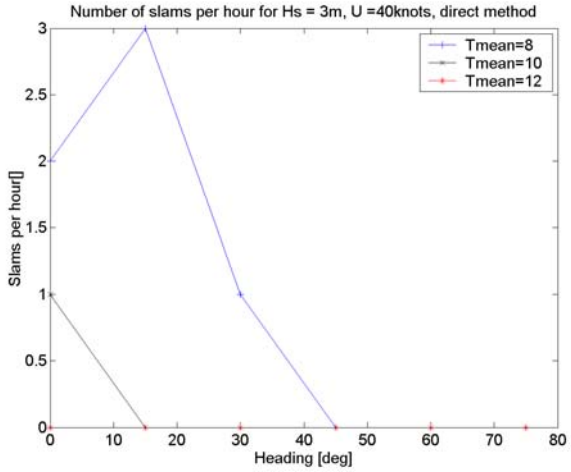

Fig. 5.10 Predicted slamming occurrence

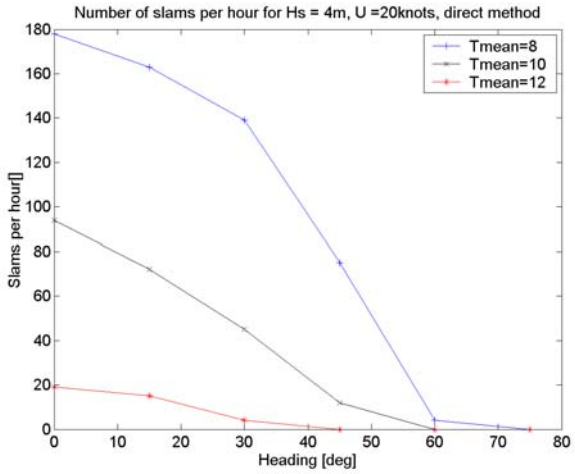

Fig. 5.11 Predicted slamming occurrence

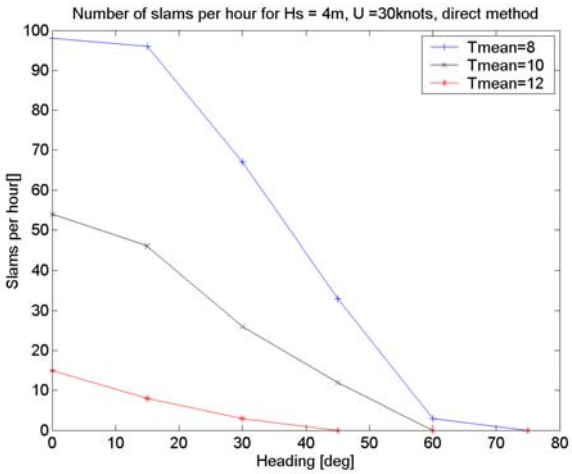

Fig. 5.12 Predicted slamming occurrence

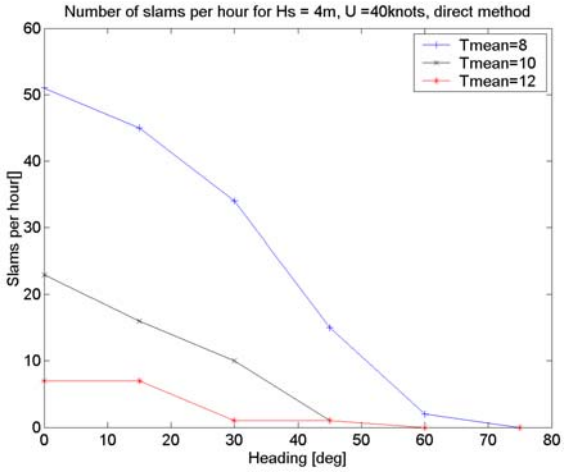

Fig. 5.13 Predicted slamming occurrence

By using the direct method the average impact velocity can be plotted, providing some insight into the severity of the slamming. Shown below are the average impact velocity plotted vs heading angle (fig. 5.14 – 5.19), plotted for the same conditions as above. The statistical uncertainty for the average impact velocity is larger than for the number of slams. Especially in marginally slamming conditions the average slamming velocity are dominated by a few events. The average impact velocity follows a similar trend as the number of slams. The maximum velocity is found for 20 knots in head sea, in a 4m Hs, 8s Tmean seastate.

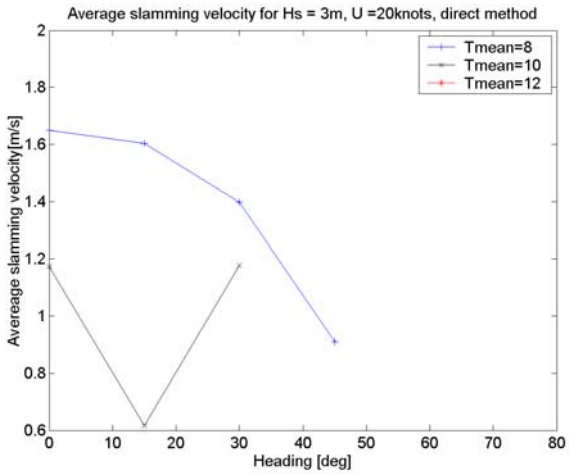

Fig. 5.14 Average impact velocity

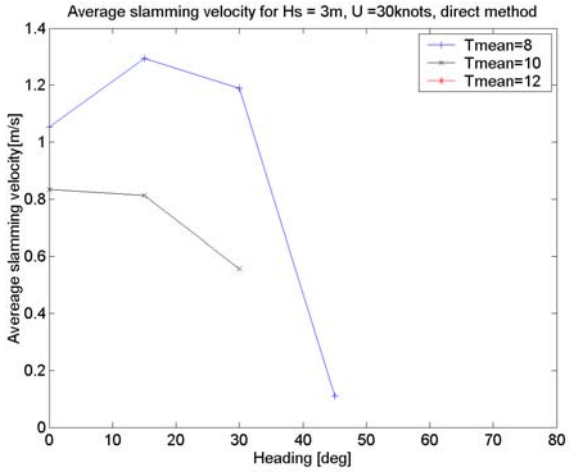

Fig. 5.15 Average impact velocity

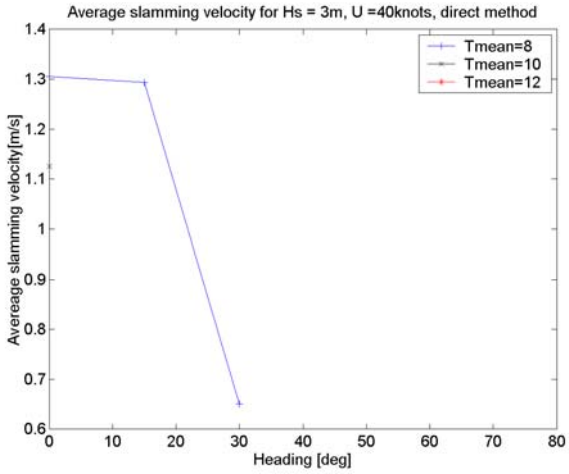

Fig. 5.16 Average impact velocity

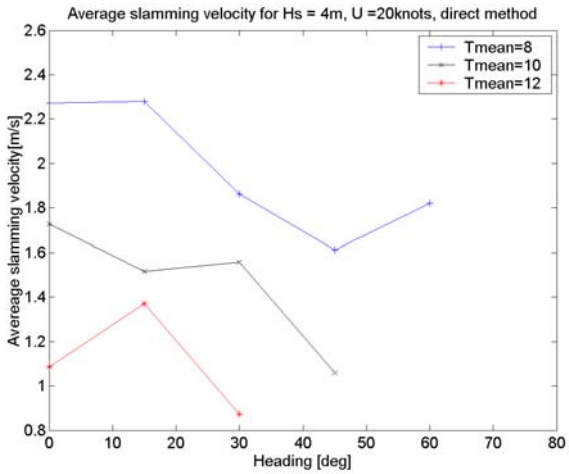

Fig. 5.17 Average impact velocity

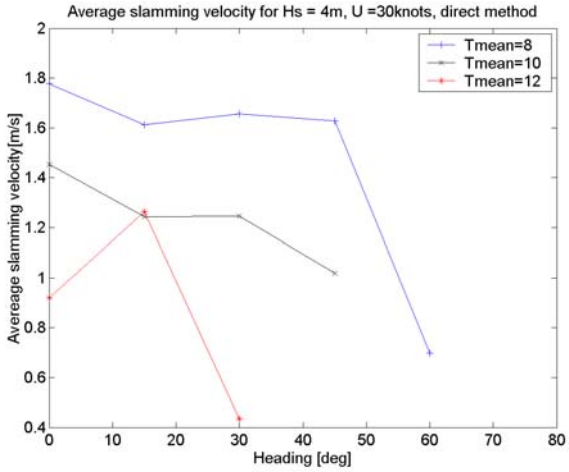

Fig. 5.18 Average impact velocity

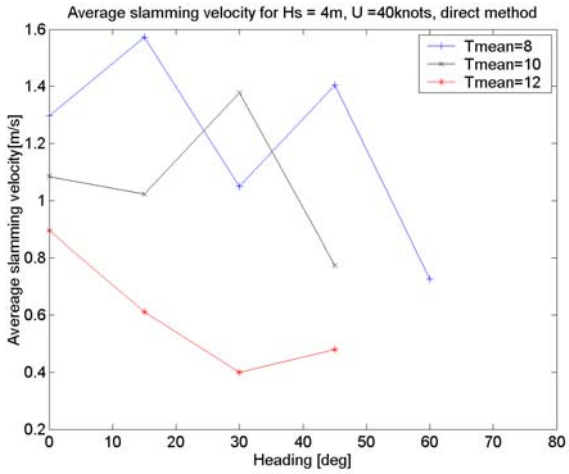

Fig. 5.19 Average impact velocity

5.1.3 Comparison

Finally, the results from the probabilistic method and the direct method are compared (fig. 5.20 –5.25). Again the same conditions are used. The results are encouraging with generally good agreement. The probabilistic method predicts a slightly higher number of slams per hour than the direct method, especially for conditions with a limited number of slamming events. Since this trend can be found in all conditions it is not believed this is caused by statistical uncertainty.

The probabilistic method assumes that the peaks of the relative motion follow the Rayleigh distribution. This is valid for a narrow banded spectrum (Faltinsen 1990), but the Bretschneider spectrum used here is not narrow banded. It is in fact extremely broad banded (Lloyd 1989), and the peaks of the wave and the relative motion will consequently not follow the Rayleigh distribution. In view of this the probabilistic method of predicting slamming occurrence must be seen as an approximate method. The probabilistic method is however preferred for rare events as the statistical uncertainty of the direct method is large for rare events.

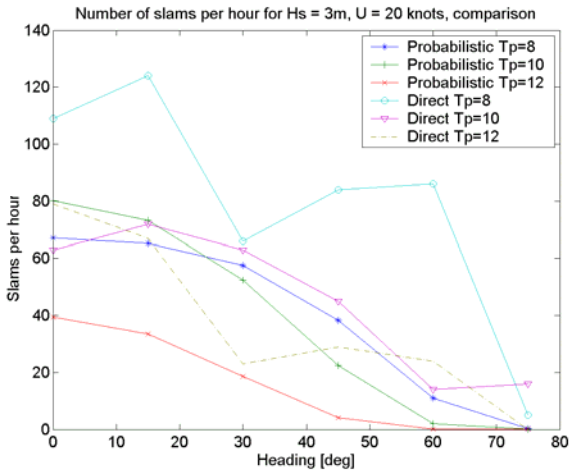

Fig. 5.20 Predicted slamming occurrence

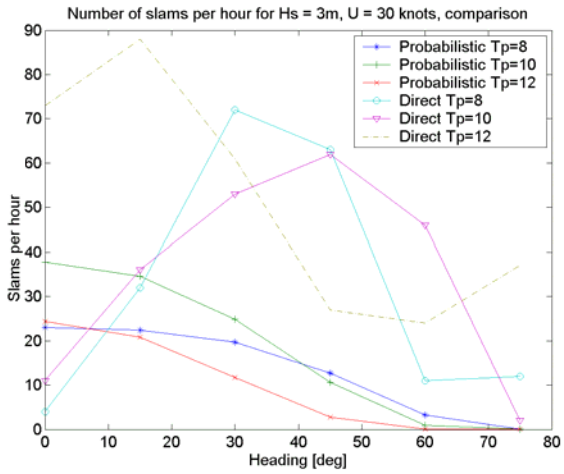

Fig. 5.21 Predicted slamming occurrence

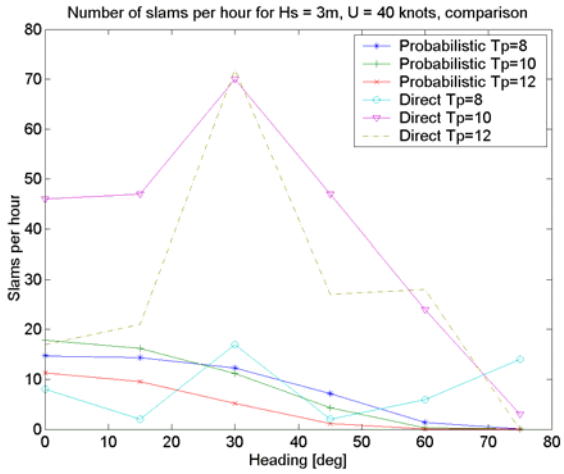

Fig. 5.22 Predicted slamming occurrence

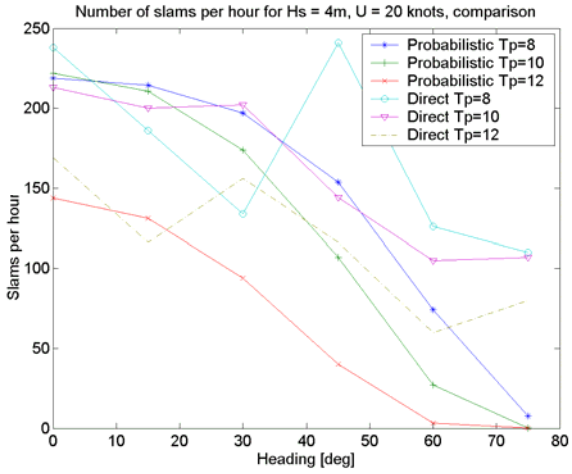

Fig. 5.23 Predicted slamming occurrence

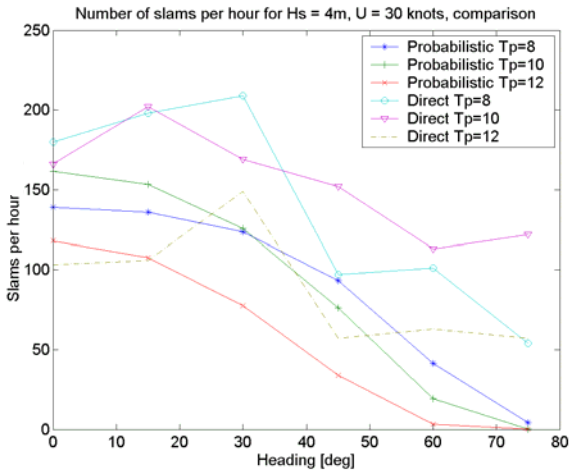

Fig. 5.24 Predicted slamming occurrence

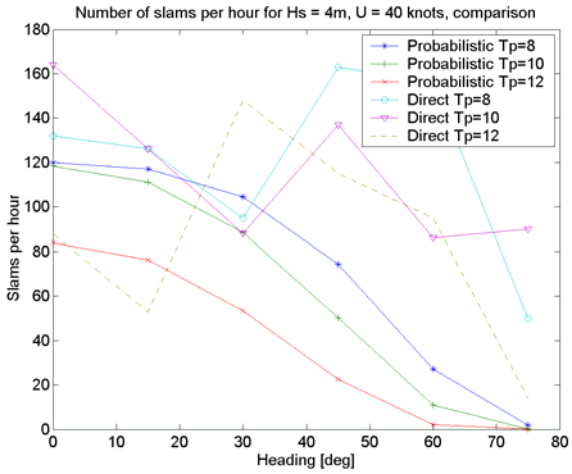

Fig. 5.25 Predicted slamming occurrence

5.2 Crowther Design 318

For crowther design 318 two motion prediction strategies were used. First the non-linear version of VERES was used, neglecting sailforces and heel angle. Although this is not a realistic situation it does provide a simple way to study the characteristics of the hull, and the effect of non-linearities can be investigated. The second method is more realistic where the sailing multihull strip theory was used to provide motion prediction. Further, only the direct method has been used for slamming identification. In the case where linear strip theory is used irregular time series were genereated prior to slamming identification. A one hour run time was chosen for all conditions. Slamming is mostly a problem for sailing

catamarans when sailing upwind, so a heading angle of 45 degrees to the waves was chosen for the analysis. This catamaran is special in that it has a central accomodation pod located between the hulls. This pod is located further aft but lower compared to the main beam. Since this is a critical location with regards to slamming the pod has deep-vee sections to reduce the impact loads. A representative point on the forward part of the pod centerline as well as a point on the underside of the mainbeam was chosen for slamming analysis.

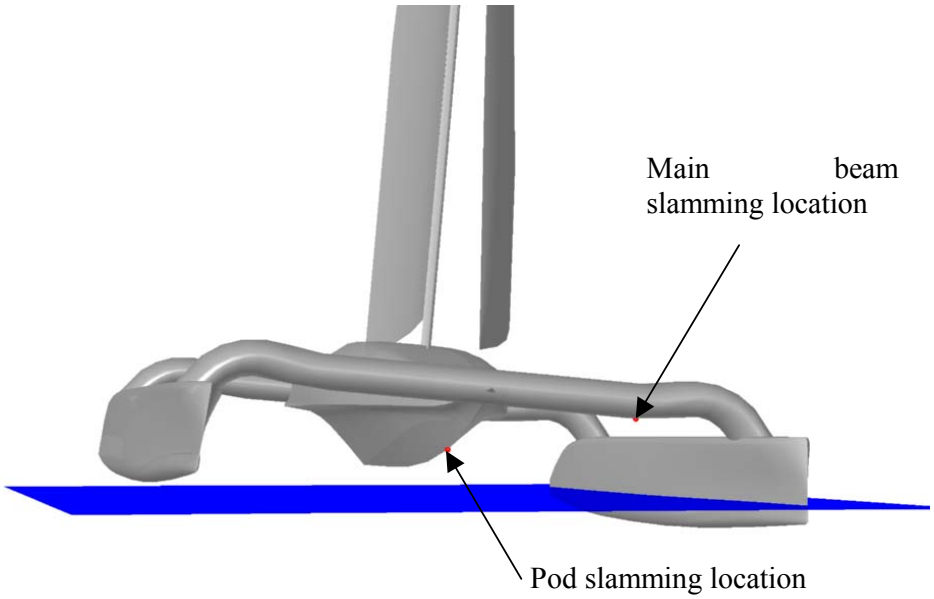

Fig. 5.26 Crowther design 318 slamming locations

5.2.1 Results from non-linear motion simulation

A total of 84 1 hour simulations were performed with the non-linear high-speed strip theory program VERES. Seastates with two different significant waveheights (Hs = 1m and Hs = 2m) were analysed, with average wave periods from 5 to 13s. The simulations were run with six different speeds, from 6 to 20 knots. The results are given below (fig. 5.27 – 5.34).

The number of slams per hour is highly dependent on the speed, waveheight and wave period, as seen on Austal hull 63. This particular hull is vulnerable to short period waves, at low speed. It is seen that the number of slamming incidents on the pod is much larger than the number of slams on the main beam.

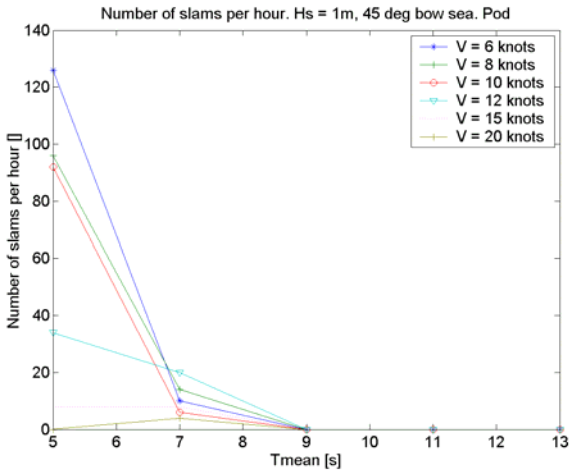

Fig. 5.27 Predicted slamming occurrence

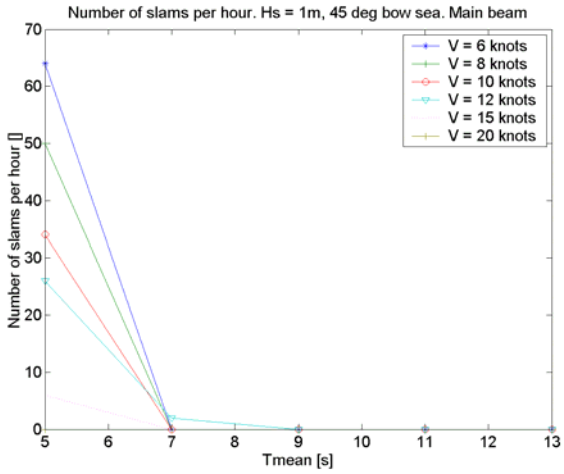

Fig. 5.28 Predicted slamming occurrence

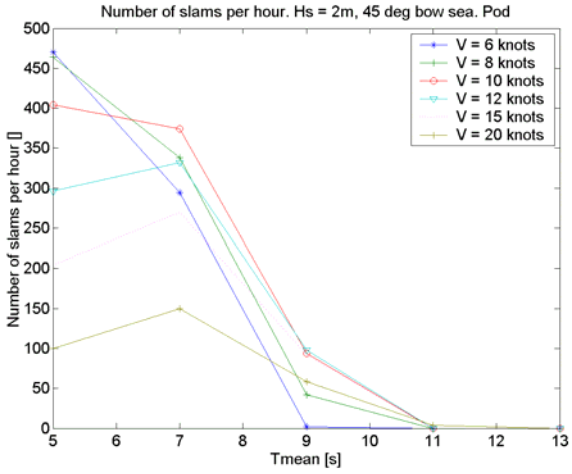

Fig. 5.29 Predicted slamming occurrence

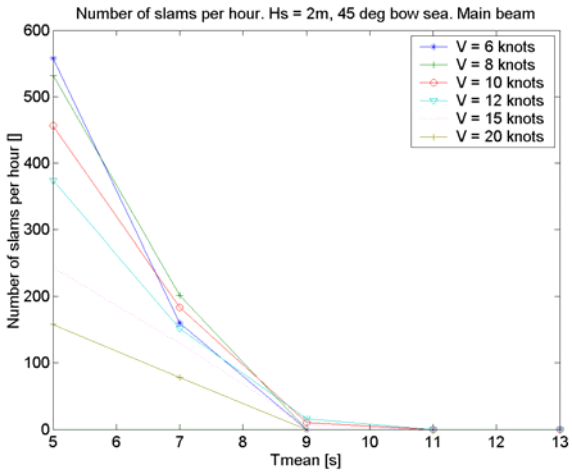

Fig. 5.30 Predicted slamming occurrence

The average impact velocity follows a similar trend, with most severe impacts at low speed in short waves. The main beam is shown to experience larger impact velocities than the pod, even though the pod will experience more frequent slamming.

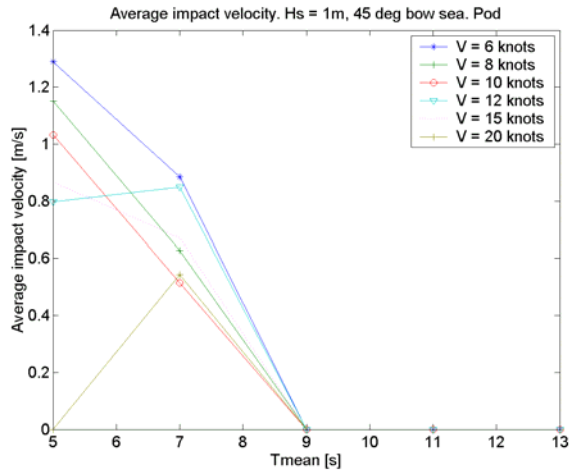

Fig. 5.31 Average impact velocity

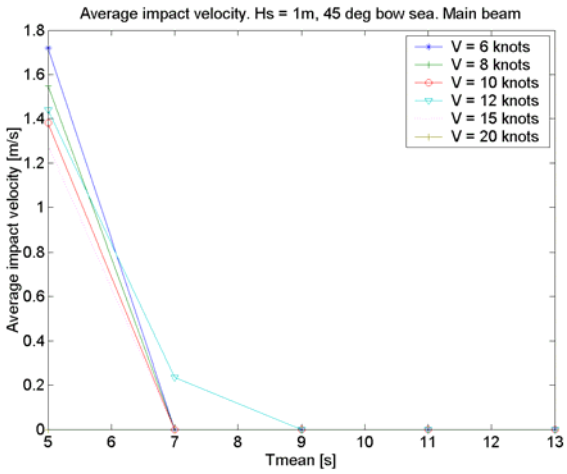

Fig. 5.32 Average impact velocity

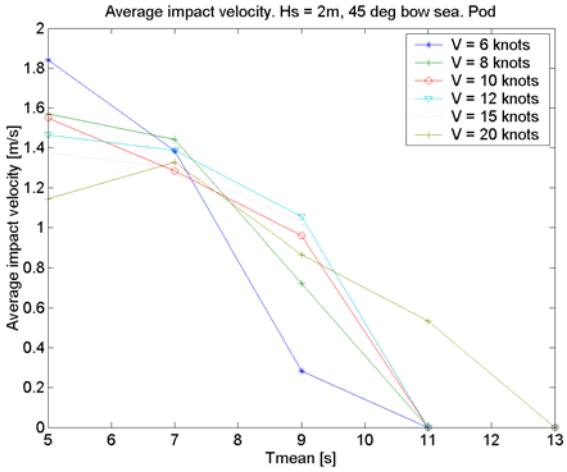

Fig. 5.33 Average impact velocity

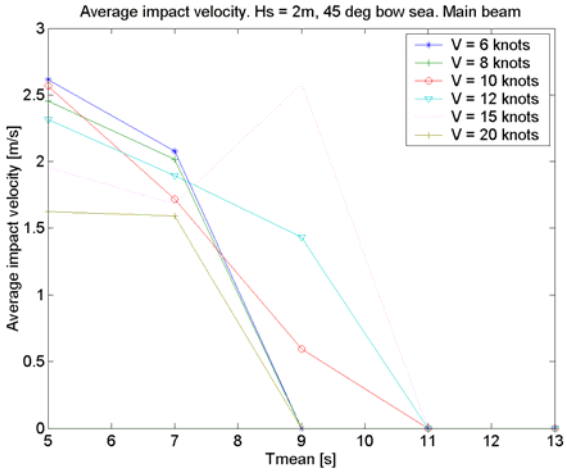

Fig. 5.34 Average impact velocity

5.2.2 Results from sailing multihull strip theory

It is assumed that the wind direction follows the wave direction. Three different speeds were chosen, 5 knots, 10 knots and 15 knots. Accurate performance data for the catamaran is not available, but it is believed that sailing at 5 knots corresponds well to sailing with very little heel angle (0 degrees). 10 knots corresponds to sailing with both hulls in the water but heeling (2 degrees) and 15 knots corresponds to sailing fully powered up with one hull flying (5 degrees). The location of the pod and main beam slamming locations change with varying heel angle, and this was incorporated in the computations. Seastates with three different significant wave heights were chosen for analysis, 0.75m, 1.5m and 2.25m, and the mean wave period was varied from 4 – 6 – 8s. No slamming was found for the seastates with Hs = 0.75m, and no further results are presented for that seastate.

The results (fig. 5.35 –5.38) show that slamming is only a problem in short waves, virtually no slamming is seen in seastates with Tmean = 6s and Tmean = 8s. Sailing at medium speed, 10 knots results in more slamming than sailing at high speed, 15 knots or low speed, 5 knots. This result is different from the result obtained earlier when the boat was sailed on one hull for all speeds, and it is obvious that modelling the ship motions at a proper sailing attitude is important for slamming. It is also clear that the pod experiences the most frequent slamming. The pod is obviously slamming quite severe both in the 1.5m seastate and the 2.25 m seastate while the main beam is in a much better position.

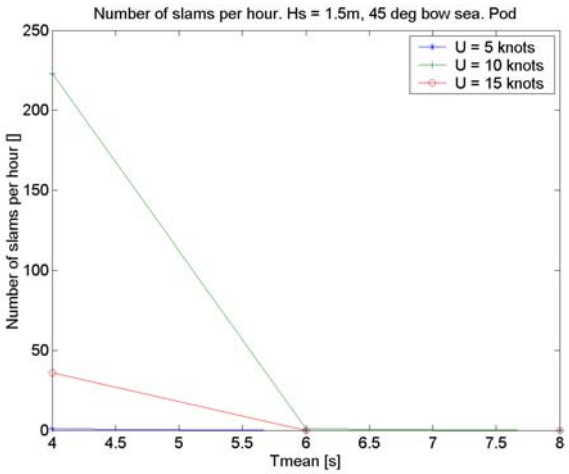

Fig. 5.35 Predicted slamming occurrence

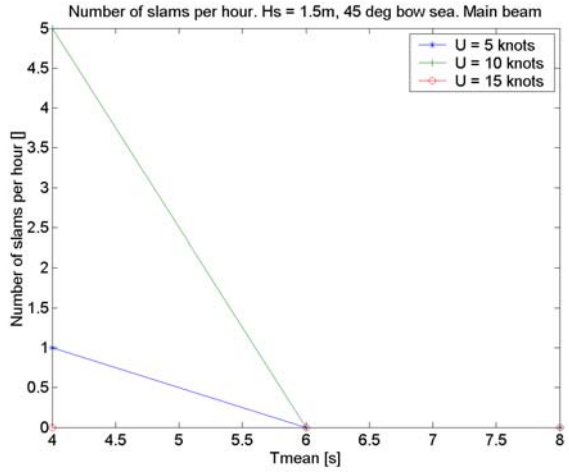

Fig. 5.36 Predicted slamming occurrence

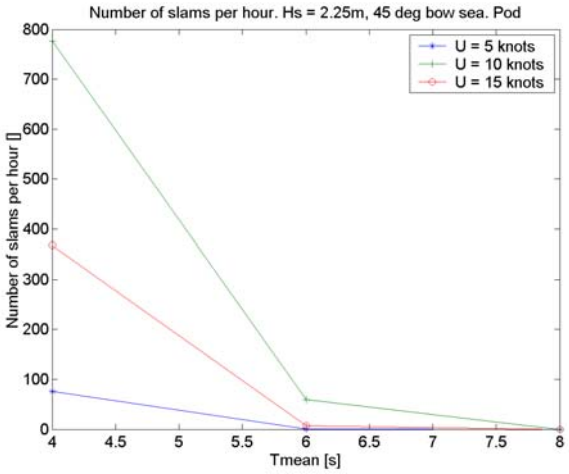

Fig. 5.37 Predicted slamming occurrence

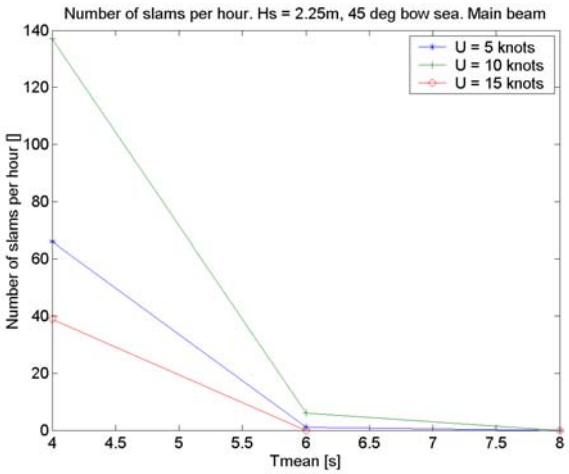

Fig. 5.38 Predicted slamming occurrence

The average impact velocities follow a similar trend, and high impact velocities are seen for the pod for seastates with Tmean = 4s. The main beam generally experiences smaller velocities.

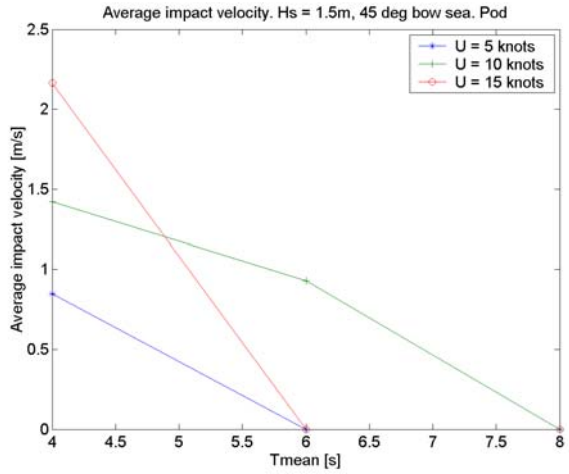

Fig. 5.39 Average impact velocity

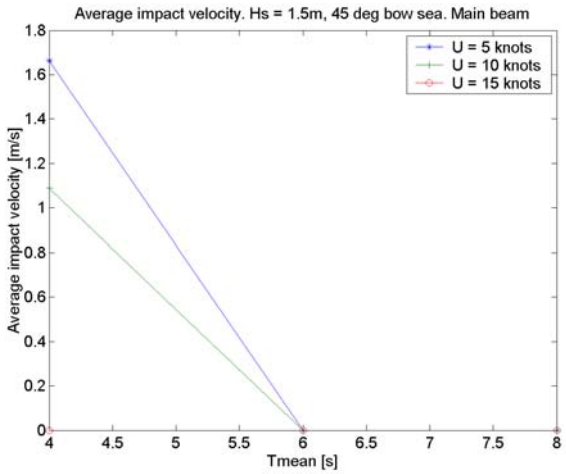

Fig. 5.40 Average impact velocity

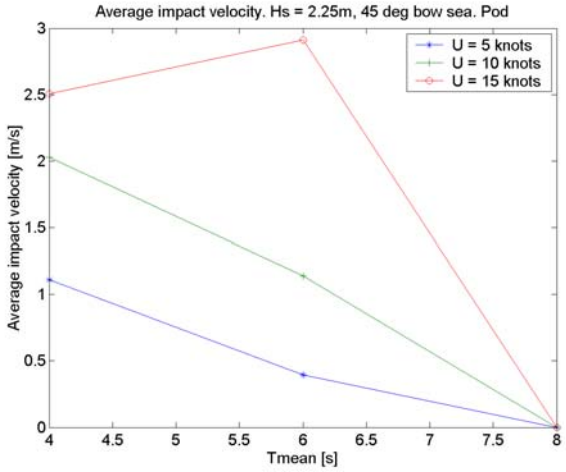

Fig. 5.41 Average impact velocity

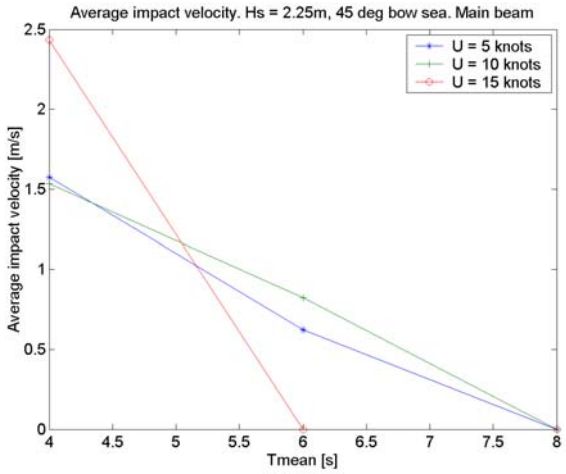

Fig. 5.42 Average impact velocity

5.3 Educat

During the seakeeping trials of Educat (described in detail in ch. 3) an attempt was made to measure slamming occurrence. Two methods were used. Firstly a purpose built slamming sensor was used to measure slamming pressure directly. Secondly, the slamming on the sidehulls could be identified from the accelerometer in the bow. The pod on Educat is mounted on rubber bushings, and each time the sidehulls were slamming a characteristic vibration of the pod occurred. Using an autocorrelation technique these slams can be identified. The wetdeck on Educat is too high for slamming to occur under normal operating conditions so it was decided to measure the slamming pressure on a small cylinder instead. The cylinder was designed so its height above the watersurface could be adjusted according to the wave conditions on the trial day (fig. 5.43).

Fig. 5.43 Slamming sensor mounted on Educat

Due to reasons discussed in chapter 7 the sensor gave unexpected low readings at speed, but it was still possible to identify slamming occurrences in at least one 10min run. The slamming pressure was recorded during the seakeeping trials.

The number of slams in a 10min full-scale run has been compared to simulated data, the results are shown in table 5.1. Simulated timeseries of the relative motion including slamming events are shown below for both locations (fig. 5.44 and fig. 5.45). The agreement is very good, but the dataset is limited.

Location	Number of slams pr 10min full-scale	Number of slams pr 10min simulation
Slamsensor	15	17
Sidehulls	198	203

Table 5.1 Full-scale slamming

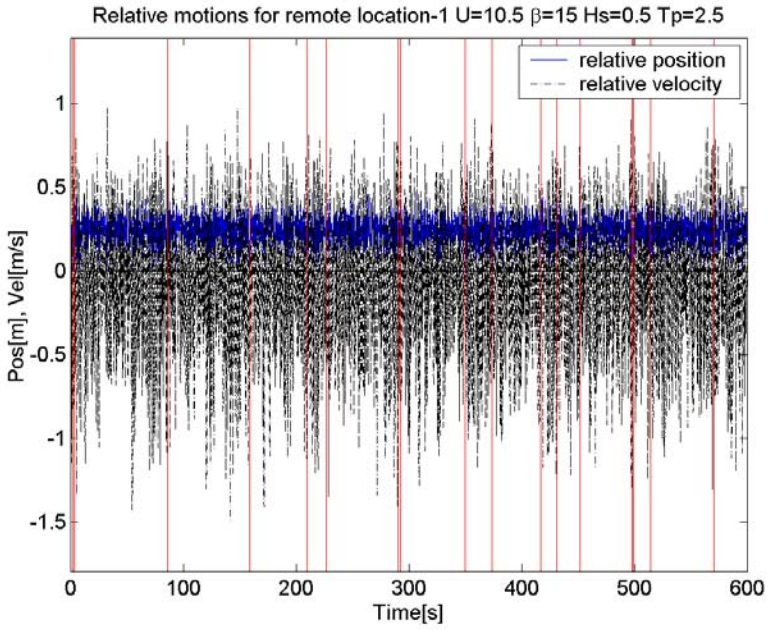

Fig. 5.44 Simulated relative motions and slamming for slamsensor

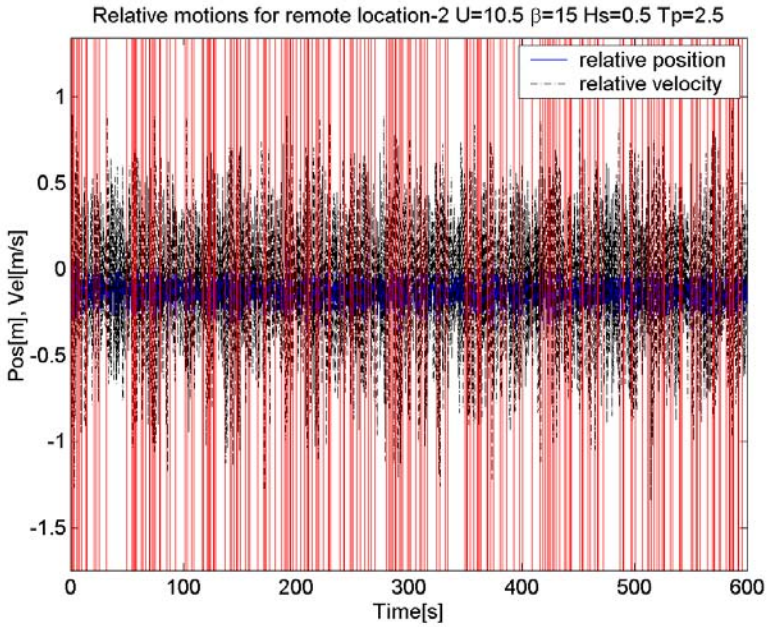

Fig. 5.45 Simulated relative motions and slamming for sidehulls

CHAPTER 6: SLAMMING PRESSURE CALCULATIONS

6.1 Calculation procedure

Having found the impact velocity at points of interest the remaining task is to calculate the slamming pressure. An existing 2-dimensional slamming theory is used to calculate slamming pressure on longitudinal strips of the wetdeck, bridgedeck or cross-beams. Forward speed effects are not included in the computations. In this work a constant velocity during the slam is used in the calculation. This is a reasonable assumption when the ship motions are not influenced by slamming. When calculating a single slam this has little importance as a non-constant velocity is easy to implement, but it reduces the workload greatly if several hundred slamming events are of interest. The latter is true if one wishes to calculate the slamming pressure distribution in an irregular seastate, which will be done in chapter 7. Also, the calculation is performed for an initially calm water surface, i.e. waves are ignored. Finally the body is assumed rigid and it is assumed no air pockets are formed during impact.

Research into the calculation of slamming pressure has not yet reached a mature stage, as evidenced by the long list of simplifications frequently used in the literature. However, several interesting theories including hydroelastic effects and 3-dimensional effects have been presented and may in time provide more accurate computations.

6.2 2-dimensional slamming theory

Local slamming pressures are calculated on 2-dimensional cross sections, according to the theory presented by Faltinsen and Zhao (Zhao & Faltinsen 1993). The computer program SLAM 2D by Marintek, Norway is one implementation of this theory and is used in the present work. For completeness

a brief description of the theory is given here, the full details can be found in (Zhao & Faltinsen 1993) and (*SLAM 2D users manual, Marintek*).

The 2 dimensional section is forced through an initially calm water surface with a velocity U. Waterdepth is infinite and the extent of the fluid domain is infinite.

Fig. 6.1 Local origin

The fluid is assumed incompressible and irrotational so that a velocity potential satisfying the Laplace equation

$$\frac{\partial^2 \phi}{\partial y^2} + \frac{\partial^2 \phi}{\partial z^2} = 0 \qquad (6.\ 1)$$

in the fluid domain exists. The pressure on the free surface is set to atmospheric pressure. This is correct at anytime except when an air pocket is formed in the initial stage of impact, this typically happens for flat sections or sections with a deadrise angle of less than 2 – 3 degrees. It is further assumed that the fluid accelerations during the impact are much larger than the gravitational acceleration and that the effect of gravity can be neglected.
Then, the dynamic and kinematic free surface conditions can be written as

$$\frac{\partial \phi}{\partial t} + \frac{1}{2}\left[\left(\frac{\partial \phi}{\partial y}\right)^2 + \left(\frac{\partial \phi}{\partial z}\right)^2\right] = 0 \ \text{ on } \ z = \zeta(y,t) \qquad (6.\ 2)$$

and

$$\frac{\partial \zeta}{\partial t} - \frac{\partial \phi}{\partial z} + \frac{\partial \phi}{\partial y}\frac{\partial \zeta}{\partial y} = 0 \text{ on } z = \zeta(y,t) \qquad (6.3)$$

$z = \zeta(y,t)$ is the free surface shape. The velocity potential is given the initial value $\phi = 0$ on the free surface. The body boundary condition is written as

$$\frac{\partial \phi}{\partial n} = -Un_3 \qquad (6.4)$$

where $\overset{\rightharpoonup}{n} = (n_2, n_3)$ is the unit normal vector to the body surface, positive direction is into the fluid domain.

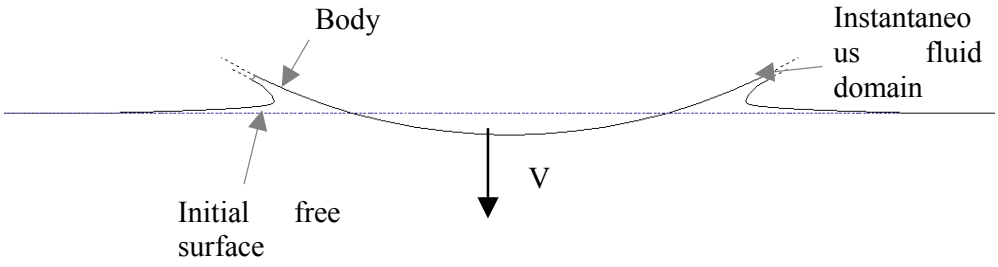

Fig. 6.2 Fluid domain

The velocity potential inside the fluid domain is given by Green's second identity,

$$2\pi\phi(y,z) = \int_S \left[\frac{\partial \phi(\eta,\zeta)}{\partial n(\eta,\zeta)}\log r - \phi(\eta,\zeta)\frac{\partial \log r}{\partial n(\eta,\zeta)}\right] ds(\eta,\zeta) \qquad (6.5)$$

where $r = \sqrt{(y-\eta)^2 + (z-\zeta)^2}$ and S is the surface enclosing Ω.

A boundary element method is used to obtain a solution close to the body. The body surface and the free surface is discretized into elements with constant velocity potential.

Far away from the body the contribution from the free surface can be represented by a vertical dipole in infinite fluid,

$$\phi(y,z) \sim \frac{A(t)z}{y^2 + z^2} \tag{6. 6}$$

and the integral over the outer part of the free surface can be written as

$$-A(t)\left(\begin{array}{l} \dfrac{\log\sqrt{(b \pm y)^2 + z^2}}{b} \pm \dfrac{y}{y^2 + z^2}\log\left(\dfrac{\sqrt{(b \pm y)^2 + z^2}}{b}\right) \\ + \dfrac{z}{y^2 + z^2}\left[\operatorname{sgn}(z)\dfrac{\pi}{2} - arctg\left(\dfrac{b \pm y}{z}\right)\right] \end{array}\right) \tag{6. 7}$$

The problem is solved as an initial value problem, with both the free surface elevation and the velocity potential set to zero at the start time. With the instantaneous velocity potential and wetted length found the pressure, force and moments can be calculated at each time instant.

The computed pressure over the instantaneous wetted length at each time step can be integrated to form both area and time averaged estimates of the impact pressure. The peak impact pressure can be extremely high, but has a very short duration and acts on a small area. If the duration of the peak impact pressure is much shorter than the natural period of the structure the peak impact pressure will not excite the structure. In this case it is important to integrate the pressure over time and area to give a realistic load-case. It is often assumed that

the slamming pressure is proportional to the impact velocity squared, and a slamming coefficient can be defined as

$$k_{slam} = \frac{p_{\max}}{\frac{1}{2}\rho|U|^2} \tag{6. 8}$$

The k factor can be calculated for a given pressure panel by SLAM2D, and is a purely geometric factor. Once it is found the slamming pressure for any impact velocity is easily calculated as

$$p = \frac{1}{2}\rho k_{slam}|U|^2 \tag{6. 9}$$

For simple geometries analytical methods can be used to determine the peak impact pressure. A simple wedge can be solved using Wagner's theory, and the k factor can easily be calculated according to (Faltinsen 1990) as

$$k_{slam} = \frac{\pi^2}{4}\cot^2\beta \text{ , where } \beta \text{ is the deadrise angle} \tag{6. 10}$$

CHAPTER 7: SLAMMING PRESSURE RESULTS

7.1 Austal Hull 63

To calculate slamming pressure on the wetdeck on Austal Hull 63 the 2 dimensional slamming analysis program SLAM 2D was used. Since there is no transverse curvature on the wetdeck it was decided to perform the analysis on a longitudinal strip on the wetdeck. Slamming is most likely to occur when the ship is pitching bow-down, and it was believed that this would provide the most realistic case for detailed analysis. As described in the previous chapter forward speed effects and the shape of the wave are not treated in the analysis. After a close examination of the structural drawings of the wetdeck it was decided to analyse a 1.4m panel, located in the forward part of the wetdeck (fig. 7.1). The length between sections is 1.4m and it is believed that damage is most likely to occur on plating between sections. In aft sections of the wetdeck it is likely that the ships own waves will reduce the airgap under the wetdeck and should be included in the analysis. Slamming on the aft part of the wetdeck is reported to be an occasional problem on smaller catamaran, but is less critical for ships in the size range analysed here. The reduction of airgap due to radiated and diffracted waves and their interaction with the incident waves are not included in the analysis.

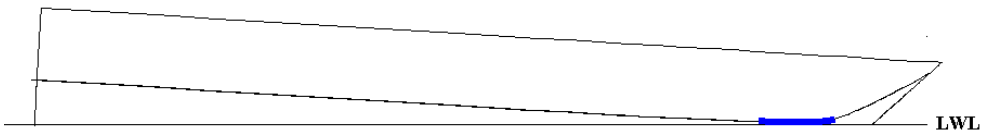

Fig. 7.1 Slamming pressure panel Austal hull 63

7.1.1 Calculated slamming pressures

The program SLAM 2D was used to calculate both the time dependent pressure history for a constant velocity impact and the k factor.

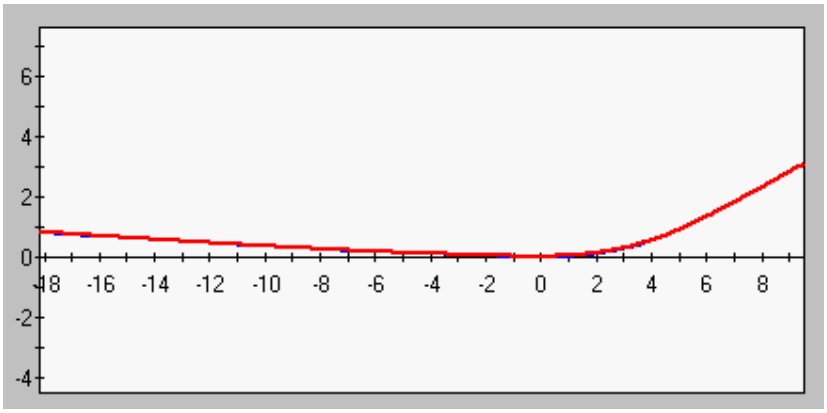

Fig. 7.2 Wetdeck section

Austal H 63 slamming pressure, 4m/s impact

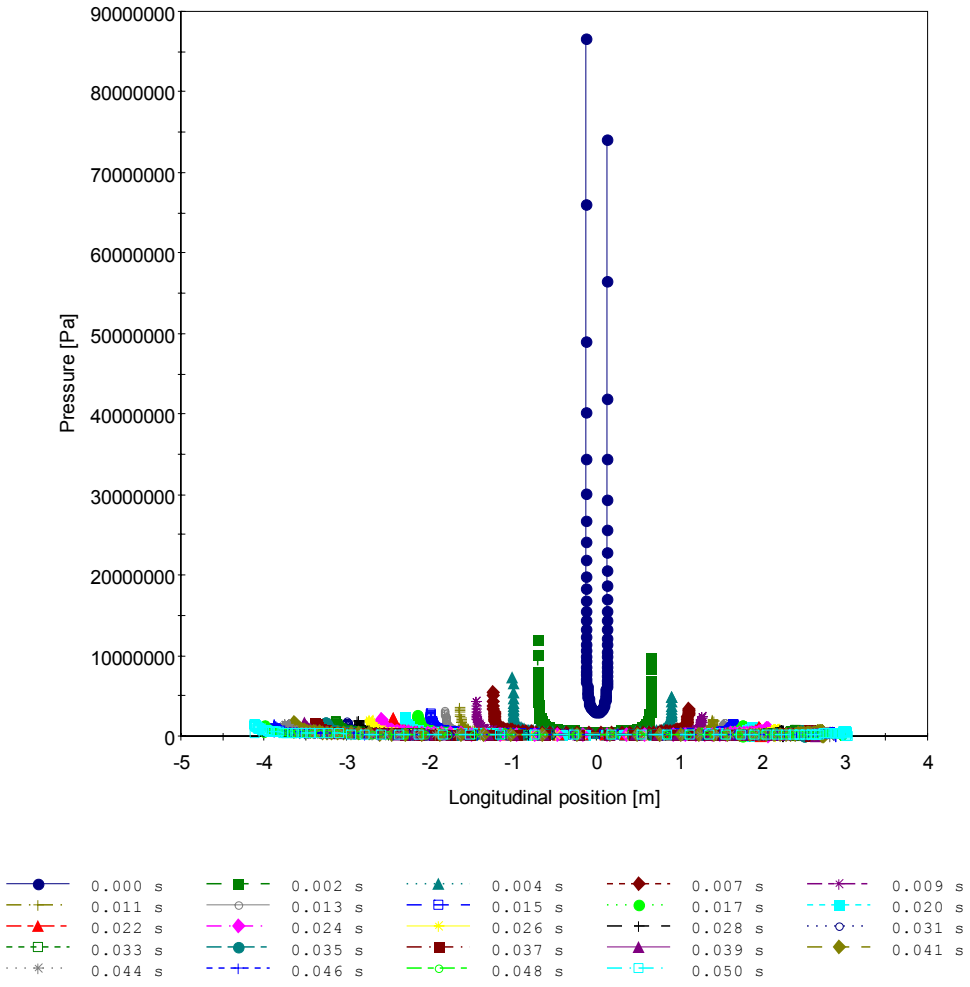

Fig. 7.3 Impact pressure time history

The impact pressure time history (fig. 7.3) for the wetdeck (fig. 7.2) shows that maximum slamming pressure is extremely high, but with a very short duration. It is possible that the peak pressure will be influenced by the creation of an air pocket and water compressibility effects, but the duration is so short that it will generally not excite the structure (Faltinsen 2002). The pressure acting on a slightly longer time scale is however much more interesting and generally easier to predict. It is also easy to see how the pressure peak moves during the slam. The highest pressure is found at the intersection of the body and the free surface, and is hence moving extremely rapid.

Austal H 63 average slamming pressure, 4m/s impact

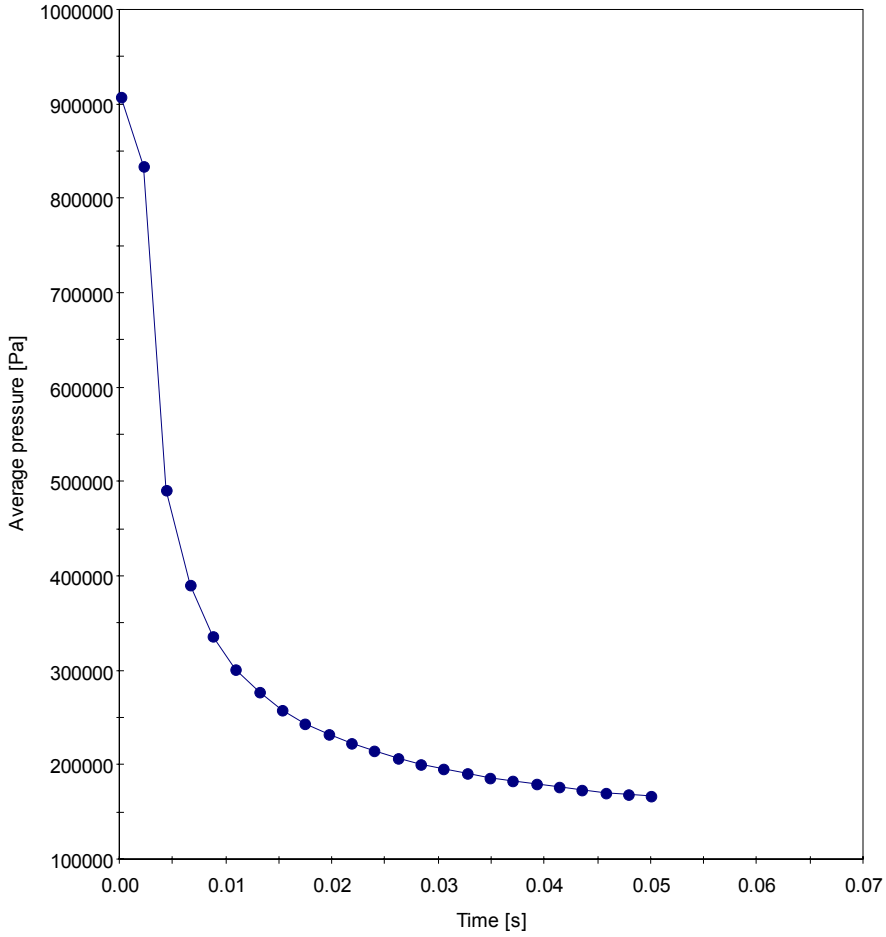

Fig. 7.4 Average impact pressure time history

Also of interest is the average pressure vs time (fig. 7.4) on a chosen pressure panel located between two stiffeners on the underside of the wetdeck. Again we see that the peak pressure is high, but much smaller than in (fig. 7.3) due to the area averaging. The non-dimensional k factor was also calculated for the pressure panel and is given below (table 7.1).

Calculated k_{slam} factor	113.7

Table 7.1 k_{slam} factor

The calculated k factor corresponds to an area averaged peak pressure of 932 kPa over the panel for the 4 m/s impact velocity shown above (fig. 7.3 and Fig. 7.4).

7.1.2 Slamming pressure distribution

Finally, using the computed impact velocities and the computed k factor the distribution of slamming pressures can be calculated in a realistic seaway. The pressure shown is the area averaged but not time averaged peak pressure. A large set of results have been calculated for a systematic variation of the seastate: Two significant waveheights, 3 and 4m. Three forward speeds, 20, 30 and 40 knots. Three wave mean periods, 8, 10 and 12s. Six headings, 0, 15, 30, 45, 60 and 75 degrees from head sea. The full results are given in appendix 2, while a few sample plots are presented below (fig. 7.5 – Fig. 7.10). Note that the axes are scaled differently for each plot to provide optimum resolution.

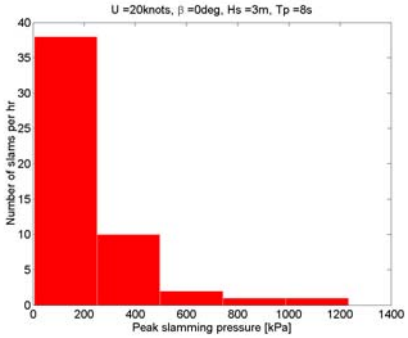

Fig. 7.5 Slamming pressure distribution

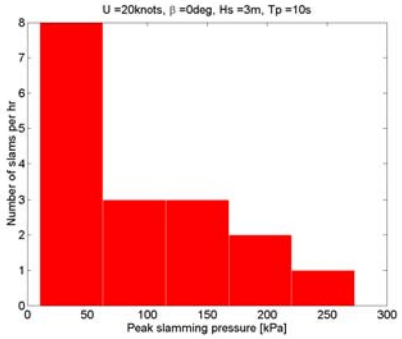

Fig. 7.6 Slamming pressure distribution

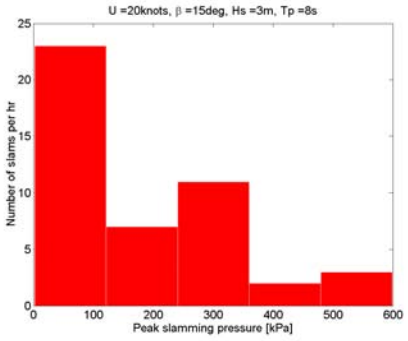

Fig. 7.7 Slamming pressure distribution

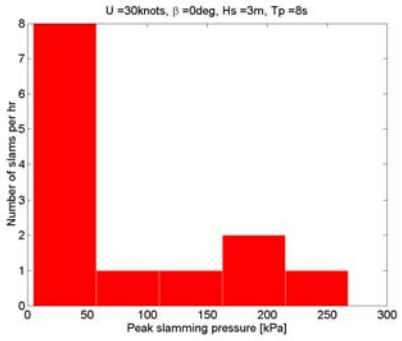

Fig. 7.8 Slamming pressure distribution

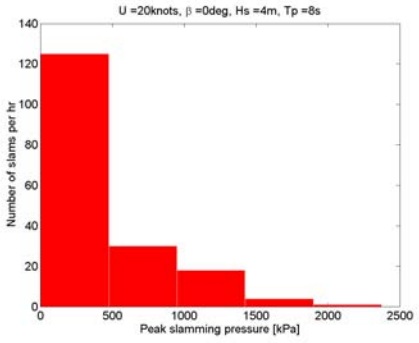

Fig. 7.9 Slamming pressure distribution

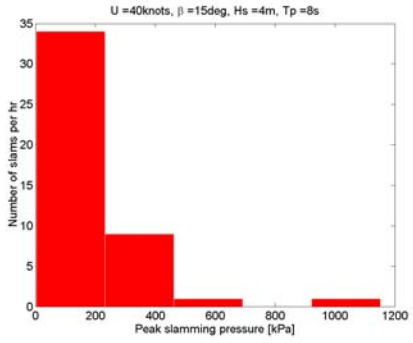

Fig. 7.10 Slamming pressure distribution

It can be clearly seen that most slamming impacts are light, with a smaller number of more severe slams. The figures also give useful information about how the slamming pressure and the number of slams change with different wave heights, wave period, speeds and headings.

For conditions where few slamming events are recorded in the one hour simulations the statistical uncertainty is large.

7.2 Crowther 318 original

The sailing catamaran Crowther design 318 has been analysed for two slamming locations, the pod and the main beam (fig. 5.26). The pod has deep vee sections, and a transverse section was chosen for analysis. The other location considered is the main beam, and here a longitudinal section was chosen for analysis.

7.2.1 Slamming pressure calculations

The pod has a wedge shaped sectional shape with a 45 degree deadrise angle (fig. 7.11). The calculation was performed with SLAM 2D, but the simple geometry meant that the computed k factor could also be checked against an analytical solution (eq. 5.10) providing a useful check of the accuracy of SLAM 2D.

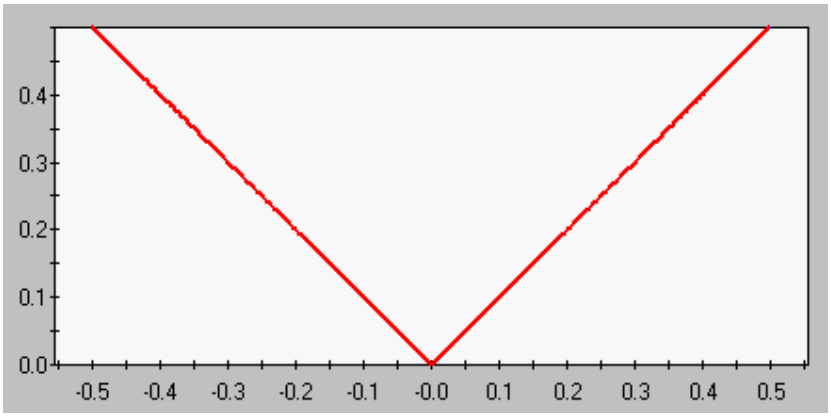

Fig. 7.11 Pod section

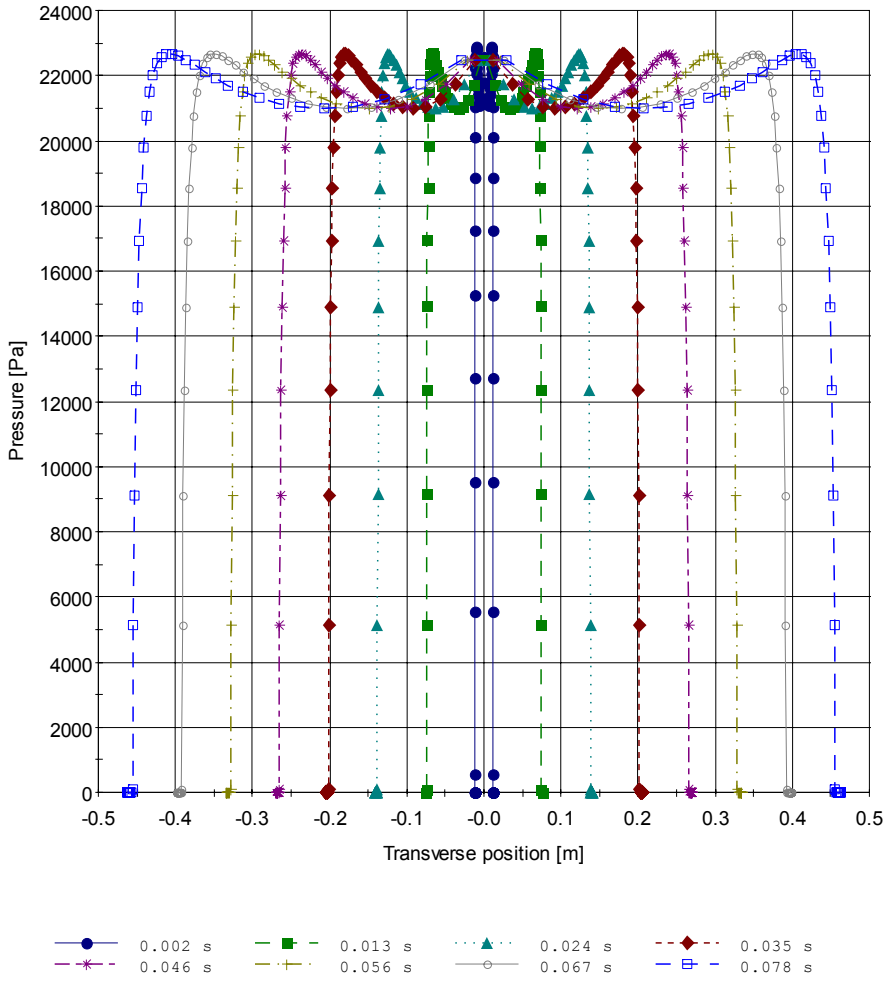

Fig. 7.12 Impact pressure time history

The impact pressure time history (fig. 7.12) shows a very different behaviour compared to the Austal wetdeck section. The peak slamming pressure is constant during the whole impact, but moves outward with the intersection of the wetted surface and the free surface. There is also a peak pressure with similar magnitude at the centreline, which was not seen for the more irregular shape of the Austal wetdeck. In general the pressure is distributed very evenly over the wetted area of the section.

Crowther 318 pod average slamming pressure, 4m/s impact

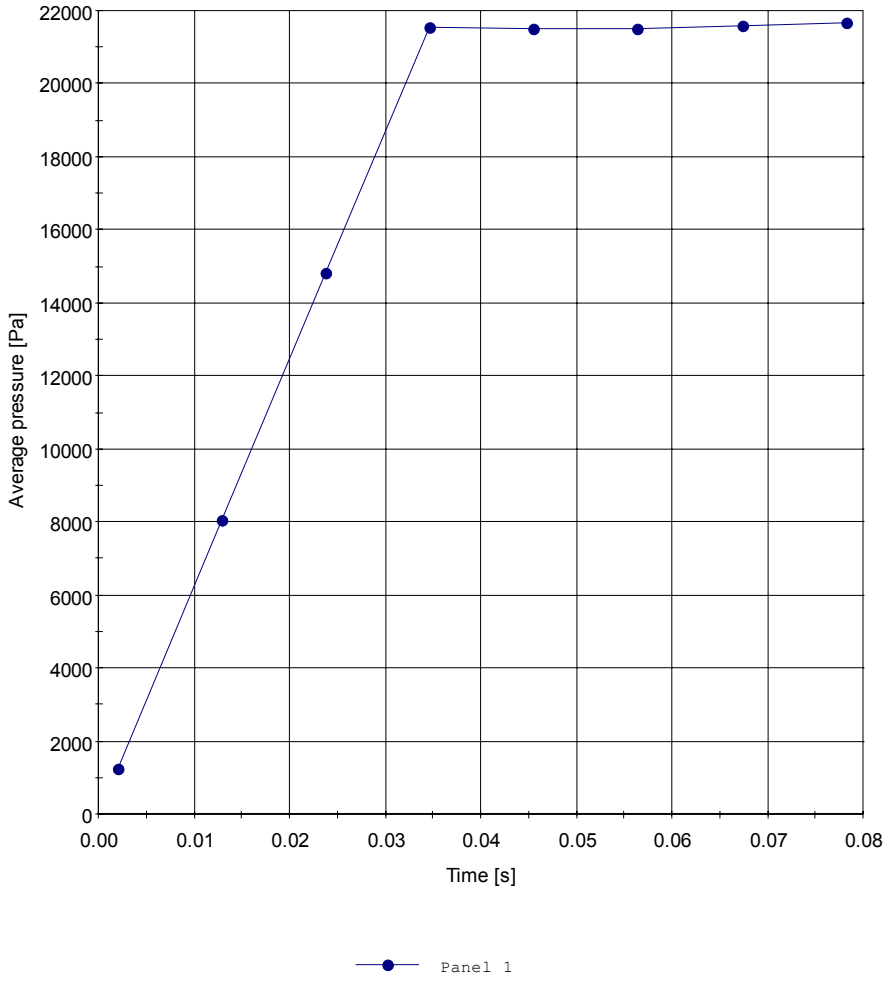

Fig. 7.13 Average impact pressure time history

The pressure panel here has a total width of 0.4m, and the average pressure rises constantly as the wetted area increases. The area averaged impact pressure time history (fig. 7.13) shows a linear rise in the average impact pressure until it reaches a steady state at 0.035 s. At 0.035s the pressure panel is fully submerged and the pressure remains constant.

The k factor was calculated by SLAM 2D and using eq. 5.10 for comparison. The results are given below (table 7.2) and show a fair agreement.

Calculated k_{slam} factor Pod	2.71
Wagner k_{slam} factor Pod	2.47

Table 7.2 Pod k_{slam} factor

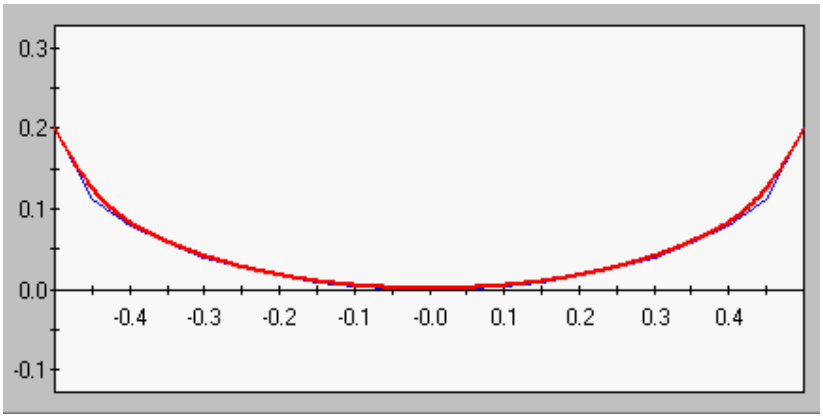

Fig. 7.14 Main beam section

Crowther 318 average slamming pressure, 4m/s impact

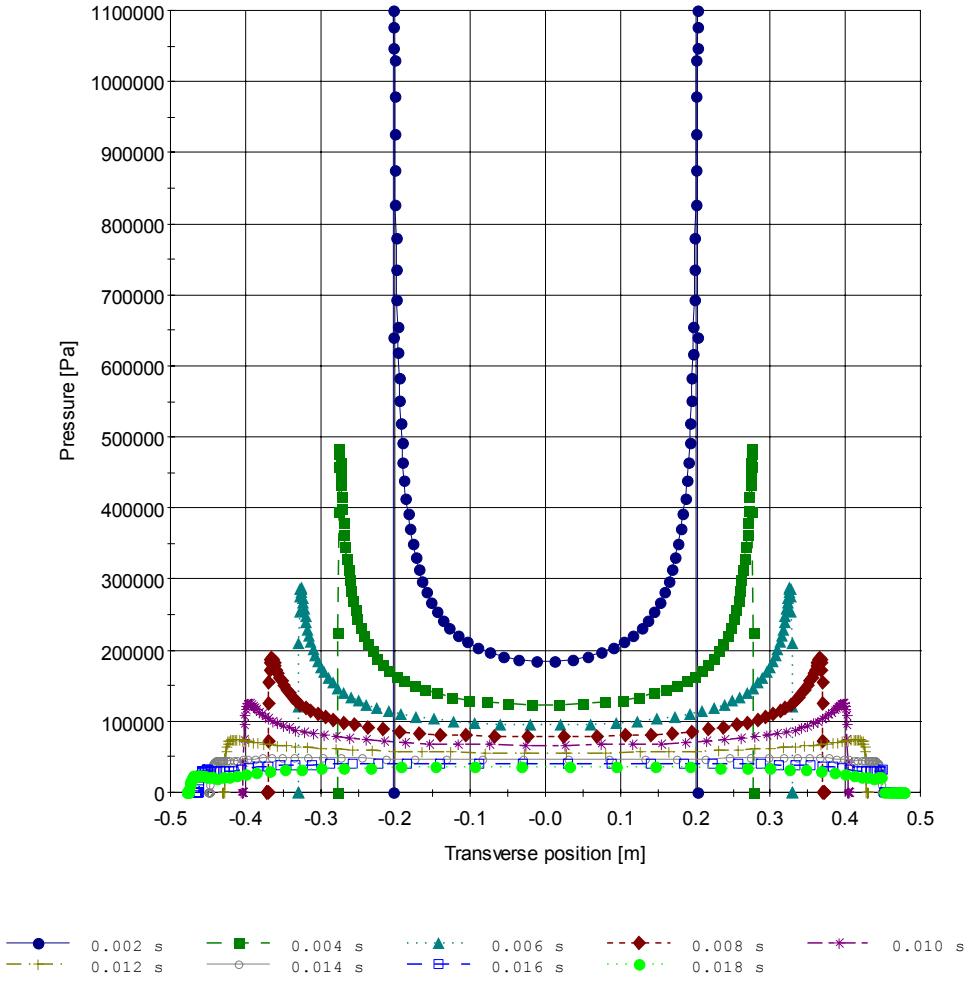

Fig. 7.15 Impact pressure time history

The impact pressure time history of the main beam (fig. 7.14 and fig. 7.15) shows a similar behaviour to the Austal wetdeck section, with a sharp pressure peak at the intersection of the body and the free surface.

Crowther 318 average slamming pressure (0.4m panel), 4m/s impact

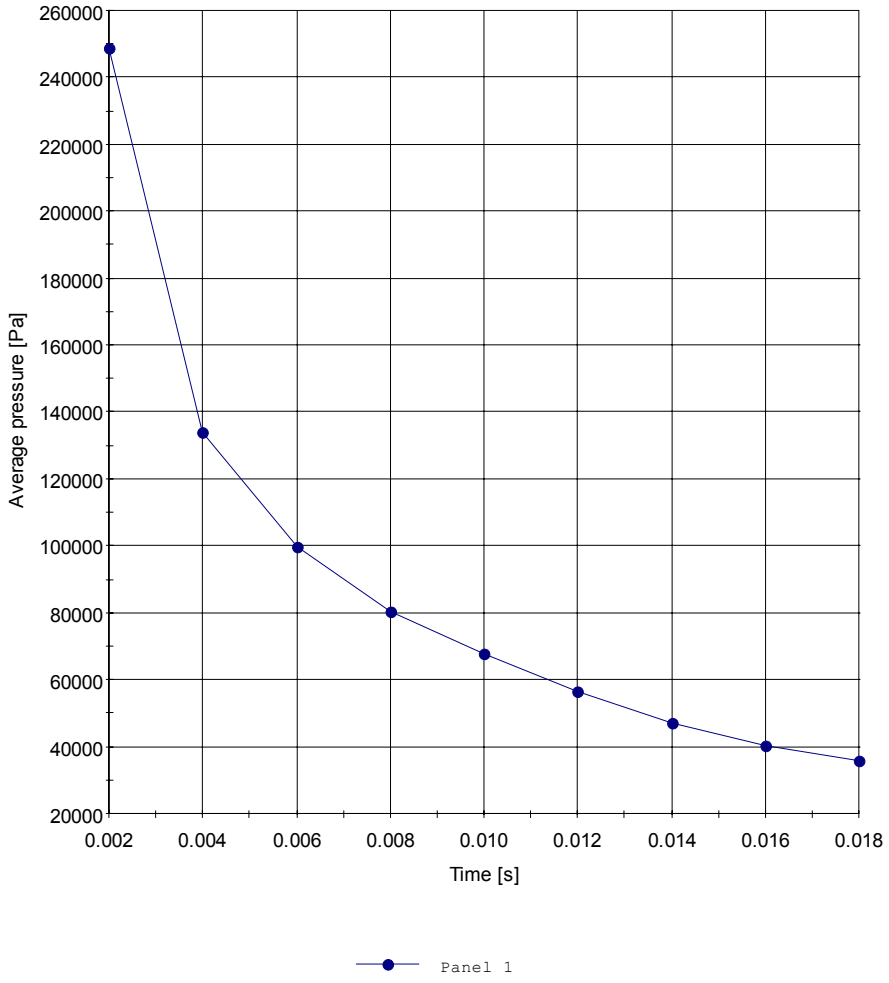

Fig. 7.16 Average impact pressure time history

The area averaged impact pressure time history on the main beam (fig. 7.16) shows a high peak pressure, but it is of very short duration. The k factor was also calculated for this section and is given below (table 7.3)

Calculated k_{slam} factor Main beam	40.8

Table 7.3 Main beam k_{slam} factor

Both from the pressure histories (fig. 7.15 and Fig. 7.16) and the calculated k factor (table 7.3) it is clear that the main beam will give much higher slamming pressures than the pod for the same impact velocity. This is an

excellent example showing how important the geometry of the section is to the impact pressure.

7.2.2 Slamming pressure distribution

Using the calculated k factors for the pod and the main beam and the impact velocities found in chapter 5 the slamming pressure distributions can be calculated and plotted in a similar way as for Austal hull 63. For Crowther design 318 two ship motion prediction methods have been used as discussed in chapter 3, one simplified using high-speed strip theory and a more complete analysis using a new strip theory for sailing multihulls. The full results are given in appendix 2, with a selected set of results given below.

Slamming pressure distributions with ship motion prediction from high-speed theory are listed below for the pod (fig. 7.17 – Fig. 7.20).

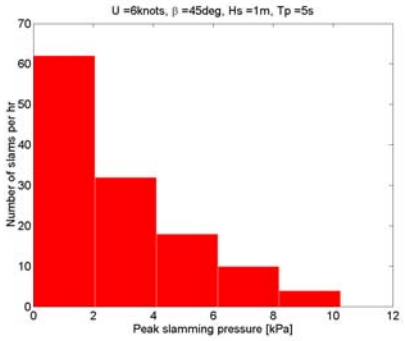

Fig. 7.17 Pod slamming pressure distribution

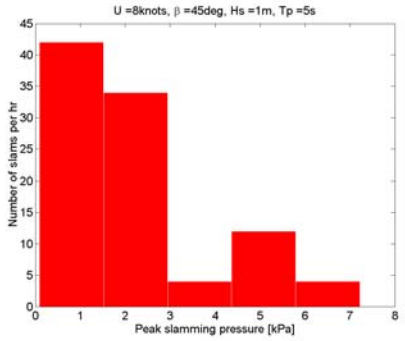

Fig. 7.18 Pod slamming pressure distribution

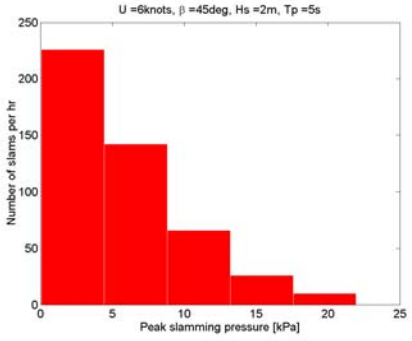

Fig. 7.19 Pod slamming pressure distribution

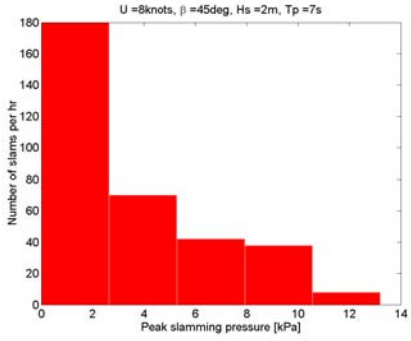

Fig. 7.20 Pod slamming pressure distribution

Sample slamming pressure distribution for the main beam are shown below (fig. 7.21 – Fig. 7.24).

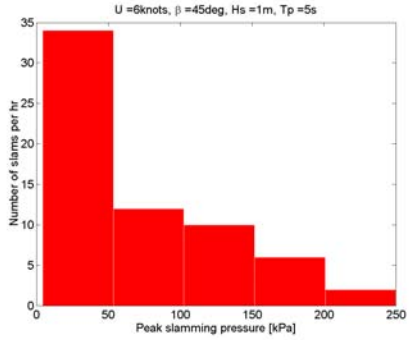

Fig. 7.21 Main beam slamming pressure distribution

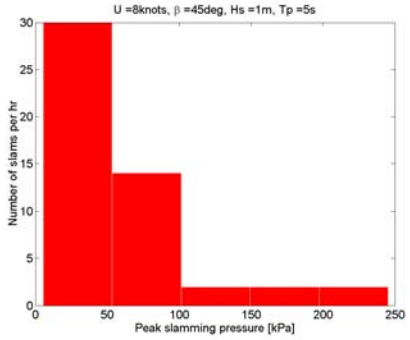

Fig. 7.22 Main beam slamming pressure distribution

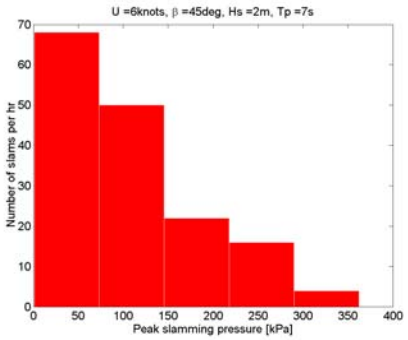

Fig. 7.23 Main beam slamming pressure distribution

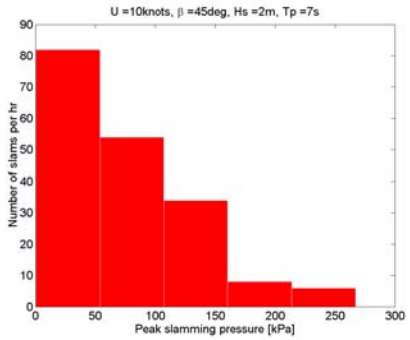

Fig. 7.24 Main beam slamming pressure distribution

Comparing the slamming pressure distributions it is clear that the pod experiences the most frequent slamming, as observed in chapter 5. More importantly however is the difference in slamming pressures observed, the main beam is exposed to much higher pressures than the pod.

Finally, slamming pressure distributions with ship motion prediction from the sailing multihulls strip theory are calculated. Sample distributions are given below for the pod (fig. 7.25 – Fig. 7.28) while the complete results are given in appendix 2.

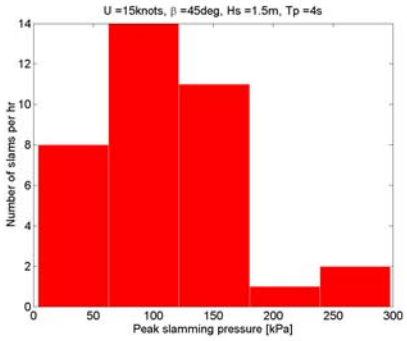

Fig. 7.25 Pod slamming pressure distribution

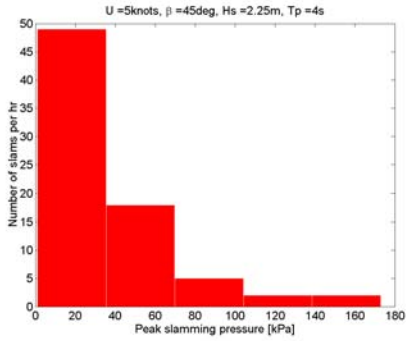

Fig. 7.26 Pod slamming pressure distribution

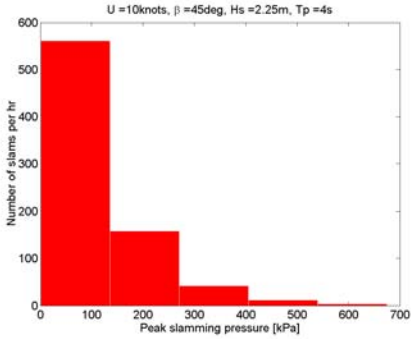

Fig. 7.27 Pod slamming pressure distribution

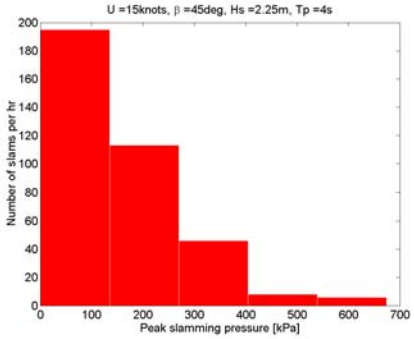

Fig. 7.28 Pod slamming pressure distribution

Similarily for the main beam (fig. 7.29 and Fig. 7.30).

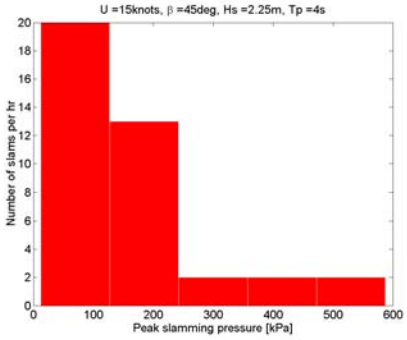

Fig. 7.29 Main beam slamming pressure distribution

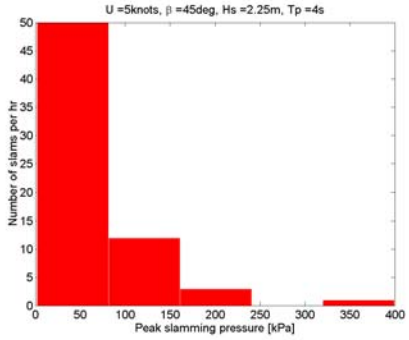

Fig. 7.30 Main beam slamming pressure distribution

7.3 Educat full-scale slamming measurements

During the full-scale trial of Educat the slamming sensor did not give the expected results. The sensor was tested before and after the trial at zero speed and was found to function satisfactory. For the majority of the slams the pressure

reading was barely noticeable even though the slamming sensor was clearly submerged. A few slams did however register as expected, a typical slam is shown below (fig. 7.31).

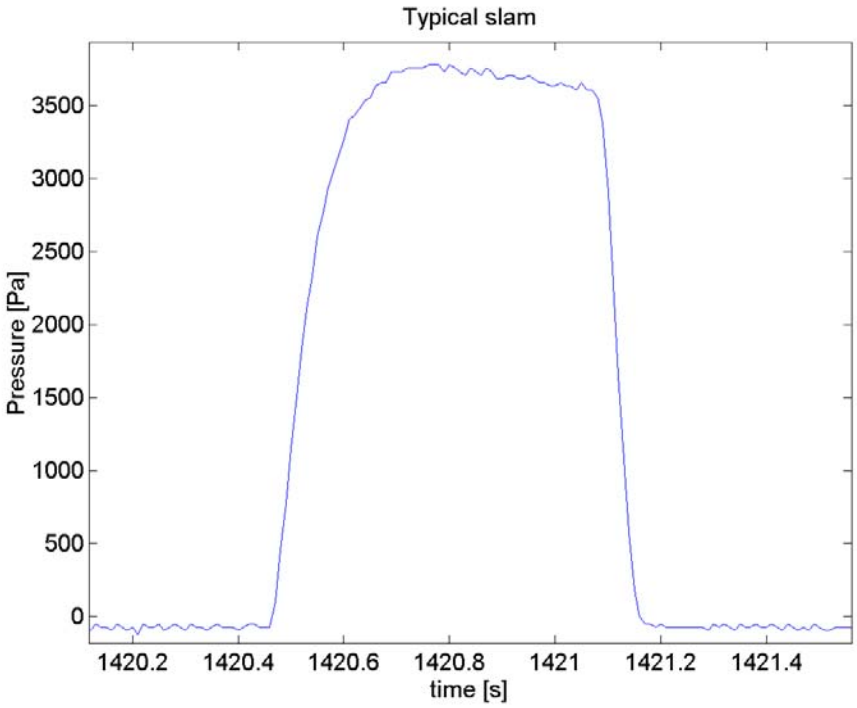

Fig. 7.31 Typical impact pressure

This can be compared to a typical slam for the same section, calculated from SLAM 2D (fig. 7.32) with an impact velocity of 1m/s. The peak value is similar, but the timescale is very different from full-scale to the calculation. If we instead look at purely hydrostatic pressure, a submergence of 0.4m corresponds to a hydrostatic pressure of 4022Pa. A submergence of 0.4m was about the largest submergence observed. It is most likely that hydrostatic pressure is dominating the slamming pressure for this slamming sensor at the low impact velocities experienced.

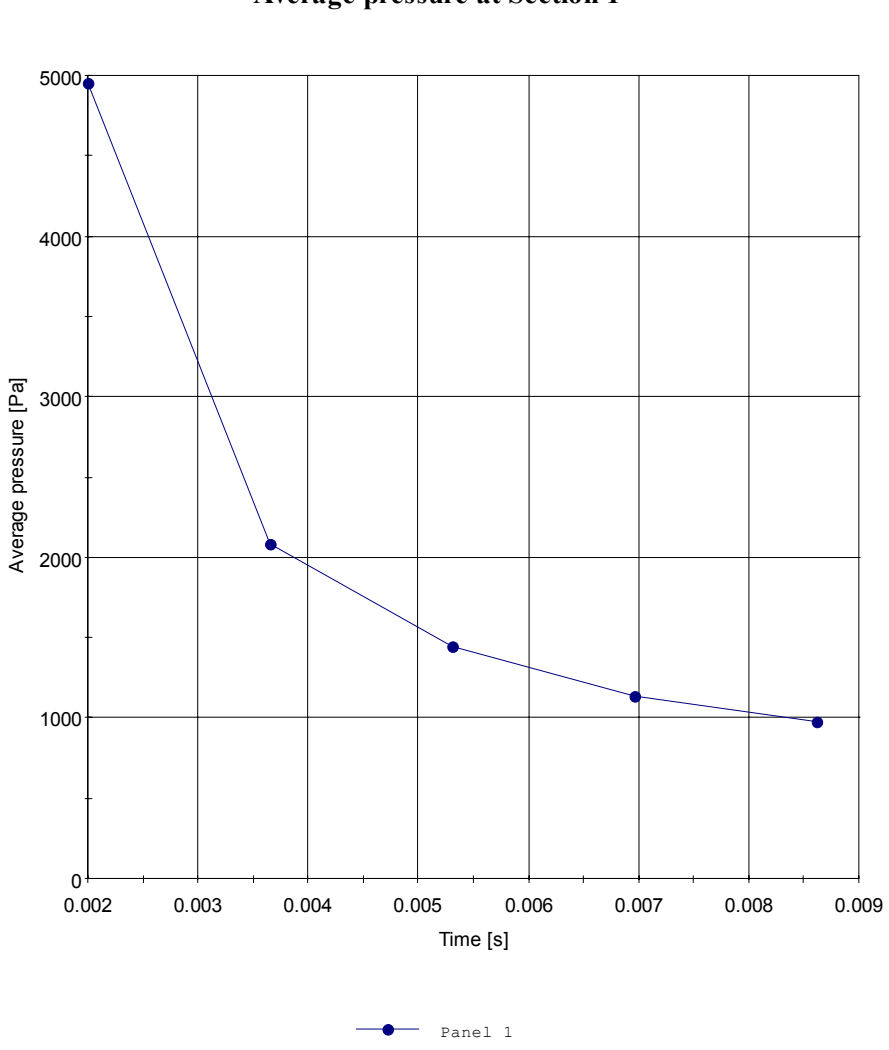

Fig. 7.32 Calculated slamming pressure, 1 m/s impact

This does not however explain why so few slams registered. During the trial it was clear that the forward speed effects on the sensor were significant. At times it looked like a separation bubble formed over the whole lower surface of the sensor at impact, and this could explain why the pressure was so low. It is also believed that the steady pressure distribution of the sensor was disadvantageous. Although the section is round we can get some insight into the problem by treating it as an infinitely long foil. This is a gross simplification as the foil here as an extremely low aspect ratio, but it is nevertheless a useful and simple way to study the pressure situation. By using a 2 dimensional airfoil

analysis program (Drela & Youngren 2001) the pressure distribution has been plotted for the section (fig. 7.33). It can be seen that a stagnation point is found on the nose of the section while a low pressure region is found along the section. From this we learn that there will be a negative pressure at forward speed, but we cannot predict the value with confidence from this method. In order for a slam to register it is however necessary to overcome this steady low pressure. For larger (real) ships this will not be a problem but for a small section operating at a high speed it can be significant.

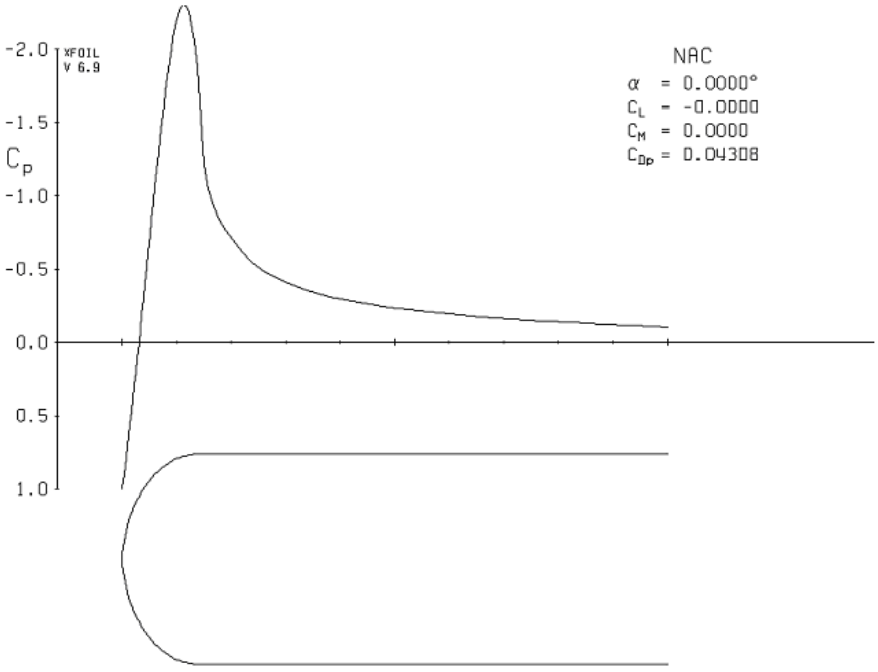

Fig. 7.33 Pressure distribution for 2D section

To further add to the confusion it is clear from the calculated slamming pressure (fig. 7.29) that the sampling rate must be extremely high in order to capture the impact pressure, especially on small sections. The importance of this has only been fully realized after the trial, but since the sensor registered test slams at zero forward speed this cannot be the only reason. It is likely that a combination of the above mentioned factors is the reason why the results were

unexpected. The final conclusion can only be that a different method to measure slamming pressure should be used in future trials.

CHAPTER 8: PARAMETRIC STUDY

8.1 Austal Hull 63

A parametric study with variation of important hullform parameters has been performed for Austal Hull 63. Austal Hull 63 is an existing vessel, but the following results are an example of a study that would be useful to designers in the initial design phase of the vessel. In this work two new hullforms were created from the base hull. One version was 10 m longer than the original hull, to study the effect of size on slamming occurrence. The cross sections of the hull were kept constant, and the displacement was increased accordingly. Another version kept the length of the base model constant but the beam of the individual hull was increased. A change in demihull beam would have a very small change on the displacement so the draft was reduced to keep the displacement constant. The location of the bridgedeck was kept constant for these variations. Two models which kept the original hull-shape but with different wetdeck location were also created. One version had the bridgedeck moved 3m aft while keeping the original height, while another version had the bridgedeck in the original longitudinal location but with the vertical clearance increased by 0.5m. The different variations are summarized in table 8.1

Hull no	Length change	Demihull beam change	Wetdeck longitudinal position change	Wetdeck vertical position change
Base	0 m	0 m	0 m	0 m
1	+ 10 m	0 m	0 m	0 m
2	0 m	+0.737 m	0 m	0 m
3	0 m	0 m	3 m aft	0 m
4	0 m	0 m	0 m	+ 0.5 m

Table 8.1 Austal Hull 63 variations

There is a distinct difference between the first two variations (length and demihull beam)and the last two (bridgedeck location). Changing the length and beam of the hull changes the seakeeping characteristics of the hull, which in turn will change the likelihood and severity of slamming. New ship motion

predictions would naturally have to be performed to predict the slamming occurrence on a modified hull form. By changing the location of the bridgedeck the seakeeping qualities of the hull are unchanged (except for slamming) and there is no need to perform new ship motion predictions. A logical design procedure is then to optimise the hull first, from a seakeeping, resistance and practical view. Then the optimum bridgedeck location can be found. If the bridgedeck location is limited then it is important to optimise the hullform.

Hull	**Number of slams per hour**	**Average impact velocity [m/s]**
Base	178	2.27
1	181	1.91
2	187	1.99
3	113	1.70
4	82	1.63

Table 8.2 Slamming results 20 knots

Hull	**Number of slams per hour**	**Average impact velocity [m/s]**
Base	98	1.78
1	107	1.76
2	112	1.73
3	69	1.43
4	33	1.64

Table 8.3 Slamming results 30 knots

Hull	**Number of slams per hour**	**Average impact velocity [m/s]**
Base	51	1.30
1	52	1.29
2	57	1.85
3	28	1.38
4	10	1.042

Table 8.4 Slamming results 40 knots

The results (table 8.2 –8.4) show that the modified hullforms have an increased number of slams. The changes are generally small. Altering the

location of the wetdeck on the other hand has a much more dramatic effect, especially increasing the wetdeck clearance. Moving the wetdeck further aft (A location in the forward part in the wetdeck is considered here) also reduces the number of impacts, due to reduced influence of pitch on the relative vertical motions.

8.2 Crowther

A parametric study of Crowther design 318 was also performed, following the same procedure as used for Austal hull 63. The sailing multihull strip theory was used for motion prediction. Two models based on the original hull were created for the study. One hull was 1m longer than the original, with unchanged cross sections. Another hull kept the original length but the waterline beam was increased and the draft reduced. Two model based on the original hull shape but with different location of the pod and the main beam were also studied. The different configurations are summarized below (table 8.5).

Hull no	**Length change**	**Demihull beam change**	**Pod/Main Beam longitudinal position change**	**Pod/Main Beam vertical position change**
Base	0 m	0 m	0 m	0 m
1	+ 1 m	0 m	0 m	0 m
2	0 m	+ 0.237 m	0 m	0 m
3	0 m	0 m	0.5 m aft	0 m
4	0 m	0 m	0 m	+ 0.25 m

Table 8.5 Crowther design 318 variations

Hull	**Number of slams per hour**	**Average impact velocity [m/s]**
Base	76	1.11
1	65	1.08
2	59	1.10
3	79	1.32
4	7	1.47

Table 8.6 Pod slamming results 5 knots

Hull	Number of slams per hour	Average impact velocity [m/s]
Base	66	1.58
1	72	1.35
2	57	1.38
3	48	1.34
4	29	1.44

Table 8.7 Main beam slamming results 5 knots

Hull	Number of slams per hour	Average impact velocity [m/s]
Base	777	2.03
1	713	1.95
2	635	1.87
3	843	2.05
4	335	2.00

Table 8.8 Pod slamming results 10 knots

Hull	Number of slams per hour	Average impact velocity [m/s]
Base	137	1.53
1	159	1.53
2	152	1.49
3	121	1.53
4	59	1.67

Table 8.9 Main beam slamming results 10 knots

Hull	Number of slams per hour	Average impact velocity [m/s]
Base	368	2.51
1	345	2.57
2	203	2.57
3	472	2.68
4	103	2.93

Table 8.10 Pod slamming results 15 knots

Hull	Number of slams per hour	Average impact velocity [m/s]
Base	39	2.43
1	50	2.39
2	32	2.13
3	26	2.58
4	9	2.59

Table 8.11 Main beam slamming results 15 knots

The results (table 8.6 - 8.11) show that a longer hull will have less slamming on the pod compared to the original design, while the reverse is true for the main beam. Increasing the demihull beam reduces slamming for all conditions. Moving the pod aft leads to increased slamming, while moving the main beam aft leads to reduced slamming. It is likely that the pod is most sensitive to heave motion since it is located close to the centre of gravity. The main beam is located further forward and is more influenced by pitch motions. This can explain why the predicted number of slams changes in a different way for these two locations for some variations.

CHAPTER 9: CONCLUSIONS

In the present work a numerical procedure for predicting slamming occurrence of catamarans is developed. The method is divided into three steps: ship motion prediction, slamming identification and slamming pressure calculations. The method is applicable for both high-speed power catamarans and sailing catamarans, the only difference being the method of ship motion prediction used. The following conclusions can be drawn from the work:

- Accurate ship motion prediction is an important factor in prediction of slamming occurrence.

- Several existing methods were used for high-speed power catamarans. Linear high-speed strip theory was found to give good predictions for ship motions of high-speed power catamarans. The non-linear theory used did not perform as expected on the hull shapes used in this work. The methods used to predict slamming occurrence will however benefit if a better non-linear seakeeping theory can be used in future work. (Note: A new version of Veres from Marintek was available after the thesis was submitted for examination. The non-linear version performed satisfactorily.)

- A new strip theory for motion prediction of sailing multihulls was developed and found to give encouraging results. Asymmetric coupling effects are found to be important for heeled multihulls. Sail-forces are found to be important for racing catamarans.

- A new direct method for identifying slamming occurrences in the time domain was developed and is especially suitable when non-linear motion simulation is used. Further the method makes no assumption about the

distribution of the relative velocity as the probabilistic method do. Since the non-linear simulations used in this work did not perform satisfactorily the full potential of this method was not realized in this work. However the method has been proven to be effective and to give good results.

- Slamming pressure calculations were performed using an existing theory. The method used was effective and provided reasonable accuracy. Development of new theories was beyond the scope of the current work, but it is believed that more advanced theories will be available in the future. Also, more work should be done in validating theoretical methods through full-scale testing but again this is beyond the current scope of work.

- A simple methodology for performing parametric varations is developed, and is expected to be very useful for designers of catamarans.

- The overall objective of predicting slamming occurrence of catamarans has been met, both for high-speed power catamarans and sailing catamarans. The methods presented allows a designer to optimize a vessel for an operational profile. The predicted slamming occurrence and slamming pressure distribution will be valuable information for the structural designer, both in designing for fatigue and extreme values.

REFERENCES

Beck, R. & Reed, A. 2001, *Modern Seakeeping Computations for Ships*, Twenty-Third Symposium on NAVAL HYDRODYNAMICS.

Bertram, V. 2000, *PRACTICAL SHIP HYDRODYNAMICS*, Butterworth-Heinemann.

Brown, K. C. & Joubert, P. N. 1990, *Pressure Loading of Aluminium Plating*, Marine Technology, Vol 27, No. 6.

Brown, K. C., Joubert, P. N. & Yan, P. 1996, *Tests on Yacht Hull Plating*, Marine Technology, Vol. 33, No. 2.

Chapman, R. B. 1975, *Free surface effects for surface forces on a surface-piercing plate oscillating in yaw and sway*, Proc. 1st Int. Conf. Numer. Ship Hydrodyn, pp333-350. David W. Taylor Naval Ship R&D Center, Bethesda, Maryland.

Drela, M. & Youngren, H. 2001, *XFOIL 6.9 User Guide*.

Faltinsen, O. M. 1983, *Bow Flow and Added Resistance of Slender Ships at High Froude Number and Low Wave Lengths*, Journal of Ship Research, Vol. 27, No.3.

Faltinsen, O. M. 1990, *Sea loads on ships and offshore structures*, Cambridge University Press.

Faltinsen, O. M. 2001, *Slamming with Application to Planing Vessels, Green Water Loading and Sloshing*, Hydrodynamics in Ship and Ocean Engineering, RIAM.

Faltinsen, O. M. 2002, *Water entry of a Wedge with Finite Deadrise Angle*, Journal of Ship Research, Vol. 46, No.1, pp. 39-51.

Faltinsen, O. M. & Zhao, R. 1991, *Numerical predictions of ship motions at high forward speed*, Phil. Trans. R. Soc. Lond. A(1991) 334, 241-252.

Frank, W. 1967, *Oscillation of Cylinders in or Below the Free Surface of Deep Fluids*, Report 2375. Washington DC: Naval Ship Research and Development Center.

Gerritsma, J. & Beukelman, W. 1967, *International Shipbuilding Progress*, International Shipbuilding Progress, vol.14, no.156.

Hayman, B., Haug, T. & Valsgård, S. 1991, *Response of Fast Craft Hull Structures to Slamming Loads*, Fast'91.

Hermundstad, O. A. 1996, *Theoretical and Experimental Hydroelastic Analysis of High Speed Vessels*, Doctoral thesis, NTNU.

Kapsenberg, G. K. & Brouwer, R. 1998, *Hydrodynamic Development for a Frigate for the 21 Century*, Practical Design of Ships and Mobile Units.

Korvin-Kroukovsky, B. V. & Jacobs, W. R. 1957, *Pitching and Heaving Motions of a Ship in Regular Waves*, Trans. SNAME, vol. 65.

Kring, D., Huang, Y. F. & Sclavounos, P. 1997, *Nonlinear Ship Motions and Wave-Induced Loads by a Rankine Method*, Twenty-First Symposium on Naval Hydrodynamics.

Kvålsvold, J. & Faltinsen, O. M. 1994, *Slamming loads on wetdecks of multihull vessels*, Proc. Conf. Hydroelasticity in Marine Technology,
Trondheim.

Larsson, L. & Eliasson, R. E. 2000, *Principles of yacht design*, International Marine.

Lewis, F. M. 1929, *The inertia of water surrounding a ship*, TSNAME.

Lloyd, A. R. J. M. 1989, *SEAKEEPING Ship behaviour in rough weather*, Ellis Horwood.

Maggi, A. & Klaka, K. 1999, *Results of a deployment of CMST Wave Recorders in the vicinity of a Datawell Wave Rider Buoy*, CMST Report C99-28.

Manganelli, P. & Wilson, P. A. 2001, *An experimental investigation of slamming on ocean racing yachts*, The 15th Chesapeake sailing yacht symposium.

Milchert, T. & Stråby, O. 1999, *Calculation and full scale measurement of slamming pressures on semi-planing V-shaped monohulls*, Hydrodynamics of High Speed Craft 24 and 25 November 1999, London.

Ochi, M. K. 1964a, *Extreme Behaviour of a Ship in Rough Seas - Slamming and Shipping of Green Water*, SNAME Transactions 1964.

Ochi, M. K. 1964b, *Prediction of occurence and severity of ship slamming at sea.*, Fifth Symp. on Naval Hydrodynamics, pp. 545-96.

O'Dea, J., Powers, E. & Zselecsky, J. 1992, *Experimental determination of non-linearities in vertical plane ship motions*, Proc. 19th symposium on Naval Hydrodynamics.

Ogilvie, T. F. & Tuck, E. O. 1969, *A Rational Strip-Theory of Ship Motion: Part I*, Department of Naval Architecture, The University of Michigan, Report No. 013.

Parga-Landa, B., Vlegels, S., Hernandez-Olivares, F. & Clark, S. D. 1999, *An analytical study of the effect of slamming pressures on the interlaminar behaviour of composite panels*, Composite Structures.

Press, W. H., Teukolsky, S. A., Vetterling, W. T. & Flannery, B. P. 1986, *Numerical Recipes in Fortran 77*, Press Syndicate of the University of Cambridge.

Rosén, A. & Garme, K. 1999, *Slamming studies on High-Speed Planing Craft through Full-Scale Trials and Simulations*, FAST'99.

Salvesen, N., Tuck, E. O. & Faltinsen, O. M. 1970, *Ship motions and sea loads*, Transactions of the Society of Naval Architects and Marine Engineers, vol 78.

SLAM 2D users manual, Marintek, http://veres.marintek.sintef.no.

Söding, H. 1969, *Eine Modifikation der Streifen-methode*, Schiffstechnik, Bd16, Heft 80.

Steinmann, P., Fach, K. & Menon, B. 1999, *Global and Slamming Sea Loads Acting on an 86m High Speed Catamaran Ferry*, FAST 99.

TSK Remote Wave height meter, operating manual.

Ursell, F. 1949, *On the heaving motion of a circular in the surface of a fluid*, QJMAM 2 218-231.

Varyani, K. S., Gatiganti, R. M. & Gerigk, M. 2000, *Motions and slamming impact on catamaran*, Ocean Engineering 27.

VERES User manual*, Marintek*, http://veres.marintek.sintef.no.

Ward, L. W. 1985, *Sailboat Bow Impact Stresses*, The seventh Chesapeake sailing yacht symposium.

Wu, M. & Moan, T. 1996, *Linear and Nonlinear Hydroelastic Analysis of High-Speed Vessels*, Journal of Ship Research, Vol. 40, No. 2.

Xia, J., Wang, Z. & Jensen, J. 1998, *Non-linear wave loads and ship responses by a time-domain strip theory*.

Zhao, R. & Faltinsen, O. M. 1993, *Water entry of two dimensional bodies*, J. Fluid Mech., 246, pp.593-612.

APPENDIX 1: BACKGROUND THEORY

STF Strip theory

The problem of a ship advancing at constant speed in regular sinusoidal waves can be studied by employing linear theory. The strip theory presented by STF is widely used, both in its original form and as a basis for more advanced theories. Since the theory is used as a basis in this work a thorough description of the theory is given in this section.

Disregarding viscous effects the fluid can be assumed irrotational, and potential flow theory can be used to describe the problem.

The velocity potential $\phi(x, y, z, t)$ must satisfy the Laplace equation,

$$\nabla^2 \phi = 0 \tag{A1. 51}$$

with the following exact boundary conditions:

$$\frac{DF}{Dt} = 0 \tag{A1. 52}$$

is the body boundary condition, where F(x,y,z) = 0 defines the hull surface.

The exact free surface condition

$$\frac{Dp}{Dt} = -\rho \frac{D}{Dt}\left(\frac{\partial \phi}{\partial t} + \frac{1}{2}\left|\nabla \phi\right|^2 + gz \right) = 0 \tag{A1. 53}$$

is enforced on the unknown free surface z = Z(x,y,t). Finally, a suitable radiation condition at infinity must be defined, ensuring that the radiated waves propagate away from the body.

Consistent with linear theory the velocity potential can be separated into two parts, one time independent contribution from the steady forward motion of

the ship and one unsteady contribution from boat motion. Adding the free stream potential Ux the total velocity potential is

$$\phi(x,y,z,t) = \left[-Ux + \phi_S(x,y,z)\right] + \phi_T(x,y,z)e^{i\omega_e t} \qquad \text{(A1. 54)}$$

To simplify the solution the boundary conditions (A1. 52) and (A1. 53) are linearized by omitting the higher order terms in the steady part of the velocity potential and all terms involving cross products between the steady and unsteady part of the velocity potential.

Furthermore, in linearizing the problem the unsteady velocity potential is decomposed into contributions from the incident wave potential ϕ_I, the diffraction potential ϕ_D and the oscillatory potential ϕ_j.

$$\phi_T = \phi_I + \phi_D + \sum_{j=1}^{6} \eta_j \phi_j \qquad \text{(A1. 55)}$$

The incident wave potential is given as

$$\phi_I = \frac{g\zeta_A}{\omega} e^{kz} e^{-ik(x\cos\beta + y\sin\beta)} \qquad \text{(A1. 56)}$$

Including only linear terms and applying Taylor expansions about the mean hull position in the hull boundary condition (A1. 52) and about the undisturbed free surface z = 0 in the free surface condition (A1. 53) the following boundary conditions must be satisfied:

The steady perturbation potential ϕ_S must satisfy the body condition

$$\frac{\partial}{\partial n}\left[-Ux + \phi_S\right] = 0 \qquad \text{(A1. 57)}$$

on the hull at mean position, and the free surface condition

$$U^2 \frac{\partial^2 \phi}{\partial x^2} + g\frac{\partial \phi_S}{\partial z} = 0 \text{ on z = 0} \qquad \text{(A1. 58)}$$

The incident wave potential ϕ_I and the diffraction potential ϕ_D must satisfy

$$\frac{\partial \phi_I}{\partial n} + \frac{\partial \phi_D}{\partial n} = 0 \text{ on the hull at mean position} \qquad \text{(A1. 59)}$$

and the free surface condition

$$\left[\left(i\omega_e - U\frac{\partial}{\partial x}\right)^2 + g\frac{\partial}{\partial z}\right](\phi_I, \phi_D) = 0 \text{ on z = 0} \qquad \text{(A1. 60)}$$

The oscillatory potential components ϕ_j (j=1..6) must satisfy

$$\frac{\partial \phi_j}{\partial n} = i\omega_e n_j + U m_j \text{ on the hull at mean position} \qquad \text{(A1. 61)}$$

and

$$\left(i\omega_e - U\frac{\partial}{\partial x}\right)^2 \phi_j + g\frac{\partial}{\partial z}\phi_j = 0 \text{ on z = 0} \qquad \text{(A1. 62)}$$

The generalized normal n_j is defined by

$$(n_1, n_2, n_3) = \vec{h} \text{ and } (n_4, n_5, n_6) = \vec{r} \times \vec{h} \qquad \text{(A1. 63)}$$

where $\vec{r} = (x, y, z)$ is the position vector with respect to the origin of the coordinate system and $\vec{h}$ is the outward unit normal vector pointing into the fluid. $m_j = 0$ for j=1 ,2, 3, 4 while

$$m_5 = n_3 \text{ and } m_6 = -n_2 \qquad \text{(A1. 64)}$$

The hull condition (A1. 61) can be further simplified by dividing the oscillatory potential into two parts,

$$\phi_j = \phi_j^0 + \frac{U}{i\omega}\phi_j^U \qquad \text{(A1. 65)}$$

where ϕ^0 will be shown to be speed independent. This results in two hull conditions

$$\frac{\partial \phi_j^0}{\partial n} = i\omega_e n_j \text{ and } \frac{\partial \phi_j^U}{\partial n} = i\omega_e m_j \qquad \text{(A1. 66)}$$

Since both ϕ^0 and ϕ^U must satisfy the Laplace equation, the same free surface equation (A1. 62) and the same radiation condition at infinity it follows from the hull conditions (A1. 66) and the relationships (A1. 64) that $\phi_j^U = 0$ for j= 1, 2, 3, 4 and that

$$\phi_5^U = \phi_3^0 \text{ while } \phi_6^U = -\phi_2^0 \qquad \text{(A1. 67)}$$

We see that the total oscillatory potential can be expressed in terms of the speed independent part of the potential:

$$\phi_j = \phi_j^0 \text{ for j=1, 2, 3, 4} \qquad \text{(A1. 68)}$$

$$\phi_5 = \phi_5^0 + \frac{U}{i\omega_e}\phi_3^0 \qquad \text{(A1. 69)}$$

$$\phi_6 = \phi_6^0 - \frac{U}{i\omega_e}\phi_2^0 \qquad \text{(A1. 70)}$$

ϕ^0 must satisfy the conditions

$$\frac{\partial \phi_j^0}{\partial n} = i\omega_e n \text{ on the mean hull position} \qquad \text{(A1. 71)}$$

and

$$\left(i\omega_e - U\frac{\partial}{\partial x}\right)^2 \phi_j^0 + g\frac{\partial \phi_j^0}{\partial z} = 0 \text{ on z = 0} \qquad \text{(A1. 72)}$$

In addition to these linear boundary conditions the potentials ϕ_S, ϕ_I, ϕ_D and ϕ_j must each satisfy the Laplace equation (A1. 51) in the fluid domain and appropriate radiation conditions at infinity.

The pressure in the fluid is obtained from the Bernoulli equation

$$p = -\rho\left(\frac{\partial\phi}{\partial t} + \frac{1}{2}|\nabla\phi|^2 + gz\right) \qquad \text{(A1. 73)}$$

The pressure can be linearized by expanding it in a Taylor series about the calm water line, including only terms of first order in ϕ_S and ϕ_T. The linearized pressure is

$$p = -\rho\left(i\omega - U\frac{\partial}{\partial x}\right)\phi_T e^{i\omega_e t} \qquad \text{(A1. 74)}$$

The hydrodynamic force and moment amplitudes are found by integrating the pressure amplitude over the hull surface

$$H_j = -\rho\int\int_S n_j\left(i\omega_e - U\frac{\partial}{\partial x}\right)\phi_T ds, j = 1..6 \qquad \text{(A1. 75)}$$

The integration is over the mean wetted surface S. H_1, H_2, H_3 are the force components in the x, y and z direction, while H_4, H_5, H_6 are the moments about the x, y and z axes. The forces and moments can be divided into two parts as

$$H_j = F_j + G_j \qquad \text{(A1. 76)}$$

where F_j is the exciting force and moment:

$$F_j = -\rho\int\int_S n_j\left(i\omega_e - U\frac{\partial}{\partial x}\right)(\phi_I + \phi_D)ds \qquad \text{(A1. 77)}$$

and G_j is the force and moment due to the body motions $\eta_{1..}\eta_{6:}$

$$G_j = -\rho \iint_S n_j \left(i\omega_e - U\frac{\partial}{\partial x} \right) \sum_{k=1}^{6} \phi_k \eta_k ds$$
$$= \sum_{k=1}^{6} T_{jk} \eta_k \qquad \text{(A1. 78)}$$

T_{jk} denotes the hydrodynamic force and moment in the jth direction per unit oscillatory displacement in the kth mode:

$$T_{jk} = -\rho \iint_S n_j \left(i\omega_e - U\frac{\partial}{\partial x} \right) \phi_k ds \qquad \text{(A1. 79)}$$

T_{jk} may be separated into real and imaginary parts as

$$T_{jk} = \omega_e{}^2 A_{jk} - i\omega_e B_{jk} \qquad \text{(A1. 80)}$$

where A_{jk} and B_{jk} are the added mass and damping forces respectively.
Finally the equation of motion can be written as

$$\sum_{k=1}^{6} \left[-\omega_e{}^2 \left(M_{jk} + A_{jk} \right) + i\omega_e B_{jk} + C_{jk} \right] \eta_k = F_j \qquad \text{(A1. 81)}$$

Hydrodynamic coeffcients

It remains to simplify the expression for T_{jk} (A1. 79) to a suitable form for calculation. A well known form of Stokes' theorem is

$$\iint_S \left(n \times \nabla \right) \times q ds = \int_C dl \times q \qquad \text{(A1. 82)}$$

where S is a surface situated in the fluid with the closed curve C as boundary. Now by letting $q = \phi U i$ for translational motions and $q = \phi U i \times r$ for rotational motions (Ogilvie & Tuck 1969)showed that the following variant of Stokes' theorem can be derived.

$$\iint_S n_j U \frac{\partial}{\partial x} \phi ds = U \iint_S m_j \phi ds - U \int_C n_j \phi dl \qquad \text{(A1. 83)}$$

For the added mass and damping coefficients we now have

$$T_{jk} = -\rho i\omega_e \iint_S n_j \phi_k ds + U\rho \iint_S m_j \phi_k ds - U\rho \int_{C_A} n_j \phi_k dl \qquad \text{(A1. 84)}$$

where C_A refers to the aftermost cross section of the ship. Now the speed independent part of T_{jk} can be defined as

$$T_{jk}^0 = -\rho i\omega_e \iint_S n_j \phi_k^0 ds \qquad \text{(A1. 85)}$$

and the speed independent part of the line integral at any cross section C_x as

$$t_{jk} = -\rho i\omega_e \int_{C_x} n_j \phi_k^0 ds \qquad \text{(A1. 86)}$$

The added mass and damping coefficients can now be expressed in terms of the speed independent terms (A1. 85) and (A1. 86) by applying the expressions for the potential (A1. 68), (A1. 69) and (A1. 70):

$$T_{jk} = T_{jk}^0 + \frac{U}{i\omega_e} t_{jk}^A \ ; \text{j,k} = 1,2,3,4$$

$$T_{5k} = T_{5k}^0 - \frac{U}{i\omega_e} T_{3k}^0 + \frac{U}{i\omega_e} t_{5k}^A \ ; \text{k} = 1,2,3,4$$

$$T_{6k} = T_{6k}^0 - \frac{U}{i\omega_e} T_{2k}^0 + \frac{U}{i\omega_e} t_{6k}^A \ ; \text{k} = 1,2,3,4$$

$$T_{j5} = T_{j5}^0 + \frac{U}{i\omega_e} T_{j3}^0 + \frac{U}{i\omega_e} t_{j5}^A - \frac{U^2}{\omega_e^{\,2}} t_{j3}^A \ ; \text{j} = 1,2,3,4$$

$$T_{j6} = T_{j6}^0 + \frac{U}{i\omega_e} T_{j2}^0 + \frac{U}{i\omega_e} t_{j6}^A + \frac{U^2}{\omega_e^{\,2}} t_{j2}^A$$

$$T_{55} = T_{55}^0 + \frac{U^2}{\omega_e^2} T_{33}^0 + \frac{U}{i\omega_e} t_{55}^A - \frac{U^2}{\omega_e{}^2} t_{53}^A$$

$$T_{66} = T_{66}^0 + \frac{U^2}{\omega_e^2} T_{22}^0 + \frac{U}{i\omega_e} t_{66}^A + \frac{U^2}{\omega_e{}^2} t_{62}^A \qquad \text{(A1. 87)}$$

To this point in the derivation no assumptions about strip theory have been made directly, but linearizing and decomposing the velocity potentials plus neglecting the steady potential the problem have made the problem suitable for a strip theory approach. It is in the calculation of the zero speed coefficients that the simplification of strip theory is introduced. If we consider that the beam and draft of the ship are much smaller than her length, then it is consistent with the previous assumptions to set ds = dxdl in the surface integral (A1. 85) so that

$$T_{jk}^0 = -\rho i\omega_e \int_L \int_{C_x} n_j \phi_k^0 dl dx = \int_L t_{jk} dx \qquad \text{(A1. 88)}$$

Exciting Forces

Looking at the exciting forces as described by (A1. 77) it is convenient to separate the contributions from the undisturbed wave, F_j^I, and contributions from diffraction forces, F_j^D,

$$F_j = F_j^I + F_j^D \qquad \text{(A1. 89)}$$

where

$$F_j^I = -\rho \int\int_S n_j \left(i\omega_e - U \frac{\partial}{\partial x} \right) \phi_I ds \qquad \text{(A1. 90)}$$

and

$$F_j^D = -\rho \int\int_S n_j \left(i\omega_e - U \frac{\partial}{\partial x} \right) \phi_D ds \qquad \text{(A1. 91)}$$

Introducing the incident wave potential ϕ_I given by (A1. 56) into (A1. 90) and using the relationship

$$\omega = \omega_e + kU\cos\beta \tag{A1. 92}$$

we have

$$F_j^I = -\rho i\omega_e \iint_S n_j \phi_I ds \tag{A1. 93}$$

or the well known Froude Krylov force.

Going back to the diffraction force (A1. 91) application of the Stokes theorem (A1. 83) gives

$$F_j^D = -\rho \iint_S \left(i\omega_e n_j - Um_j\right)\phi_D ds - \rho U \int_{CA} n_j \phi_D dl \tag{A1. 94}$$

The sectional Froude Krylov force is written as

$$f_j(x) = ge^{-ikx\cos\beta} \int_C N_j e^{-iky\cos\beta} e^{kz} dl \text{ , j = 2,3,4} \tag{A1. 95}$$

and the sectional diffraction force is written as

$$h_j(x) = \omega e^{-ikx\cos\beta} \int_C \left(iN_3 - N_2\sin\beta\right) \times e^{-iky\cos\beta} e^{kz} \psi_j dl \text{ , } j = 2,3,4 \tag{A1. 96}$$

where ψ_j is the two dimensional potential.

Finally the total exciting forces are written as

$$F_j = \rho\zeta_A \int_L \left(f_j + h_j\right)dx + \rho\zeta_A \frac{U}{i\omega_e} h_j^A \text{ , j=2,3,4} \tag{A1. 97}$$

$$F_5 = -\rho\zeta_A \int_L \left[x\left(f_3 + h_3\right) + \frac{U}{i\omega_e} h_3 \right] dx - \rho\zeta_A \frac{U}{i\omega_e} x_A h_3^A \qquad \text{(A1. 98)}$$

$$F_6 = \rho\zeta_A \int_L \left[x\left(f_2 + h_2\right) + \frac{U}{i\omega_e} h_2 \right] dx + \rho\zeta_A \frac{U}{i\omega_e} x_A h_2^A \qquad \text{(A1. 99)}$$

where h^A refers to $h_j(x)$ evaluated at the aftermost station.

High-speed strip theory

The high-speed strip theory tries to incorporate important forward speed effects on the flow around the ship while still keeping the computational efficiency of strip theory. The theory incorporates the divergent wave system created by the ship at forward speed, but neglects the transverse wave system. This can be justified when the waveform parameter $\tau = \omega U/g > ¼$. This corresponds to the situation where no waves propagate forward.

In the derivation of the theory a slenderness parameter ε is introduced. The parameter ε is a measure for the beam/length ratio or draft length ratio and is small for a slender ship. It is assumed that $\frac{\partial f}{\partial x} = O\left(f\varepsilon^{-1/2}\right), \frac{\partial f}{\partial y} = O\left(f\varepsilon^{-1}\right)$ and $\frac{\partial f}{\partial z} = O\left(f\varepsilon^{-1}\right)$ where f is any flow parameter in the near field. This differs from conventional strip theory that implies $\frac{\partial f}{\partial x} = O(f)$. Further, the x component of the unit normal vector of the hull, n_1 is assumed to be $O(\varepsilon)$.

Given here is the theory as implemented in the linear high-speed strip theory VERES (VERES User manual, Marintek).Note: The coordinate system used in the high-speed strip theory is different than used in the previous section. The high-speed strip theory uses a coordinate system with the x-axis pointing backwards. Formulating the forced motion problem in terms of linear potential theory the potentials are rewritten as

$$\phi = e^{-i(\omega/U)x}\varphi(y,z) \qquad \text{(A1. 100)}$$

where the time dependency is in the first part. The problem is reduced to solving the two dimensional Laplace equation

$$\frac{\partial \varphi}{\partial y^2} + \frac{\partial \varphi}{dx^2} = 0\,,\ r = 1..m \qquad \text{(A1. 101)}$$

With the following boundary conditions:

The free surface condition

$$U^2 \frac{\partial \varphi}{\partial x^2} + g \frac{\partial \varphi}{dz^2} = 0 \text{ on z} = 0 \qquad \text{(A1. 102)}$$

and the body boundary conditions

$$\frac{\partial \varphi_j}{\partial n} = i\omega_e n - U m_j \text{, j=2..6} \qquad \text{(A1. 103)}$$

for the radiation potentials and

$$\frac{\partial \varphi_D}{\partial n} = (in_1 - n_3)\omega\zeta_A e^{kz + i(\omega/U) - iky\sin\beta} \qquad \text{(A1. 104)}$$

for the diffraction potentials. Further, the velocity potentials and their x derivatives are set to zero at the bow, and a solution can be reached by stepping downstream. The procedure requires that there are no waves propagated upstream, satisfied when $\tau = \omega U / g > 1/4$. The validity of setting the value of the potentials to zero at the bow has been questioned. This is likely to influence the calculation of the resistance more than the seakeeping problem, and it is believed it can be justified for slender high-speed hulls with a fine entrance. The total solution can be found by applying (A1. 100). The added mass and damping coefficients are calculated as

$$T_{jk} = \rho \iint_S n_j \left(i\omega_e + U \frac{\partial}{\partial x} \right) \phi_k \, ds \qquad \text{(A1. 105)}$$

and the exciting forces are calculated as

$$F_j = \rho \iint_S n_j \left(i\omega\phi_I + i\omega_e \phi_D + U \frac{\partial \phi_D}{\partial x} \right) ds \qquad \text{(A1. 106)}$$

The resulting motions are calculated as in linear strip theory. The description of the non-linear time-domain version of the high-speed strip theory can be found in Wu & Moan (1996) and is not explained here. While

conventional strip theory today can be seen as mature, at least in its linear form, the high-speed strip theory and similar theories are still subject to research work.

APPENDIX 2: SLAMMING PRESSURE DISTRIBUTIONS

Austal Hull 63

Below are plotted slamming pressure distributions for Austal Hull 63 in seastates where Hs is kept constant at 3m while speed, heading and wave mean period are varied systematically. The same conditions as shown in chapter 5 are used: Three forward speeds, 20, 30 and 40 knots. Three wave mean periods, 8, 10 and 12s. Six headings, 0, 15, 30, 45, 60 and 75 degrees from head sea. All conditions where slamming is observed are plotted (fig. A.2.1 – A.2.18)

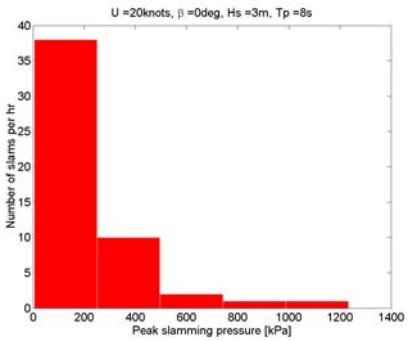

Figure A.2.1 Austal Hull 63 impact pressure distribution

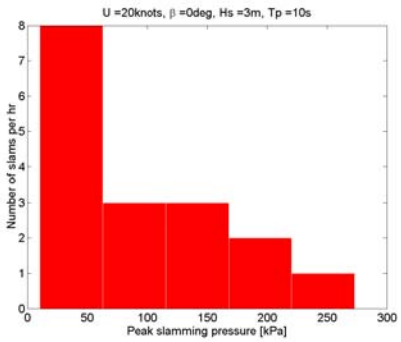

Figure A.2.2 Austal Hull 63 impact pressure distribution

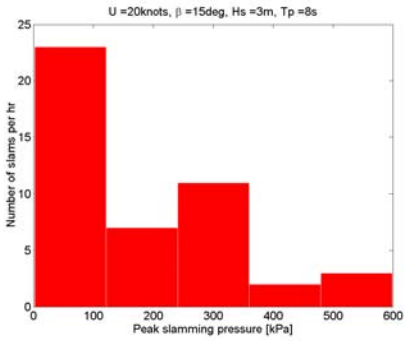

Figure A.2.3 Austal Hull 63 impact pressure distribution

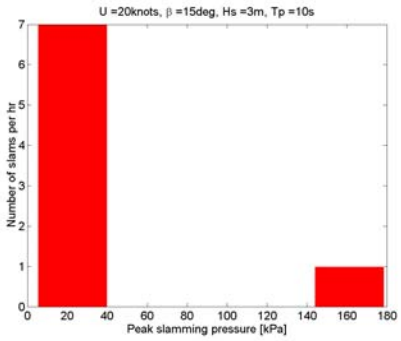

Figure A.2.4 Austal Hull 63 impact pressure distribution

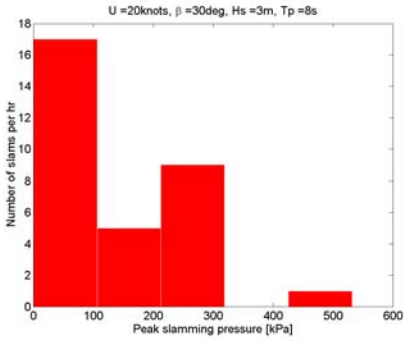

Figure A.2.5 Austal Hull 63 impact pressure distribution

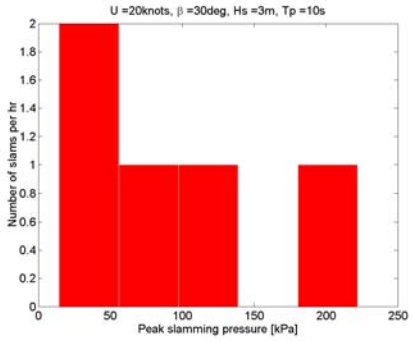

Figure A.2.6 Austal Hull 63 impact pressure distribution

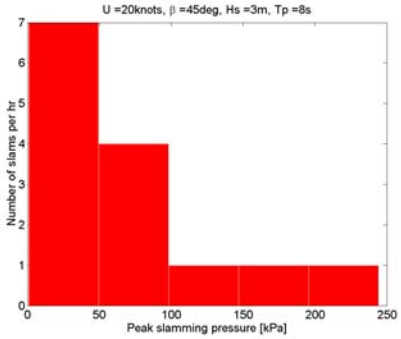

Figure A.2.7 Austal Hull 63 impact pressure distribution

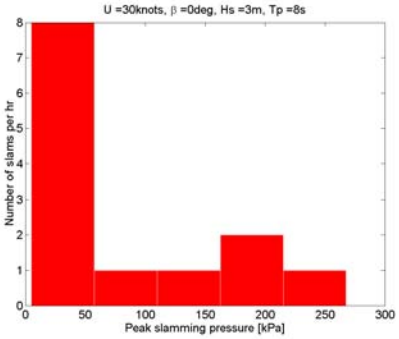

Figure A.2.8 Austal Hull 63 impact pressure distribution

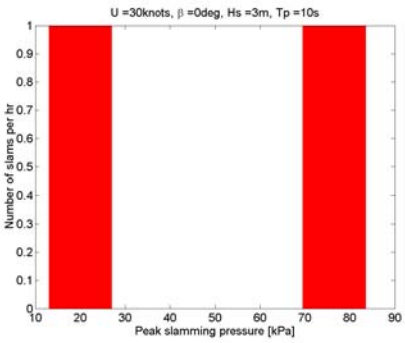

Figure A.2.9 Austal Hull 63 impact pressure distribution

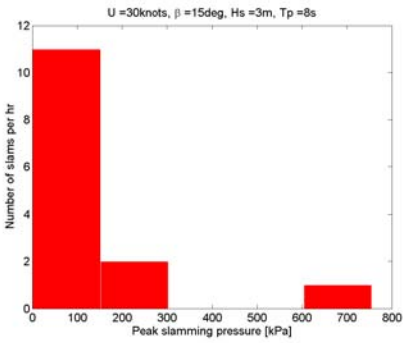

Figure A.2.10 Austal Hull 63 impact pressure distribution

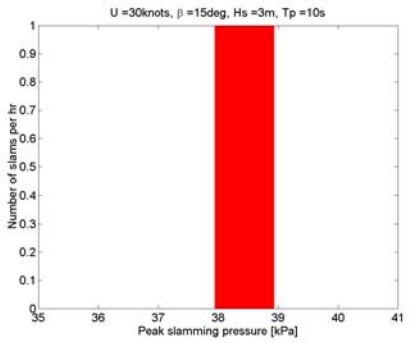

Figure A.2.11 Austal Hull 63 impact pressure distribution

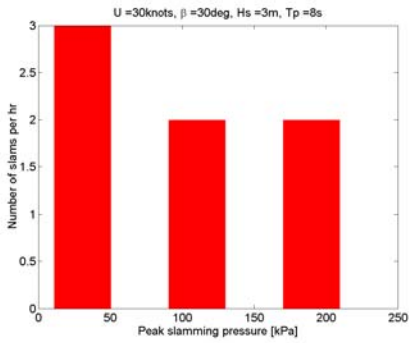

Figure A.2.12 Austal Hull 63 impact pressure distribution

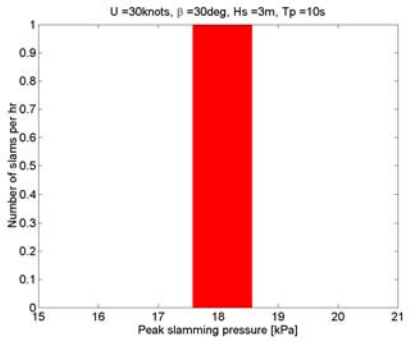

Figure A.2.13 Austal Hull 63 impact pressure distribution

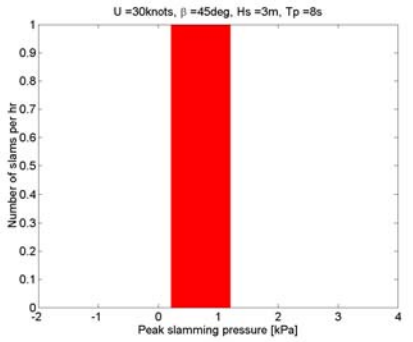

Figure A.2.14 Austal Hull 63 impact pressure distribution

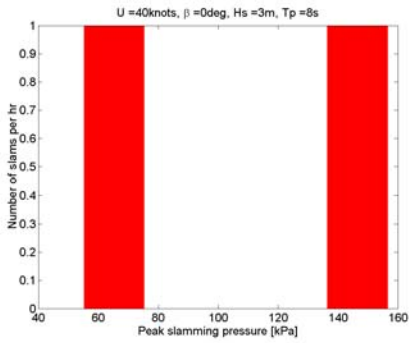

Figure A.2.15 Austal Hull 63 impact pressure distribution

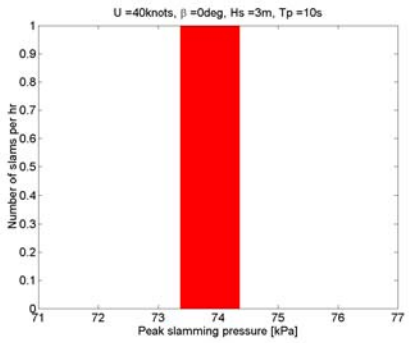

Figure A.2.16 Austal Hull 63 impact pressure distribution

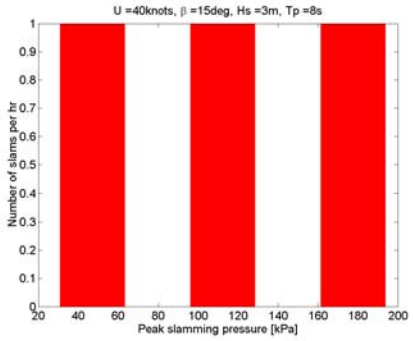

Figure A.2.17 Austal Hull 63 impact pressure distribution

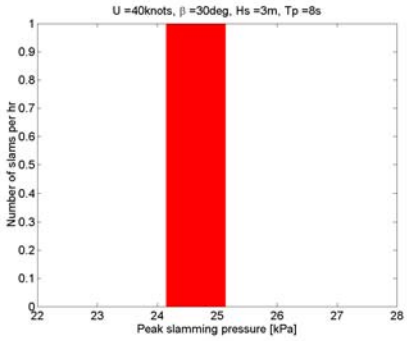

Figure A.2.18 Austal Hull 63 impact pressure distribution

The exercise is repeated with a significant wave height of 4m, while the speed, wave period and heading are varied as above (fig. A.2.19 – A.2.55).

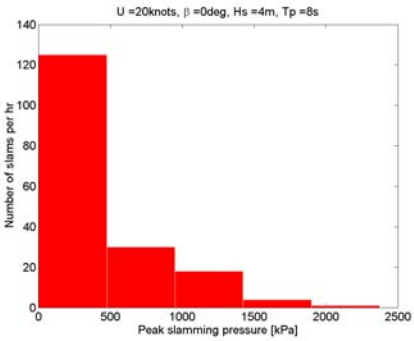

Figure A.2.19 Austal Hull 63 impact pressure distribution

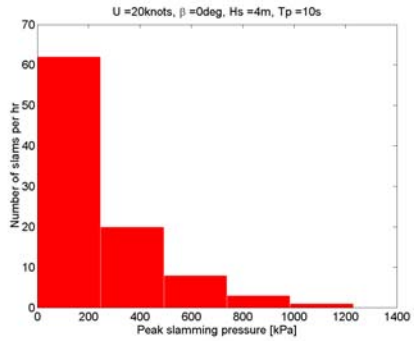

Figure A.2.20 Austal Hull 63 impact pressure distribution

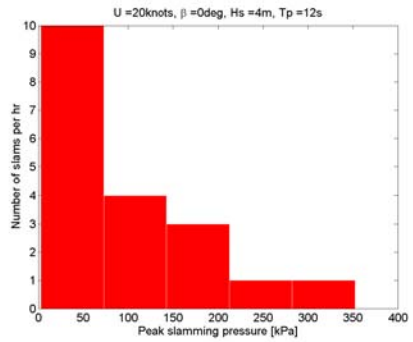

Figure A.2.21 Austal Hull 63 impact pressure distribution

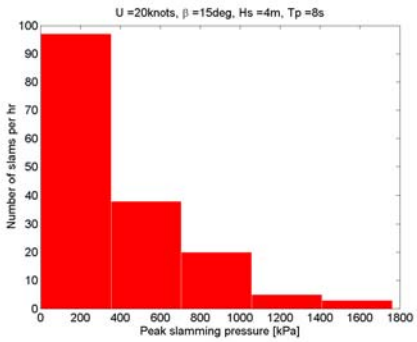

Figure A.2.22 Austal Hull 63 impact pressure distribution

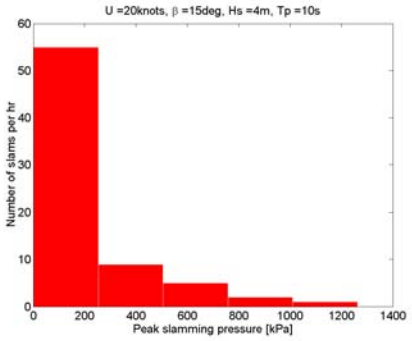

Figure A.2.23 Austal Hull 63 impact pressure distribution

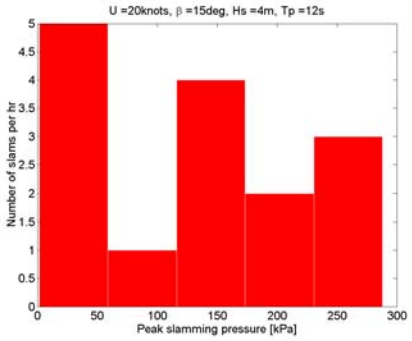

Figure A.2.24 Austal Hull 63 impact pressure distribution

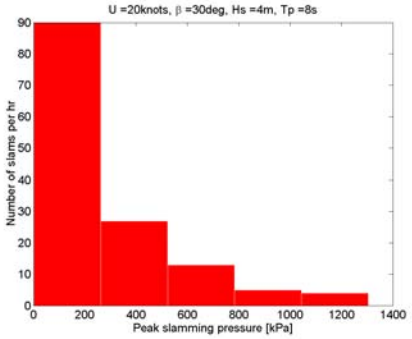

Figure A.2.25 Austal Hull 63 impact pressure distribution

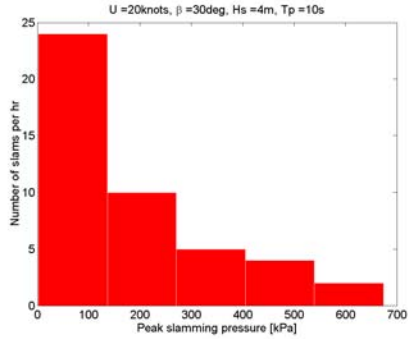

Figure A.2.26 Austal Hull 63 impact pressure distribution

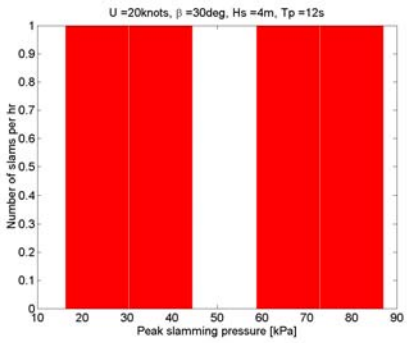

Figure A.2.27 Austal Hull 63 impact pressure distribution

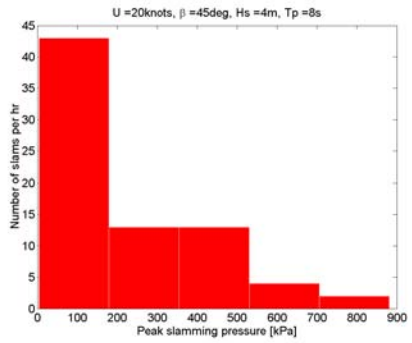

Figure A.2.28 Austal Hull 63 impact pressure distribution

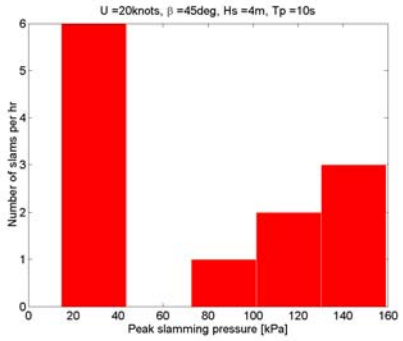

Figure A.2.29 Austal Hull 63 impact pressure distribution

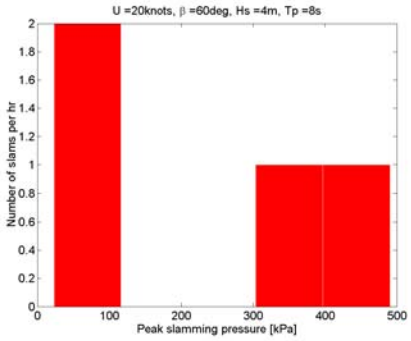

Figure A.2.30 Austal Hull 63 impact pressure distribution

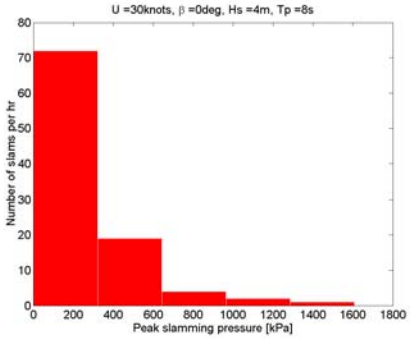

Figure A.2.31 Austal Hull 63 impact pressure distribution

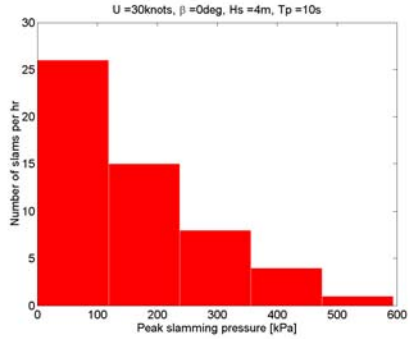

Figure A.2.32 Austal Hull 63 impact pressure distribution

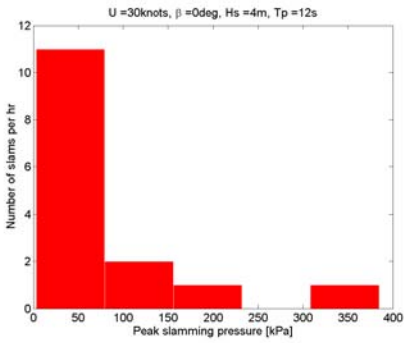

Figure A.2.33 Austal Hull 63 impact pressure distribution

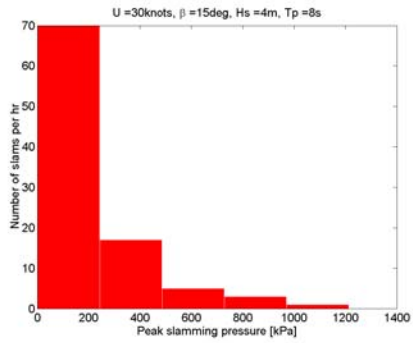

Figure A.2.34 Austal Hull 63 impact pressure distribution

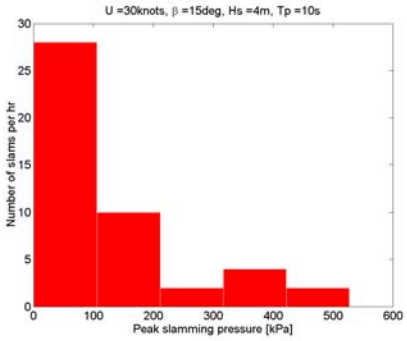

Figure A.2.35 Austal Hull 63 impact pressure distribution

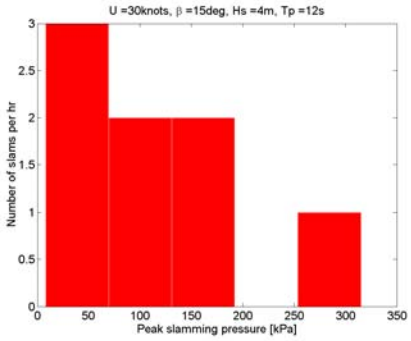

Figure A.2.36 Austal Hull 63 impact pressure distribution

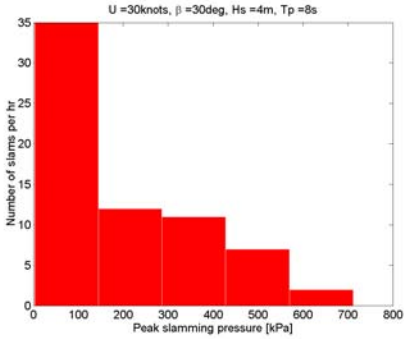

Figure A.2.37 Austal Hull 63 impact pressure distribution

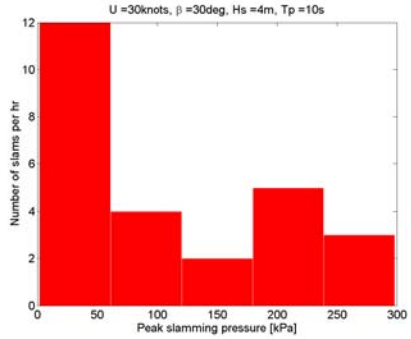

Figure A.2.38 Austal Hull 63 impact pressure distribution

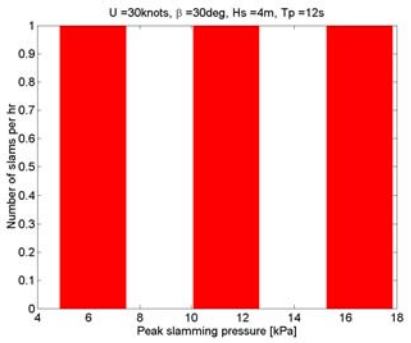

Figure A.2.39 Austal Hull 63 impact pressure distribution

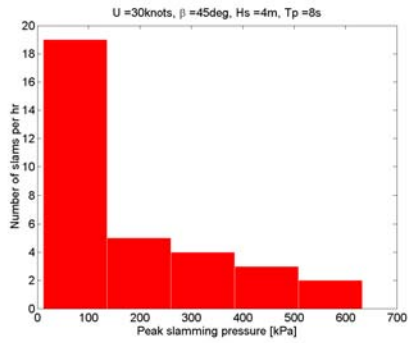

Figure A.2.40 Austal Hull 63 impact pressure distribution

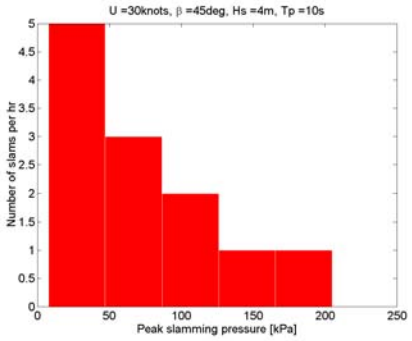

Figure A.2.41 Austal Hull 63 impact pressure distribution

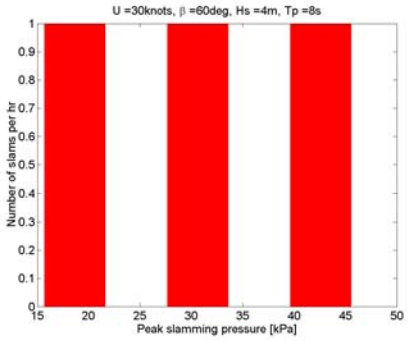

Figure A.2.42 Austal Hull 63 impact pressure distribution

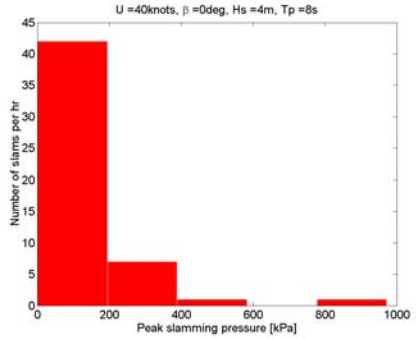

Figure A.2.43 Austal Hull 63 impact pressure distribution

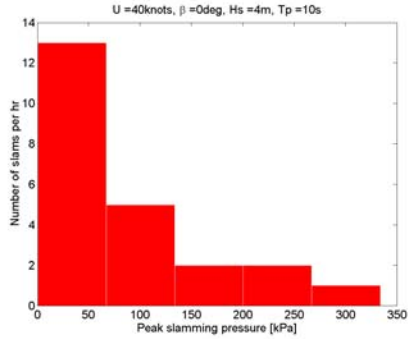

Figure A.2.44 Austal Hull 63 impact pressure distribution

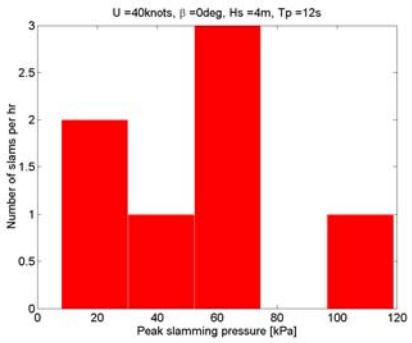

Figure A.2.45 Austal Hull 63 impact pressure distribution

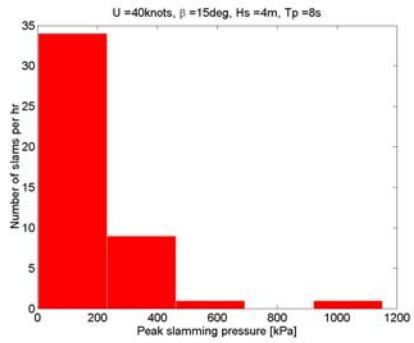

Figure A.2.46 Austal Hull 63 impact pressure distribution

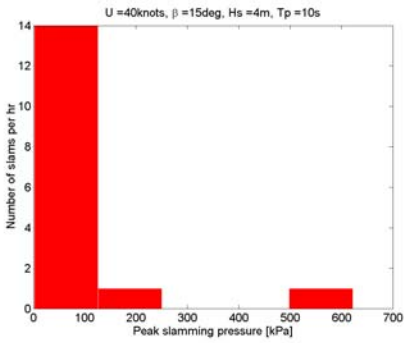

Figure A.2.47 Austal Hull 63 impact pressure distribution

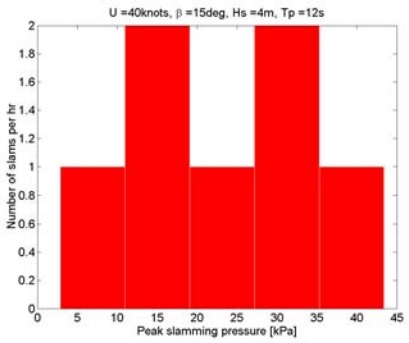

Figure A.2.48 Austal Hull 63 impact pressure distribution

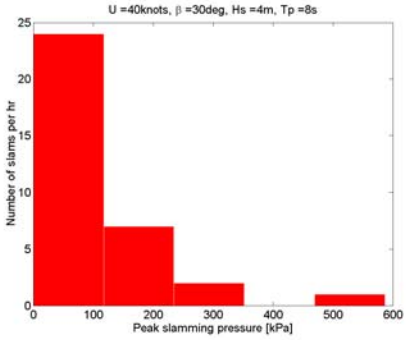

Figure A.2.49 Austal Hull 63 impact pressure distribution

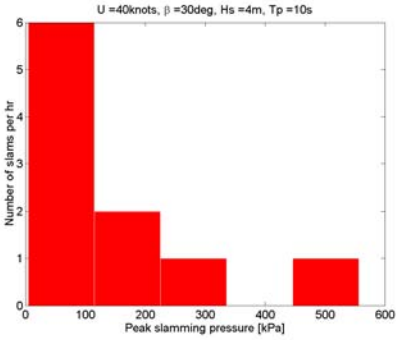

Figure A.2.50 Austal Hull 63 impact pressure distribution

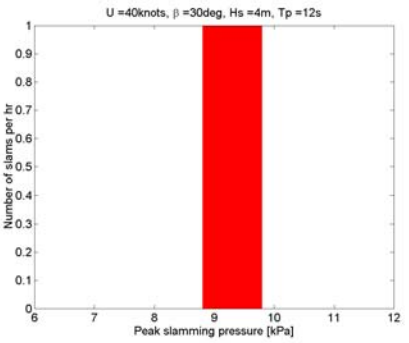

Figure A.2.51 Austal Hull 63 impact pressure distribution

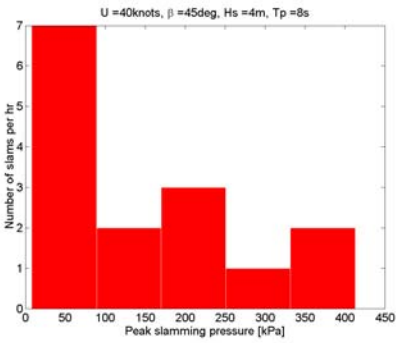

Figure A.2.52 Austal Hull 63 impact pressure distribution

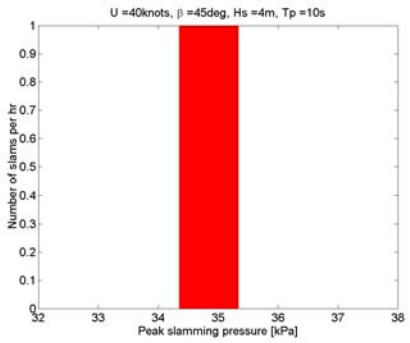

Figure A.2.53 Austal Hull 63 impact pressure distribution

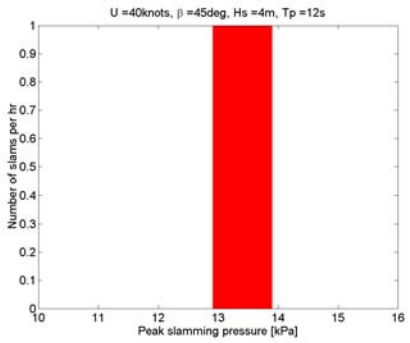

Figure A.2.54 Austal Hull 63 impact pressure distribution

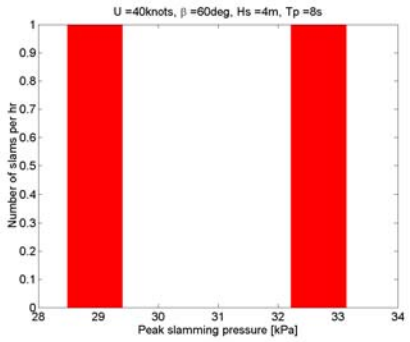

Figure A.2.55 Austal Hull 63 impact pressure distribution

Crowther 318 original

Slamming pressure distributions in a 1m seastate with ship motion prediction from high-speed theory are listed below for the pod (fig. A.2.56 – A.2.66).

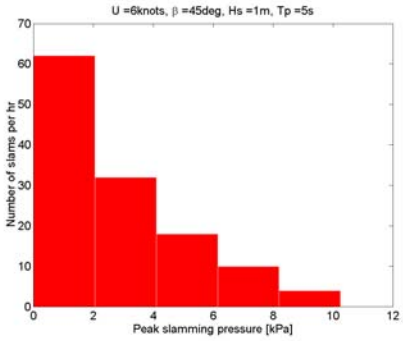

Figure A.2.56 Crowther design 318 impact pressure distribution

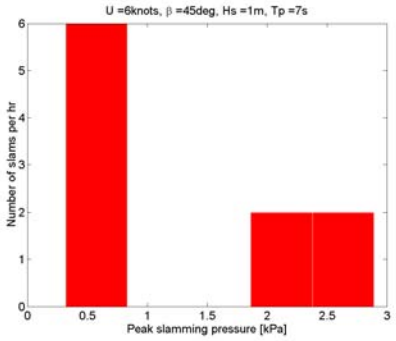

Figure A.2.57 Crowther design 318 impact pressure distribution

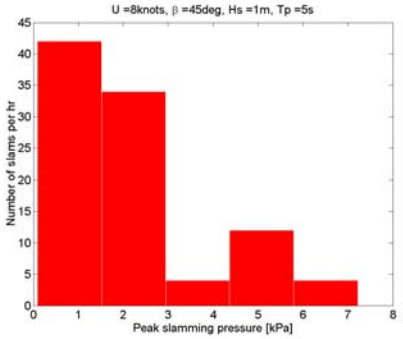

Figure A.2.58 Crowther design 318 impact pressure distribution

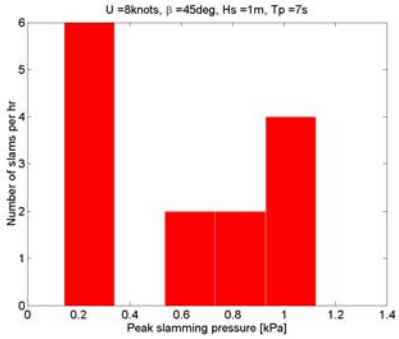

Figure A.2.59 Crowther design 318 impact pressure distribution

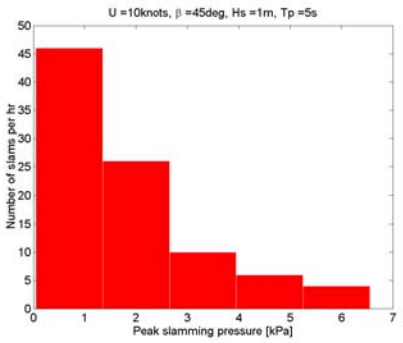

Figure A.2.60 Crowther design 318 impact pressure distribution

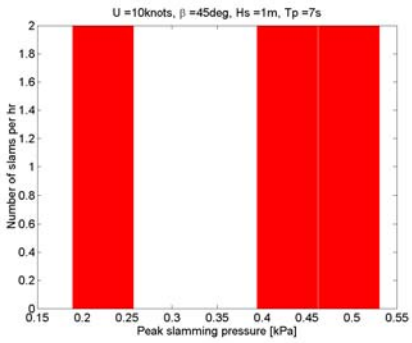

Figure A.2.61 Crowther design 318 impact pressure distribution

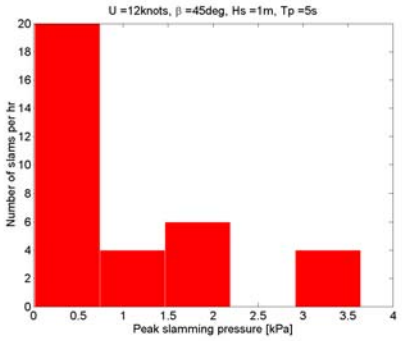

Figure A.2.62 Crowther design 318 impact pressure distribution

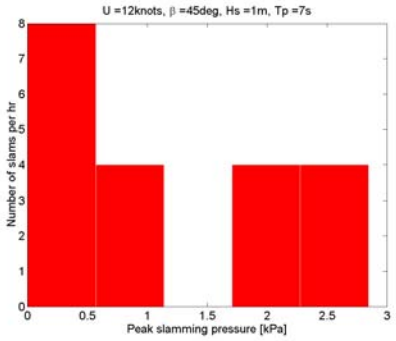

Figure A.2.63 Crowther design 318 impact pressure distribution

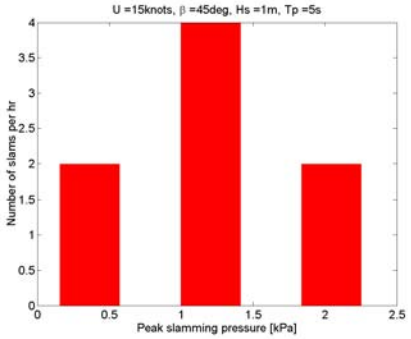

Figure A.2.64 Crowther design 318 impact pressure distribution

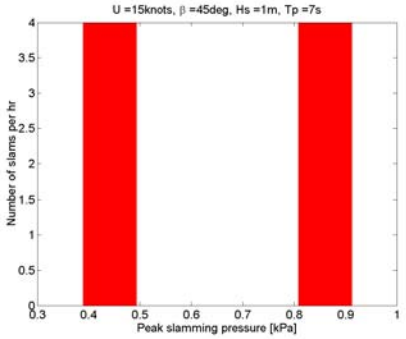

Figure A.2.65 Crowther design 318 impact pressure distribution

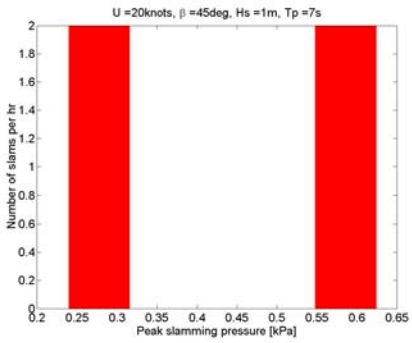

Figure A.2.66 Crowther design 318 impact pressure distribution

Slamming pressure distributions in a 1m seastate with ship motion prediction from high-speed theory are listed below for the main beam (fig. A.2.67 – A.2.71).

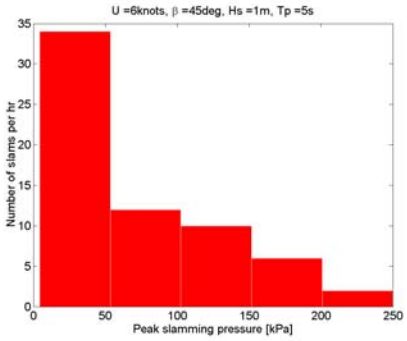

Figure A.2.67 Crowther design 318 impact pressure distribution

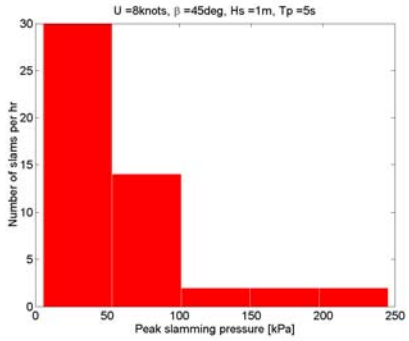

Figure A.2.68 Crowther design 318 impact pressure distribution

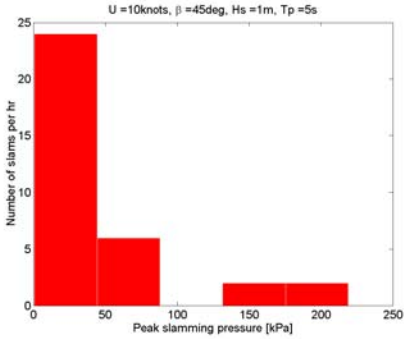

Figure A.2.69 Crowther design 318 impact pressure distribution

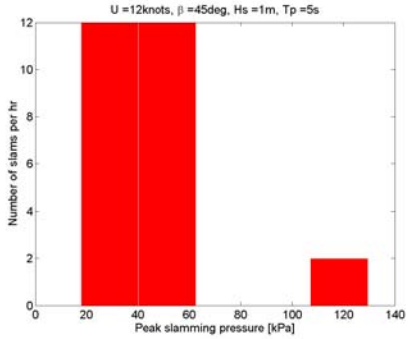

Figure A.2.70 Crowther design 318 impact pressure distribution

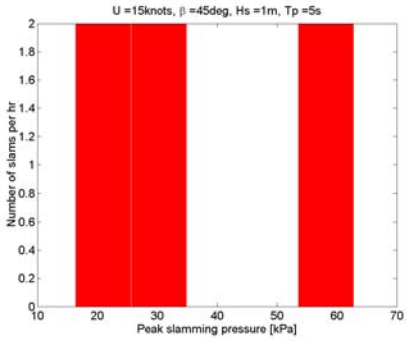

Figure A.2.71 Crowther design 318 impact pressure distribution

Slamming pressure distributions in a 2m seastate with ship motion prediction from high-speed theory are listed below for the pod (fig. A.2.72 – A.2.90).

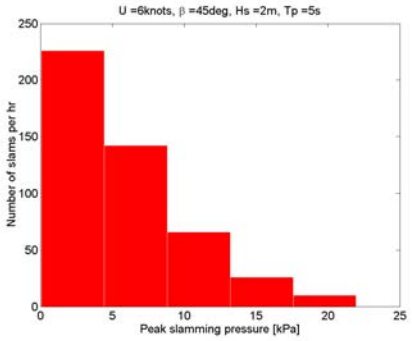

Figure A.2.72 Crowther design 318 impact pressure distribution

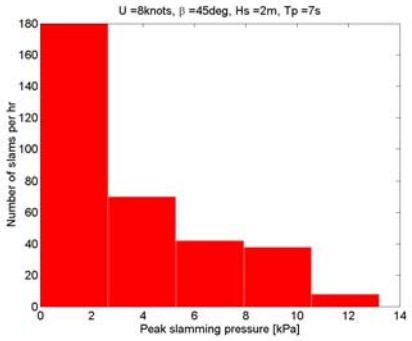

Figure A.2.73 Crowther design 318 impact pressure distribution

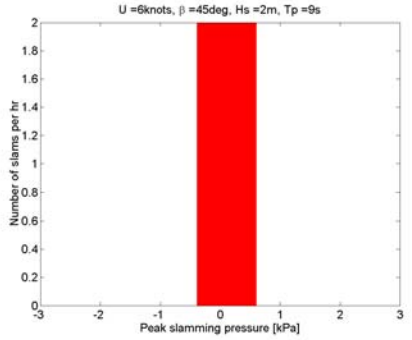

Figure A.2.74 Crowther design 318 impact pressure distribution

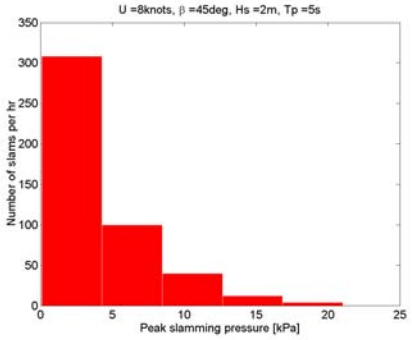

Figure A.2.75 Crowther design 318 impact pressure distribution

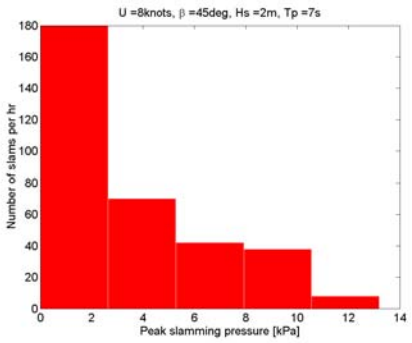

Figure A.2.76 Crowther design 318 impact pressure distribution

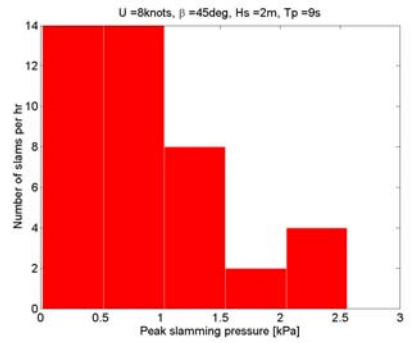

Figure A.2.77 Crowther design 318 impact pressure distribution

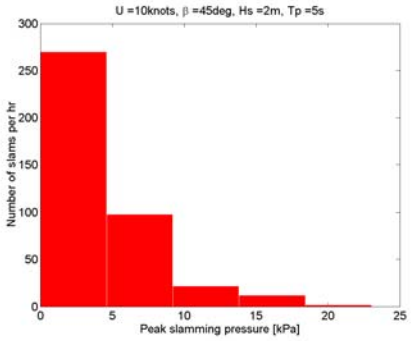

Figure A.2.78 Crowther design 318 impact pressure distribution

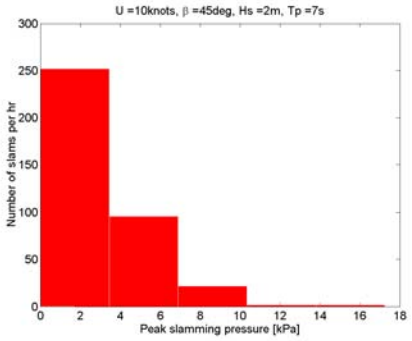

Figure A.2.79 Crowther design 318 impact pressure distribution

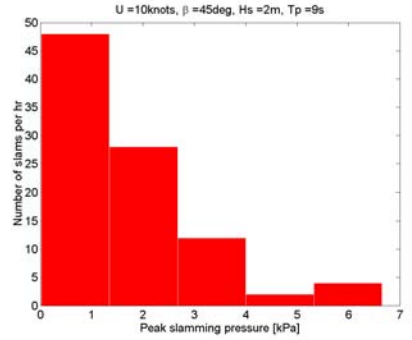

Figure A.2.80 Crowther design 318 impact pressure distribution

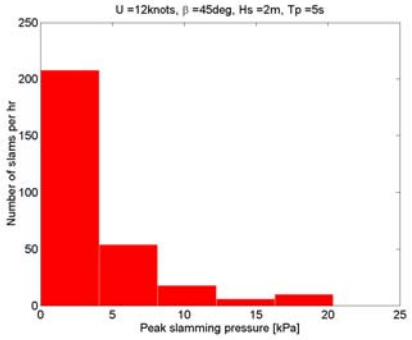

Figure A.2.81 Crowther design 318 impact pressure distribution

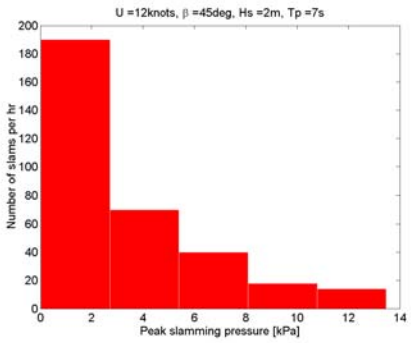

Figure A.2.82 Crowther design 318 impact pressure distribution

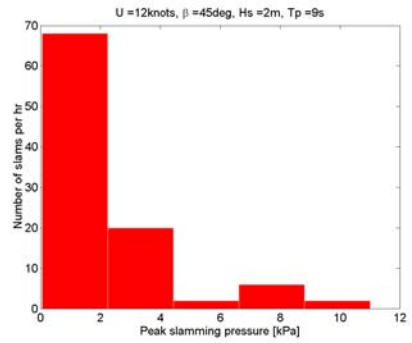

Figure A.2.83 Crowther design 318 impact pressure distribution

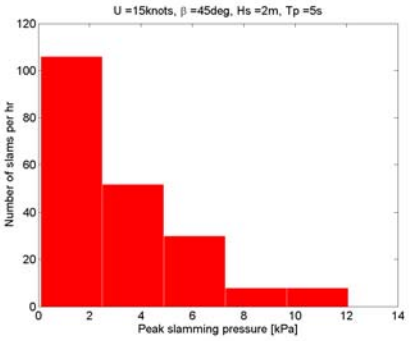

Figure A.2.84 Crowther design 318 impact pressure distribution

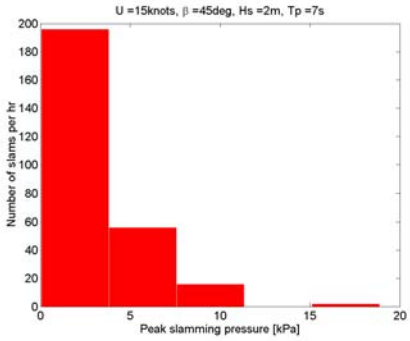

Figure A.2.85 Crowther design 318 impact pressure distribution

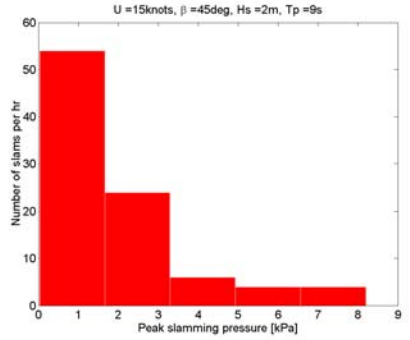

Figure A.2.86 Crowther design 318 impact pressure distribution

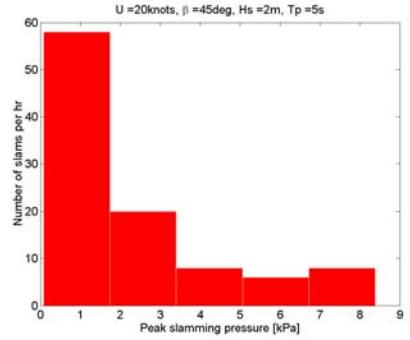

Figure A.2.87 Crowther design 318 impact pressure distribution

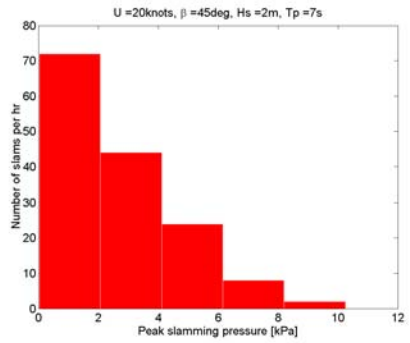

Figure A.2.88 Crowther design 318 impact pressure distribution

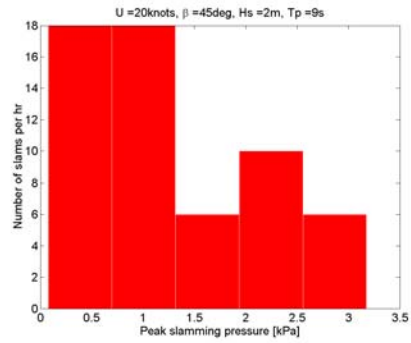

Figure A.2.89 Crowther design 318 impact pressure distribution

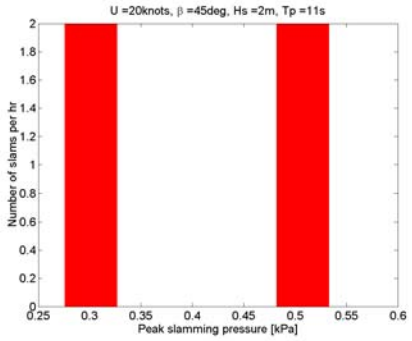

Figure A.2.90 Crowther design 318 impact pressure distribution

Slamming pressure distributions in a 2m seastate with ship motion prediction from high-speed theory are listed below for the main beam (fig. A.2.91 – A.2.105).

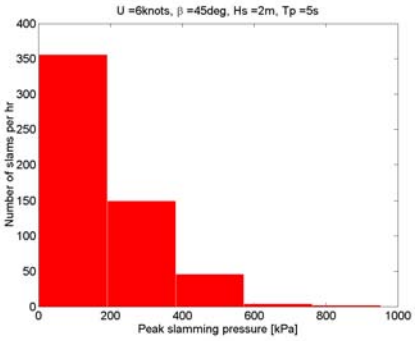

Figure A.2.91 Crowther design 318 impact pressure distribution

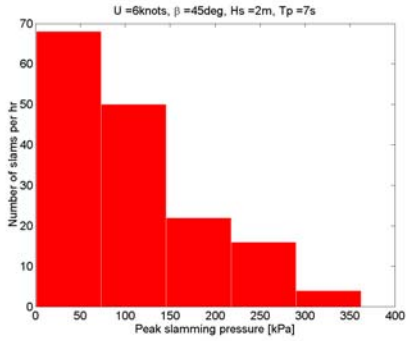

Figure A.2.92 Crowther design 318 impact pressure distribution

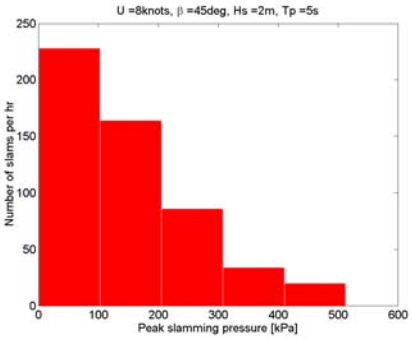

Figure A.2.93 Crowther design 318 impact pressure distribution

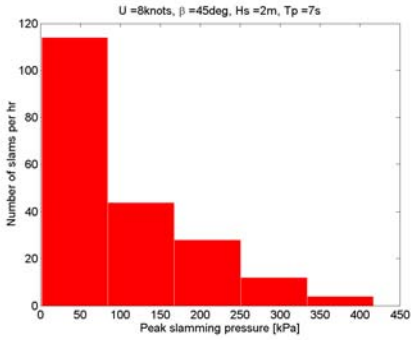

Figure A.2.94 Crowther design 318 impact pressure distribution

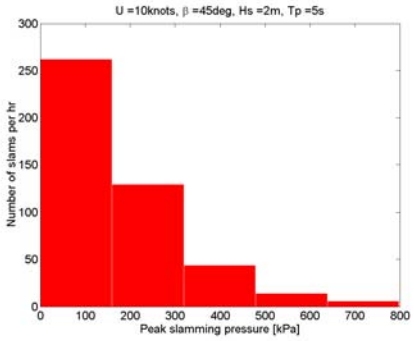

Figure A.2.95 Crowther design 318 impact pressure distribution

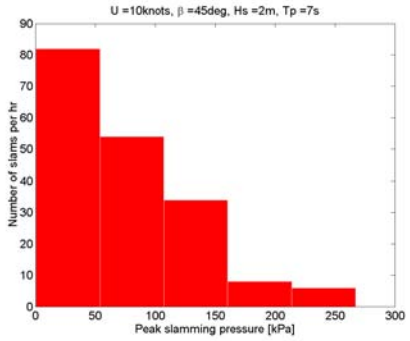

Figure A.2.96 Crowther design 318 impact pressure distribution

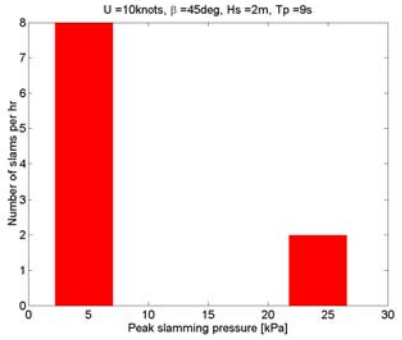

Figure A.2.97 Crowther design 318 impact pressure distribution

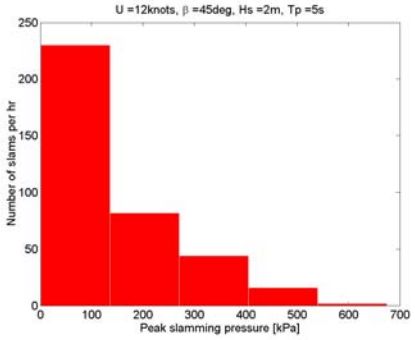

Figure A.2.98 Crowther design 318 impact pressure distribution

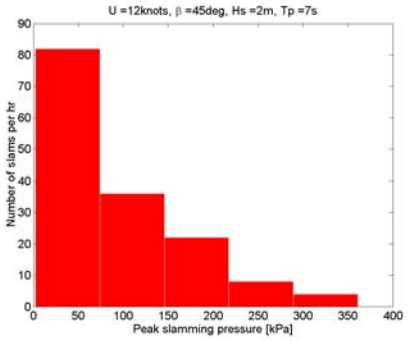

Figure A.2.99 Crowther design 318 impact pressure distribution

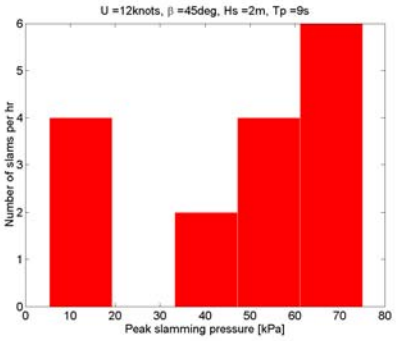

Figure A.2.100 Crowther design 318 impact pressure distribution

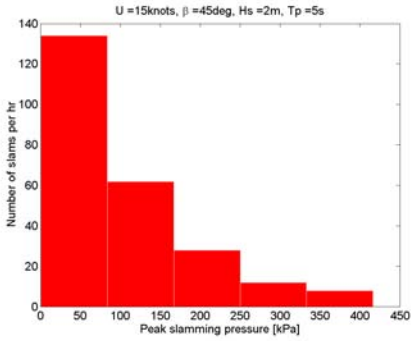

Figure A.2.101 Crowther design 318 impact pressure distribution

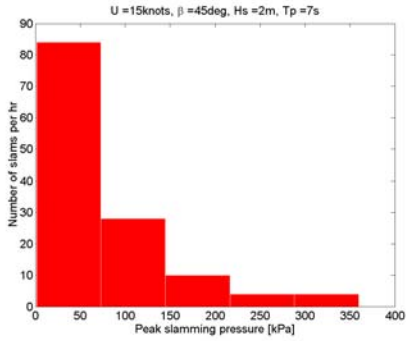

Figure A.2.102 Crowther design 318 impact pressure distribution

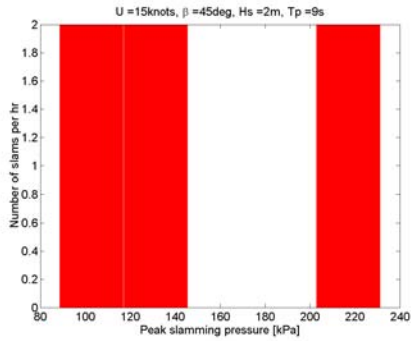

Figure A.2.103 Crowther design 318 impact pressure distribution

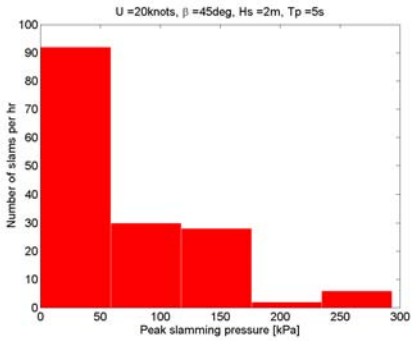

Figure A.2.104 Crowther design 318 impact pressure distribution

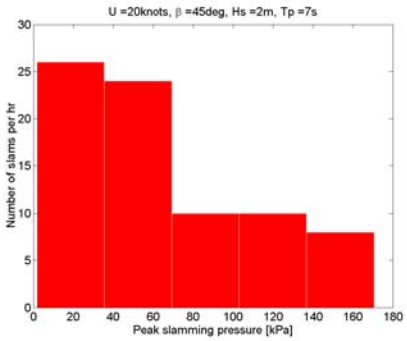

Figure A.2.105 Crowther design 318 impact pressure distribution

Slamming pressure distributions in a 1.5m seastate with ship motion prediction from sailing multihull strip theory are listed below for the pod (fig. A.2.106 – A.2.109).

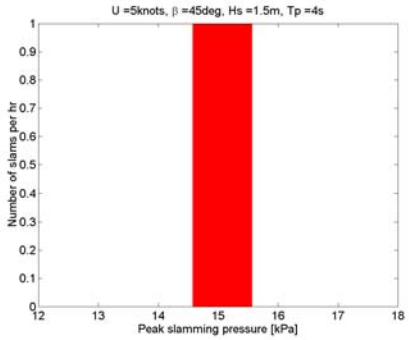

Figure A.2.106 Crowther design 318 impact pressure distribution

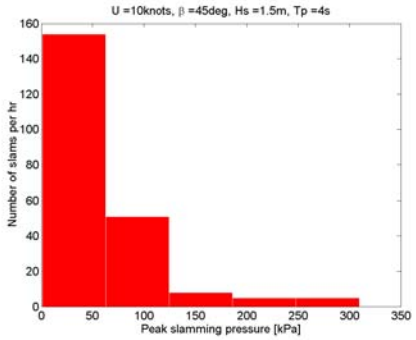

Figure A.2.107 Crowther design 318 impact pressure distribution

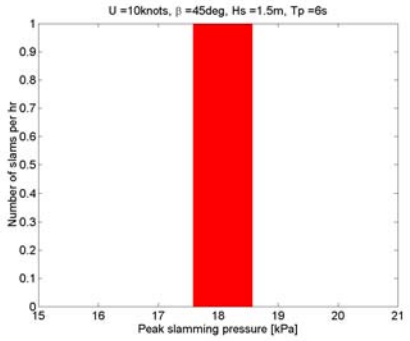

Figure A.2.108 Crowther design 318 impact pressure distribution

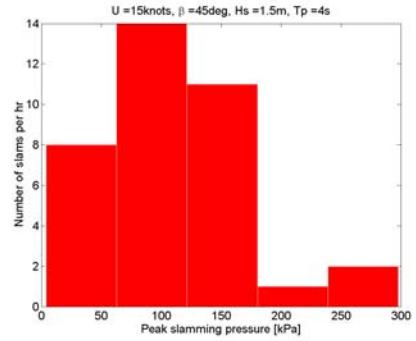

Figure A.2.109 Crowther design 318 impact pressure distribution

Slamming pressure distributions in a 1.5m seastate with ship motion prediction from sailing multihull strip theory are listed below for the main beam (fig. A.2.110 – A.2.111).

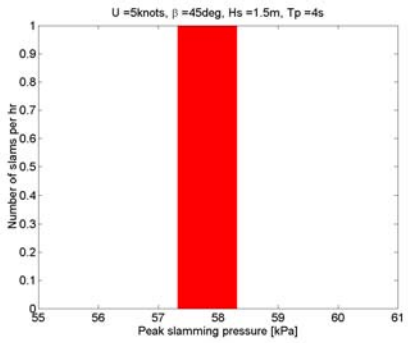

Figure A.2.110 Crowther design 318 impact pressure distribution

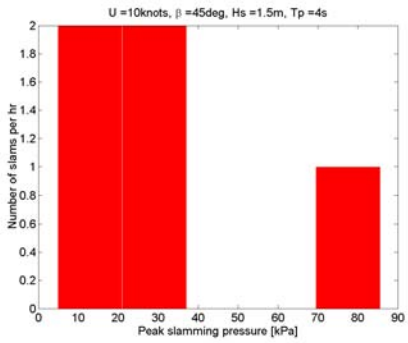

Figure A.2.111 Crowther design 318 impact pressure distribution

Slamming pressure distributions in a 2.25m seastate with ship motion prediction from sailing multihull strip theory are listed below for the pod (fig. A.2.112 – A.2.117).

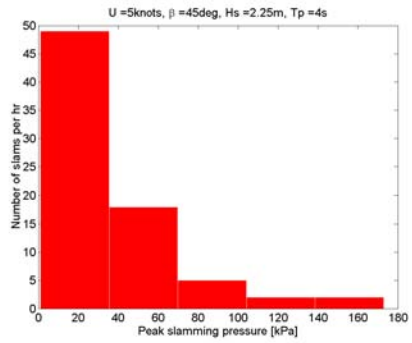

Figure A.2.112 Crowther design 318 impact pressure distribution

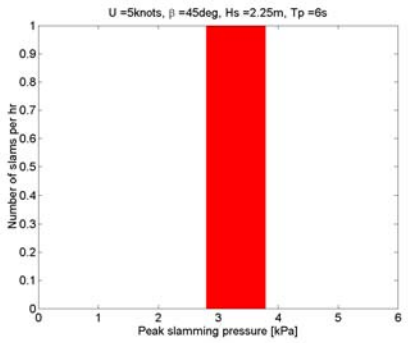

Figure A.2.113 Crowther design 318 impact pressure distribution

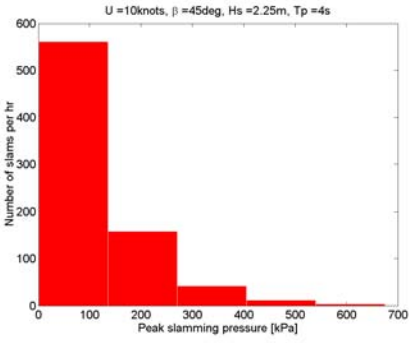

Figure A.2.114 Crowther design 318 impact pressure distribution

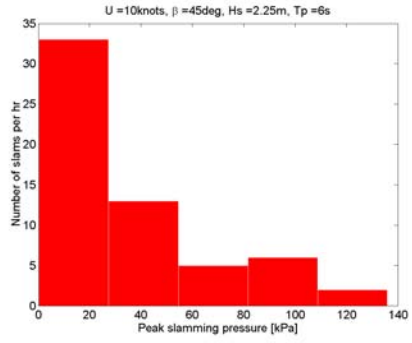

Figure A.2.115 Crowther design 318 impact pressure distribution

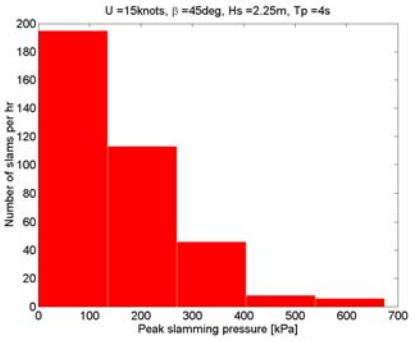

Figure A.2.116 Crowther design 318 impact pressure distribution

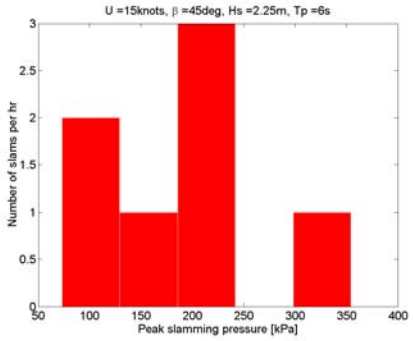

Figure A.2.117 Crowther design 318 impact pressure distribution

Slamming pressure distributions in a 2.25m seastate with ship motion prediction from sailing multihull strip theory are listed below for the main beam (fig. A.2.118 – A.2.122).

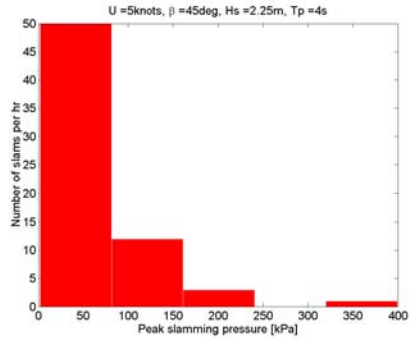

Figure A.2.118 Crowther design 318 impact pressure distribution

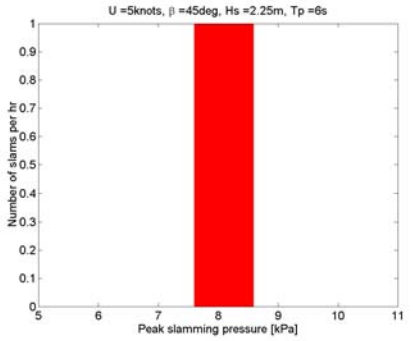

Figure A.2.119 Crowther design 318 impact pressure distribution

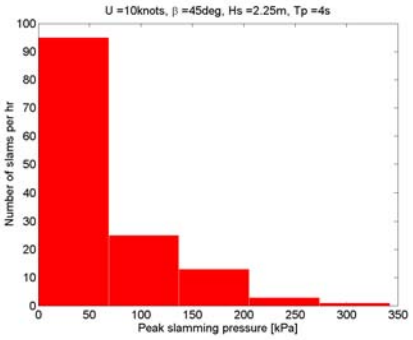

Figure A.2.120 Crowther design 318 impact pressure distribution

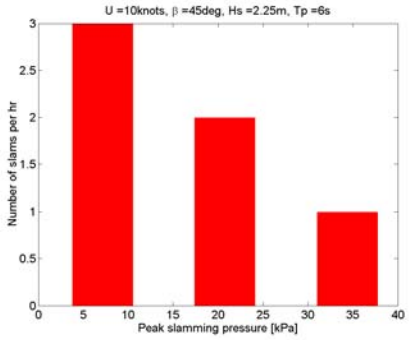

Figure A.2.121 Crowther design 318 impact pressure distribution

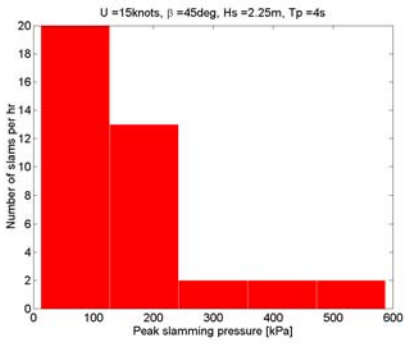

Figure A.2.122 Crowther design 318 impact pressure distribution

APPENDIX 3: FULL-SCALE EQUIPMENT

Data Acquisition system

The data acquisition system consists of a portable laptop computer with a 12 bit 16 channel data acquisition card through the PCMCIA interface. To avoid aliasing a filter is used between the data acquisition card and the sensors. The filter is a 3^{rd} order low pass (Butterworth) filter with an additional 5^{th} order switched capacitor filter. The filter was set at 20 Hz.

An application was written in Labview to log the data to file. A near real time graphical display of the data was also included in the application for monitoring purposes during the trials.

Sensors

The sensors used were one TSS motion sensor, two linear accelerometers and one slamming pressure sensor.

The TSS sensor measures heave, roll and pitch displacements. It has an array of three linear accelerometers and three angular rate sensor. An internal signal processor filters the data and calculates the displacements. The data is available both in analog format and a digital format. The digital format is the preferred format, but the analog format was used for synchronisation with other equipment.

As described in chapter 5 it was decided to make a special sensor to measure the slamming pressure. Apart from being able to measure the slamming pressure on a cylinder with known geometry it was also important that the sensor could be adjusted vertically so the number of slams could be tuned to the sea conditions on the day of the trial. The slamming sensor itself consisted of a small cylinder, pointing forward. A pressure sensor was already available, and it was decided to use this.

To avoid trapped air in the pressure sensor and the pressure tap it was decided to fill the cylinder with fluid. A rubber membrane transfers the pressure from outside the cylinder to the fluid inside. As water is incompressible and the tension in the membrane can be neglected the pressure of both sides of the membrane will always be equal. The pressure sensor measures the pressure in the fluid inside the cylinder, and will always operate in fluid. Care was taken to evacuate all air bubbles from the fluid before use. A drawing of the sensor is shown below (fig. A.1.8). Prior to use the sensor was calibrated for steady pressure and found to be very sensitive and give linear results.

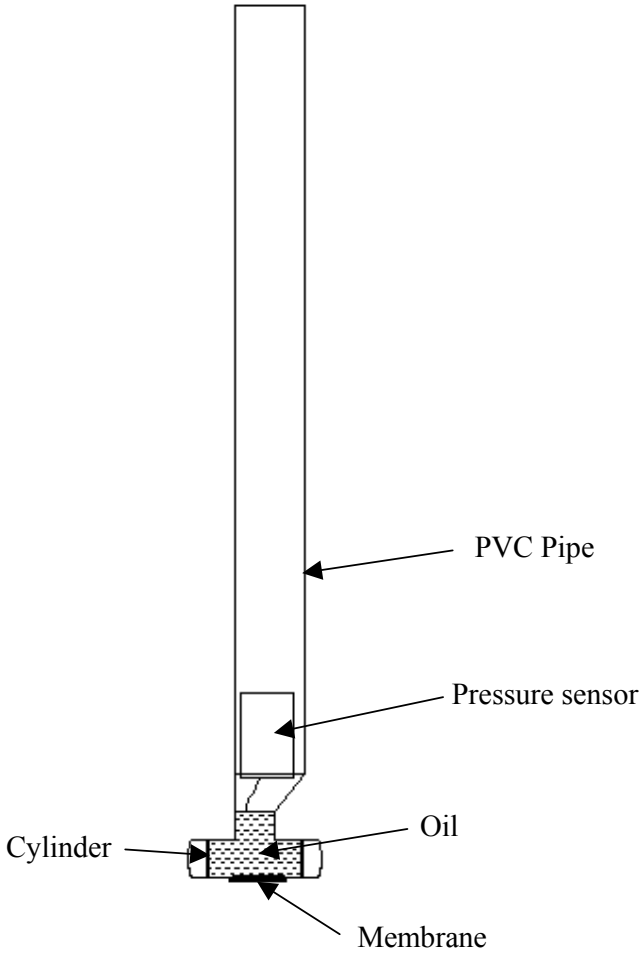

Fig. A.1.8 Slamming Sensor